EUROPEAN ORGANISATION FOR NUCLEAR RESEARCH (CERN)

Submitted to: JHEP

CERN-EP-2017-206
7th December 2017

Measurement of the Higgs boson coupling properties in the $H \to ZZ^* \to 4\ell$ decay channel at $\sqrt{s} = 13$ TeV with the ATLAS detector

The ATLAS Collaboration

The coupling properties of the Higgs boson are studied in the four-lepton decay channel using 36.1 fb^{-1} of pp collision data from the LHC at a centre-of-mass energy of 13 TeV collected by the ATLAS detector. Cross sections are measured for the four key production modes in several exclusive regions of the Higgs boson production phase space and are interpreted in terms of coupling modifiers. The inclusive cross section times branching ratio for $H \to ZZ^*$ decay and for a Higgs boson absolute rapidity below 2.5 is measured to be $1.73^{+0.24}_{-0.23}(\text{stat.})^{+0.10}_{-0.08}(\text{exp.})\pm0.04(\text{th.})$ pb compared to the Standard Model prediction of 1.34 ± 0.09 pb. In addition, the tensor structure of the Higgs boson couplings is studied using an effective Lagrangian approach for the description of interactions beyond the Standard Model. Constraints are placed on the non-Standard-Model CP-even and CP-odd couplings to Z bosons and on the CP-odd coupling to gluons.

1 Introduction

The observation of the Higgs boson by the ATLAS and CMS experiments [1, 2] with the LHC Run-1 data at centre-of-mass energies of $\sqrt{s} = 7$ TeV and 8 TeV has been a major step towards the understanding of the mechanism of electroweak (EW) symmetry breaking [3–5]. Further measurements of the spin, parity and couplings of the new particle have shown no significant deviation from the predictions for the Standard Model (SM) Higgs boson [6–10]. The increased centre-of-mass energy and higher integrated luminosity of the LHC Run-2 data allows the study of the Higgs boson properties in greater detail and an improved search for deviations from the SM predictions.

In this paper, the measurement of the Higgs boson coupling properties is performed in the four-lepton decay channel, $H \to ZZ^* \to 4\ell$, where $\ell \equiv e$ or μ, using 36.1 fb^{-1} of Run-2 pp collision data collected by the ATLAS experiment at a centre-of-mass energy of 13 TeV. Due to its clear signature and high signal-to-background ratio, this channel provides good signal sensitivity. The largest background is the continuum $(Z^{(*)}/\gamma^*)(Z^{(*)}/\gamma^*)$ production, referred to as ZZ^* hereafter. For the studied four-lepton invariant mass range of 118 GeV $< m_{4\ell} <$ 129 GeV, there are also small but non-negligible background contributions from Z + jets and $t\bar{t}$ production with two prompt leptons.

The Higgs boson spin, parity and coupling properties have been studied in this channel with Run-1 data by the ATLAS and CMS experiments [6, 7, 11–13]. In this paper, the Higgs boson couplings to SM particles are studied using two analysis approaches. In the first approach, the Higgs boson production cross sections are analyzed based on different production modes in several exclusive regions of the production phase space, testing whether it is compatible with the SM predictions. An interpretation in terms of coupling modifiers within the κ framework [14, 15] is given, assuming a SM tensor structure ($J^P = 0^+$) for all couplings. In the second approach, the tensor structure of the Higgs boson couplings is studied, probing for admixtures of CP-even and CP-odd interactions in theories beyond the SM (BSM) in addition to the corresponding SM interactions. Both analyses are performed assuming that the studied resonance is a single particle state with spin-0 and a mass of 125.09 GeV based on experimental results obtained with the LHC Run-1 data [16]. It is assumed that the total width of the resonance is small compared the experimental resolution and the interference effects between the signal and SM backgrounds are neglected due to the small contribution.

The paper is organized as follows. A brief introduction of the ATLAS detector is given in Section 2. The analysis strategy describing the two analysis approaches is outlined in Section 3. In Section 4 the data as well as the simulated signal and background samples are described. The selection and categorization of the Higgs boson candidate events, as well as the discriminating observables used in the measurement, are described in Section 5, while the signal and background modelling is detailed in Sections 6 and 7, respectively. The experimental and theoretical systematic uncertainties (Section 8) are taken into account for the statistical interpretation of the data, with the results presented in Section 9. Concluding remarks are given in Section 10.

2 ATLAS detector

The ATLAS detector [17] is a multi-purpose particle detector with a forward-backward symmetric cylindrical geometry.[1] It consists of an inner tracking detector (ID) in a 2 T axial magnetic field covering the pseudorapidity range $|\eta| < 2.5$. A new innermost silicon pixel layer [18] (IBL) was added to the ID after the Run-1 data-taking. The ID is surrounded by the electromagnetic and hadronic calorimeters up to $|\eta| = 4.9$ and by the muon spectrometer (MS) extending up to $|\eta| = 2.7$. The magnetic field for the MS is provided by a set of toroids with a field integral ranging between 2 Tm and 6 Tm across most of the detector. The trigger and data-acquisition system is based on two levels of online event selection: a hardware-based first-level trigger and a software-based high-level trigger employing algorithms similar to those for the offline particle reconstruction.

3 Analysis strategy

The Higgs boson couplings to heavy SM vector bosons (W and Z) and gluons are studied by measuring the cross sections for different production modes and by probing BSM contributions in tensor couplings. In both approaches, the reconstructed Higgs boson candidate events are classified into different categories. The categories are defined to be sensitive to different Higgs boson production modes, which in turn also provides sensitivity to the BSM contributions. The event yields in each category serve as the final discriminant for both the cross section and the tensor structure studies. There are nine reconstructed event categories defined for the cross-section measurement, one of which is additionally split into two separate ones for the tensor structure studies to improve their sensitivity. For the cross-section measurement, there are also additional discriminating observables introduced in reconstructed event categories with a sufficiently high number of events. These observables are defined using dedicated boosted decision trees (BDTs) [19].

3.1 Classification of the Higgs boson production modes

The Higgs boson production cross section times the branching ratio of the decay into Z boson pairs, $\sigma \cdot B(H \to ZZ^*)$, is measured in several dedicated mutually exclusive regions of the phase space based on the production process. For simplicity, these regions are called "production bins". The measured cross sections can then be interpreted in terms of the Higgs boson couplings with the advantage that the major theoretical uncertainties enter only at this interpretation level. The definitions of the production bins shown in Figure 1 (shaded area) are based on particle-level events produced by dedicated event generators closely following the framework of simplified template cross sections [15]. The bins are chosen in such a way that the measurement precision is maximized and at the same time possible BSM contributions can be isolated. All production bins are defined for Higgs bosons with rapidity $|y_H| < 2.5$ and no requirements placed on the particle-level leptons. Two sets of production bins are considered since a more inclusive phase-space region usually reduces the statistical uncertainty of the measurement but at the cost of a larger theoretical uncertainty.

[1] ATLAS uses a right-handed coordinate system with its origin at the nominal interaction point (IP) in the centre of the detector and the z-axis along the beam pipe. The x-axis points from the IP to the centre of the LHC ring, and the y-axis points upward. Cylindrical coordinates (r, ϕ) are used in the transverse plane, with ϕ being the azimuthal angle around the beam pipe. The pseudorapidity is defined in terms of the polar angle θ as $\eta = -\ln\tan(\theta/2)$.

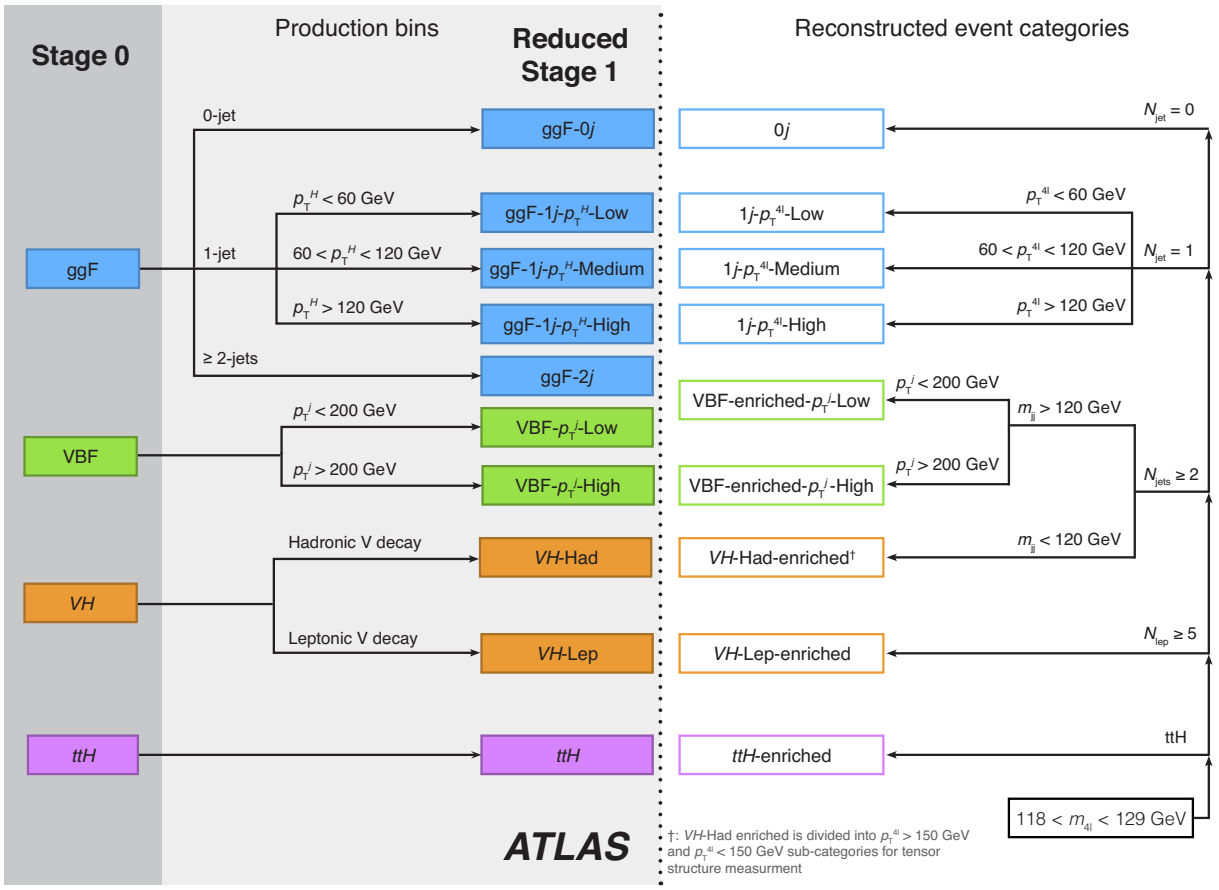

Figure 1: The phase-space regions (production bins) for the measurement of the Higgs boson production cross sections defined for two stages at the particle level and the corresponding reconstructed event categories.

For the first set (Stage 0) [15], production bins are simply defined according to the Higgs boson production vertex: gluon–gluon fusion (ggF), vector boson fusion (VBF) and associated production with top quark pairs (ttH) or vector bosons (VH), where V is a W or a Z boson. The bbH Higgs boson production bin is not included because there is insufficient sensitivity to measure this process with the current integrated luminosity. This production mode has an acceptance similar to gluon–gluon fusion, and their contributions are therefore considered together in the analysis. The sum of their contributions is referred to in the following as gluon–gluon fusion.

For the second set (reduced Stage 1), a more exclusive set of production bins is defined. This set is obtained by the merging of those production bins of the original Stage-1 set from Ref. [15] which cannot be measured separately in the $H \to ZZ^* \to 4\ell$ channel with the current data sample. The gluon–gluon fusion process is split into events with zero, one or at least two particle-level jets. The particle-level jets are built from all stable particles (all particles with $c\tau > 1$ mm) including neutrinos, photons and leptons from hadron decays or produced in the shower. All decay products from the Higgs boson, as well as the leptons and neutrinos from decays of the signal V bosons are removed, while decay products from hadronically decaying signal V bosons are included in the inputs to the particle-level jet building. The anti-k_t jet reconstruction algorithm [20], implemented in the FastJet package [21], with a radius parameter

$R = 0.4$ is used and jets are required to have $p_{\mathrm{T}} > 30$ GeV. The 1-jet bin is further split into three bins with the Higgs boson transverse momentum p_{T}^{H} below 60 GeV, between 60 GeV and 120 GeV, and above 120 GeV. The reduced Stage-1 gluon–gluon fusion bins are correspondingly denoted by ggF-0j, ggF-1j-p_{T}^{H}-Low, ggF-1j-p_{T}^{H}-Med, ggF-1j-p_{T}^{H}-High and ggF-2j. The VBF production bin is split into two bins with the transverse momentum of the leading jet, p_{T}^{j1}, below and above 200 GeV (VBF-p_{T}^{j}-Low and VBF-p_{T}^{j}-High, respectively). The former bin is expected to be dominated by SM events, while the latter is sensitive to potential BSM contributions. For VH production, separate bins with hadronically (VH-Had) and leptonically (VH-Lep) decaying vector bosons are considered. The leptonic V boson decays include the decays into τ leptons and into neutrino pairs. The ttH production bin remains the same as for Stage 0.

Figure 1 also summarizes the corresponding categories of reconstructed events in which the cross-section measurements are performed and which are described in more detail in Section 5. There is a dedicated reconstructed event category for each production bin except for ggF-2j. This process contributes strongly in all reconstructed event categories containing events with at least two jets and can therefore be measured in these categories.

3.2 Tensor structure of Higgs boson couplings

In order to study the tensor structure of the Higgs boson couplings to SM gauge bosons, interactions of the Higgs boson with these SM particles are described in terms of the effective Lagrangian of the Higgs characterization model [22],

$$\begin{aligned}\mathcal{L}_0^V =& \Bigg\{ \kappa_{\mathrm{SM}} \left[\frac{1}{2} g_{HZZ} Z_\mu Z^\mu + g_{HWW} W_\mu^+ W^{-\mu} \right] \\ &- \frac{1}{4} \left[\kappa_{Hgg} g_{Hgg} G^a_{\mu\nu} G^{a,\mu\nu} + \tan\alpha \kappa_{Agg} g_{Agg} G^a_{\mu\nu} \tilde{G}^{a,\mu\nu} \right] \\ &- \frac{1}{4} \frac{1}{\Lambda} \left[\kappa_{HZZ} Z_{\mu\nu} Z^{\mu\nu} + \tan\alpha \kappa_{AZZ} Z_{\mu\nu} \tilde{Z}^{\mu\nu} \right] \\ &- \frac{1}{2} \frac{1}{\Lambda} \left[\kappa_{HWW} W^+_{\mu\nu} W^{-\mu\nu} + \tan\alpha \kappa_{AWW} W^+_{\mu\nu} \tilde{W}^{-\mu\nu} \right] \Bigg\} \mathcal{X}_0. \end{aligned} \tag{1}$$

The additional terms in the Lagrangian involving couplings to fermions are not considered since the present analysis is not sensitive to these couplings. The model is based on an effective field theory description which assumes there are no new BSM particles below the energy scale Λ. The cut-off scale Λ is set to 1 TeV, supported by the current experimental results showing no evidence of new physics below this scale. The notation of Eq. (1) follows the notation of Eq. (2.4) in Ref. [22] with $\mathcal{X}_0$ defining a new bosonic state of spin 0 and with the difference that the dimensionless coupling parameters κ are redefined by dividing them by $\cos\alpha$, where α is the mixing angle between the 0^+ and 0^- CP states implying CP-violation for $\alpha \neq 0$ and $\alpha \neq \pi$. In this way the prediction for the SM Higgs boson is given by $\kappa_{\mathrm{SM}} = 1$ and $\kappa_{Hgg} = 1$ with the values of the BSM couplings set to zero. In this analysis, only the effective Lagrangian terms with coupling parameters κ_{HVV}, κ_{AVV} and κ_{Agg} are considered as possible BSM admixtures to the corresponding SM interactions. These terms describe the CP-even (scalar) and CP-odd (pseudo-scalar) BSM interaction with vector bosons and the CP-odd BSM interaction with gluons, respectively. The BSM couplings are assumed to be the same for W and Z bosons (i.e. $\kappa_{HWW} = \kappa_{HZZ} \equiv \kappa_{HVV}$ and $\kappa_{AWW} = \kappa_{AZZ}$

$\equiv \kappa_{AVV}$). The value of α is arbitrarily set to $\pi/4$ such that the CP-odd couplings can be more simply denoted by $\kappa_{AVV} \tan\alpha \Rightarrow \kappa_{AVV}$ and $\kappa_{Agg} \tan\alpha \Rightarrow \kappa_{Agg}$.

In the previous Run-1 analysis [11], the Higgs-related BSM interactions with heavy vector bosons were studied only in Higgs boson decays. In this analysis, the impact of BSM contributions on both the decay rates and the production cross sections in different production modes is taken into account. The κ_{HVV} and κ_{AVV} parameters contribute the most to VH and VBF Higgs boson production in the four-lepton decay mode since the coupling is present in both the production and decay vertices. The κ_{Agg} parameter mostly affects the ggF production.

4 Signal and background simulation

The production of the SM Higgs boson via ggF, VBF and VH (including $gg \to ZH$) production mechanisms was modelled with the POWHEG-BOX v2 Monte Carlo (MC) event generator [23, 24], interfaced to EvtGen v1.2.0 [25] for properties of the bottom and charm hadron decays, using the PDF4LHC next-to-leading-order (NLO) set of parton distribution functions (PDF) [26]. The gluon–gluon fusion Higgs boson production is accurate to next-to-next-to-leading order (NNLO) in the strong coupling, using the POWHEG method for merging the NLO Higgs + jet cross section with the parton shower, and the MiNLO method [27] to simultaneously achieve NLO accuracy for inclusive Higgs boson production. A reweighting procedure, employing the Higgs boson rapidity, was applied using the HNNLO program [28, 29]. The matrix elements of the VBF and VH production mechanisms were calculated up to NLO in QCD. For VH production, the MiNLO method was used to merge 0- and 1-jet events [30]. The $gg \to ZH$ contribution was modelled at leading order (LO) in QCD. The production of a Higgs boson in association with a top (bottom) quark pair was simulated at NLO with MadGraph5_aMC@NLO v2.2.3 (v2.3.3) [31, 32] , using the CT10nlo PDF set [33] for ttH production and the NNPDF23 PDF set [34] for bbH production. For the ggF, VBF, VH and bbH production mechanisms, the PYTHIA 8 [35] generator was used for the $H \to ZZ^* \to 4\ell$ decay as well as for the parton shower model using a set of tuned parameters called the AZNLO tune [36]. For the ttH production mechanism, the Herwig++ [37] event generator was used with the UEEE5 tune [38]. All signal samples were simulated for the Higgs boson with a mass $m_H = 125.00$ GeV. Wherever relevant, the signal mass distribution is shifted to the reference value of 125.09 GeV.

The Higgs boson production cross sections and decay branching ratios, as well as their uncertainties, were taken from Refs. [14, 26, 34, 39–66]. The ggF production was calculated with next-to-next-to-next-to-leading order (N^3LO) accuracy in QCD and has NLO electroweak (EW) corrections applied. For VBF production, full NLO QCD and EW calculations were used with approximate NNLO QCD corrections. The VH production was calculated at NNLO in QCD and NLO EW corrections are applied. The ttH and bbH processes were calculated to NLO accuracy in QCD. The branching ratio for the $H \to ZZ^* \to 4\ell$ decay with $m_H = 125.09$ GeV was predicted to be 0.0125% [60] in the SM using PROPHECY4F [62, 63], which includes the complete NLO QCD and EW corrections, and the interference effects between identical final-state fermions. Table 1 summarizes the production cross sections and branching ratios for the $H \to ZZ^* \to 4\ell$ decay for $m_H = 125.09$ GeV.

Additional ggF, VBF and VH signal samples with different values of the BSM couplings κ_{Agg}, κ_{HVV} and κ_{AVV} were generated with MadGraph5_aMC@NLO and are used for the signal modelling as a function of the BSM couplings as explained in Section 6. The ggF simulation includes samples at NLO QCD accuracy for zero, one and two additional partons merged with the FxFx merging scheme [31, 67], while

Table 1: The predicted SM Higgs boson production cross sections (σ) for ggF, VBF and associated production with a W or Z boson or with a $t\bar{t}$ or $b\bar{b}$ pair in pp collisions for $m_H = 125.09$ GeV at $\sqrt{s} = 13$ TeV [14, 26, 34, 39–66]. The quoted uncertainties correspond to the total theoretical systematic uncertainties calculated by adding in quadrature the QCD scale and PDF+α_s uncertainties. The decay branching ratio (B) with the associated uncertainty for $H \to ZZ^*$ and $H \to ZZ^* \to 4\ell$ with $\ell = e, \mu$, is also given.

Production process		σ [pb]
ggF	$(gg \to H)$	48.5 ± 2.4
VBF	$(qq' \to Hqq')$	3.78 ± 0.08
WH	$(q\bar{q}' \to WH)$	1.369 ± 0.028
ZH	$(q\bar{q}/gg \to ZH)$	0.88 ± 0.04
ttH	$(q\bar{q}/gg \to t\bar{t}H)$	0.51 ± 0.05
bbH	$(q\bar{q}/gg \to b\bar{b}H)$	0.49 ± 0.12
Decay process		B [$\cdot 10^{-4}$]
$H \to ZZ^*$		264 ± 6
$H \to ZZ^* \to 4\ell$		1.250 ± 0.027

the VBF and VH simulations are accurate to LO in α_s. Equivalent VBF and VH processes were also generated at NLO QCD accuracy and used to estimate the relative uncertainties of higher-order QCD effects as a function of the BSM coupling parameters.

The ZZ^* continuum background from quark–antiquark annihilation was modelled using Sherpa 2.2.2 [68–70], which provides a matrix element calculation accurate to NLO in α_s for 0-, and 1-jet final states and LO accuracy for 2- and 3-jet final states. The merging was performed with the Sherpa parton shower [71] using the ME+PS@NLO prescription [72]. The NLO EW corrections were applied as a function of the invariant mass of the ZZ^* system m_{ZZ^*} [73, 74].

The gluon-induced ZZ^* production was modelled by gg2VV [75] at LO in QCD. The higher-order QCD effects for the $gg \to ZZ^*$ continuum production have been calculated for massless quark loops [76–78] in the heavy top-quark approximation [79], including the $gg \to H^* \to ZZ$ processes [80, 81]. The simulated LO samples are scaled by the K-factor of 1.7±1.0, defined as the ratio of the higher-order and the leading-order cross section predictions.

The WZ background was modelled using POWHEG-BOX v2 interfaced to PYTHIA 8 and EvtGen v1.2.0 for properties of the bottom and charm hadron decays. The triboson backgrounds ZZZ, WZZ, and WWZ with four or more prompt leptons were modelled using Sherpa 2.1.1. The simulation of $t\bar{t}+Z$ events with both top quarks decaying semi-leptonically and the Z boson decaying leptonically was performed with MadGraph interfaced to PYTHIA 8 and the total cross section was normalized to the prediction which includes the two dominant terms at both the LO and the NLO in a mixed perturbative expansion in the QCD and EW couplings [56].

The modelling of events containing Z bosons with associated jets was performed using the Sherpa 2.2.2 generator. Matrix elements were calculated for up to two partons at NLO and four partons at LO using Comix [69] and OpenLoops [70], and merged with the Sherpa parton shower [71] using the ME+PS@NLO prescription [72]. The NNPDF3.0 NNLO PDF set was used in conjunction with dedicated parton shower parameters tuning developed by the Sherpa authors. Simulated samples were normalized

to the data-driven estimate described in Section 7. As a cross-check, this estimate was compared to the theory prediction obtained with FEWZ [82, 83] at NNLO in α_s.

The $t\bar{t}$ background was modelled using POWHEG-BOX v2 interfaced to PYTHIA 6 [84] for parton showering, hadronisation, and the underlying event and to EvtGen v1.2.0 for properties of the bottom and charm hadron decays.

Generated events were processed through the ATLAS detector simulation [85] within the Geant4 framework [86] and reconstructed the same way as the data. Additional pp interactions in the same and nearby bunch crossings (pile-up) are included in the simulation. The pile-up events were generated using PYTHIA 8 with the A2 set of tuned parameters [87] and the MSTW2008LO PDF set [88]. The simulation samples were weighted to reproduce the observed distribution of the mean number of interactions per bunch crossing in the data.

5 Event selection

5.1 Event reconstruction

The selection and categorization of the Higgs boson candidate events rely on the reconstruction and identification of electrons, muons and jets, closely following the analyses reported in Refs. [11, 89].

Collision vertices are reconstructed from ID tracks with transverse momentum $p_{\mathrm{T}} > 400$ MeV. The vertex with the highest $\sum p_{\mathrm{T}}^2$ is selected as the primary vertex. Events are required to have at least one collision vertex with at least two associated tracks.

Electron candidates are reconstructed from ID tracks that are matched to energy clusters in the electromagnetic calorimeter [90]. A Gaussian-sum filter algorithm [91] is used to compensate for radiative energy losses in the ID. Electron identification is based on a likelihood discriminant combining the measured track properties, electromagnetic shower shapes and quality of the track–cluster matching. The "loose" likelihood criteria applied in combination with track hit requirements provide an electron efficiency of 95% [90]. Electrons are required to have $E_{\mathrm{T}} > 7$ GeV and $|\eta| < 2.47$, with their energy calibrated as described in Ref. [92].

Muon candidate reconstruction [93] within $|\eta| < 2.5$ is primarily performed by a global fit of fully reconstructed tracks in the ID and the MS. In the central detector region ($|\eta| < 0.1$), which has a limited MS geometrical coverage, muons are also identified by matching a fully reconstructed ID track to either an MS track segment (segment-tagged muons) or a calorimetric energy deposit consistent with a minimum-ionizing particle (calorimeter-tagged muons). For these two cases, the muon momentum is determined by the ID track alone. In the forward MS region ($2.5 < |\eta| < 2.7$) outside the ID coverage, MS tracks with hits in the three MS layers are accepted and combined with forward ID tracklets, if they exist (stand-alone muons). Calorimeter-tagged muons are required to have $p_{\mathrm{T}} > 15$ GeV. For all other muon candidates, the minimum transverse momentum is 5 GeV instead of the 6 GeV threshold in the Run-1 publication [11], increasing the signal acceptance in the four-muon final state by about 7%. At most one calorimeter-tagged or stand-alone muon is allowed per event.

Jets are reconstructed from noise-suppressed topological clusters [94] in the calorimeter using the anti-k_t algorithm with a radius parameter $R = 0.4$. The jet four-momentum is corrected for the calorimeter's non-compensating response, signal losses due to noise threshold effects, energy lost in non-instrumented

regions, and contributions from pile-up [95]. Jets are required to have $p_{\mathrm{T}} > 30$ GeV and $|\eta| < 4.5$. Jets from pile-up are rejected using a jet-vertex-tagger discriminant [96] based on the fraction of the jet's tracks that come from the primary vertex. Jets with $|\eta| < 2.5$ containing b-hadrons are identified using the MV2c20 b-tagging algorithm [97, 98] at an operating point with 70% b-tagging efficiency.

Ambiguities are resolved if electron, muon or jet candidates are reconstructed from the same detector information. If a reconstructed electron and muon share the same ID track, the muon is rejected if it is calorimeter-tagged; otherwise the electron is rejected. Reconstructed jets geometrically overlapping in a cone of radius R = 0.2 with electrons or muons are also removed.

5.2 Selection of the Higgs boson candidates

Events are triggered by a combination of unprescaled single-lepton, dilepton and trilepton triggers with p_{T} and E_{T} thresholds increasing slightly during the data-taking periods due to an increasing peak luminosity. The lowest-threshold triggers are complemented by triggers with higher thresholds but looser lepton selection criteria. The global trigger efficiency for signal events passing the final selection is 98%.

At least two same-flavour and opposite-charge lepton pairs are required in the final state, resulting in one or more possible lepton quadruplets in each event. The three highest-p_{T} leptons in each quadruplet must have transverse momenta above 20 GeV, 15 GeV and 10 GeV, respectively. The lepton pair with the invariant mass m_{12} (m_{34}) closest (second closest) to the Z boson mass in each quadruplet is referred to as the leading (subleading) lepton pair. Based on the lepton flavour, each quadruplet is classified into one of the following decay channels: 4μ, $2e2\mu$, $2\mu2e$ and $4e$, with the first two leptons always representing the leading lepton pair. In each subchannel, only the quadruplet containing the leading lepton pair with an invariant mass closest to the Z boson mass is accepted.

The leading lepton pair must satisfy 50 GeV $< m_{12} <$ 106 GeV. The subleading lepton pair is required to have a mass $m_{\mathrm{min}} < m_{34} <$ 115 GeV, where m_{min} is 12 GeV for the four-lepton invariant mass $m_{4\ell}$ below 140 GeV, rising linearly to 50 GeV at $m_{4\ell} = 190$ GeV and then remaining at 50 GeV for all higher $m_{4\ell}$ values. In the $4e$ and 4μ channels, the two alternative opposite-charge lepton pairings within a quadruplet must have a dilepton mass above 5 GeV to suppress the J/ψ background. The two lepton pairs within the quadruplet must have an angular separation of $\Delta R = \sqrt{(\Delta y)^2 + (\Delta\phi)^2} > 0.1$ (0.2) for same-flavour (different-flavour) lepton pairs. Each electron (muon) must have a transverse impact parameter significance $|d_0|/\sigma(d_0)$ below 5 (3) to suppress the background from heavy-flavour hadrons. Reducible background from the Z+jets and $t\bar{t}$ processes is further suppressed by imposing track-based and calorimeter-based isolation criteria on each lepton. The scalar sum of the p_{T} of the tracks lying within a cone of $\Delta R = 0.3$ (0.2) around the muon (electron) is required to be smaller than 15% of the lepton p_{T} (E_{T}). Similarly, the sum of the calorimeter E_{T} deposits in a cone of $\Delta R = 0.2$ around the muon (electron) is required to be less than 30% (20%) of the lepton E_{T}. The calorimeter-based isolation requirement is applied after correcting for the pile-up and underlying-event contributions as well as removing the energy deposits from the remaining three leptons. If there is more than one decay channel per event with a quadruplet satisfying the above selection criteria, the quadruplet from the channel with highest efficiency is chosen as the Higgs boson candidate. The signal selection efficiencies are 31%, 21%, 17% and 16%, in the 4μ, $2e2\mu$, $2\mu2e$ and $4e$ channels, respectively.

In case of VH-Lep or ttH production, there may be additional leptons present in the event, together with the selected quadruplet. There is therefore a possibility that some of the quadruplet leptons do not originate from a Higgs boson decay, but rather from the V boson or top quark decays. To improve the lepton

pairing in such cases, a matrix-element-based pairing method is used for all events containing at least one additional lepton with p_{T} >12 GeV and which satisfies the same identification and isolation criteria as the four quadruplet leptons. For all possible quadruplet combinations which pass the above selection, a matrix element for the Higgs boson decay is computed at LO using the MadGraph5_aMC@NLO [31] generator. The quadruplet with the largest matrix element value is selected as the final Higgs boson candidate.

In order to improve the four-lepton mass reconstruction, the reconstructed final-state radiation (FSR) photons in Z boson decays are accounted for using the same strategy as in the Run-1 data analysis [11, 99]. After the FSR correction, the lepton four-momenta of the leading lepton pair are recomputed by means of a Z-mass-constrained kinematic fit. The fit uses a Breit–Wigner Z line shape, and a single Gaussian function per lepton to model the momentum response function for the expected resolution of each lepton. The Z boson mass constraint improves the resolution of the four-lepton invariant mass $m_{4\ell}$ by about 15%. The expected mass resolution for the Higgs boson with a mass m_H = 125.09 GeV is 1.6 GeV, 1.7 GeV, 2.1 GeV and 2.4 GeV in the 4μ, $2e2\mu$, $2\mu2e$ and $4e$ channels, respectively. Finally, to compensate for an increased reducible background due to lowering the muon p_{T} threshold to 5 GeV, the four quadruplet leptons are required to originate from a common vertex point. A requirement corresponding to a signal efficiency of 99.5% is imposed in all decay channels on the χ^2 value from the fit of the four lepton tracks to their common vertex.

The Higgs boson candidates within a mass window of 118 GeV $< m_{4\ell} <$ 129 GeV are selected to study the properties of the Higgs boson.

5.3 Categorization of reconstructed Higgs boson event candidates

In order to gain sensitivity to different Higgs boson production modes, reconstructed events are classified into several exclusive categories based on the presence of jets and additional leptons in the final state as outlined in Figure 1. The classification of events is performed in the following order. First, events are classified as enriched in the ttH process (ttH-enriched) by requiring at least one b-tagged jet in the event. In addition, there must be at least four additional jets or one additional lepton with $p_{\mathrm{T}} > 12$ GeV together with at least two jets. The additional lepton is required to satisfy the same isolation, impact parameter and angular separation requirements as the leptons in the quadruplet. Events with additional leptons but not satisfying the above jet requirements compose the next category enriched in VH production with leptonic vector boson decays (VH-Lep-enriched).

The remaining events are classified according to their jet multiplicity into events with no jets, exactly one jet or at least two jets. Among events with at least two jets there are significant contributions from the VBF and VH production modes in addition to ggF. These events are divided into two categories according to the invariant mass m_{jj} of the two leading jets. The requirement of $m_{jj} \leq 120$ GeV enhances the VH production mode with hadronically decaying vector bosons (VH-Had-enriched). For $m_{jj} > 120$ GeV, the VBF Higgs boson signal is enhanced, and these events are further classified according to the transverse momentum of the leading jet into events with p_{T}^{j1} below (VBF-enriched-p_{T}^{j}-Low) and above 200 GeV (VBF-enriched-p_{T}^{j}-High). Events with zero or one jet in the final state are expected to be dominated by the ggF process. Following the particle-level definition of production bins from Section 3.1, the 1-jet category is further split into three categories with the four-lepton transverse momentum $p_{\mathrm{T}}^{4\ell}$ smaller than 60 GeV ($1j$-$p_{\mathrm{T}}^{4\ell}$-Low), between 60 and 120 GeV ($1j$-$p_{\mathrm{T}}^{4\ell}$-Med), and larger than 120 GeV ($1j$-$p_{\mathrm{T}}^{4\ell}$-High). The largest number of ggF events and the highest ggF purity are expected in the zero-jet category ($0j$).

For the tensor structure measurement, the BSM interactions are expected to be more prominent at higher Higgs boson and jet transverse momenta. Thus, in addition to the splitting of events with a VBF-like topology according to p_{T}^{j1}, the *VH*-Had-enriched category is further divided into two categories with four-lepton transverse momentum $p_{\mathrm{T}}^{4\ell}$ below and above 150 GeV: *VH*-Had-enriched-$p_{\mathrm{T}}^{4\ell}$-Low and *VH*-Had-enriched-$p_{\mathrm{T}}^{4\ell}$-High, respectively.

The expected number of signal events is shown in Table 2 for each Stage-0 production bin and separately for each reconstructed event category. The ggF and *bbH* contributions are shown separately in order to compare their relative contributions, but both are included in the same (ggF) production bin. The highest *bbH* event yield is expected in the $0j$ category since the jets tend to be more forward than in the *ttH* process, thus escaping the acceptance of the *ttH* selection criteria. The included systematic uncertainties are detailed in Section 8. The signal composition in terms of the reduced Stage-1 production bins is shown in Figure 2.

Table 2: The expected number of SM Higgs boson events with a mass $m_H = 125.09$ GeV in the mass range $118 < m_{4\ell} < 129$ GeV for an integrated luminosity of 36.1 fb^{-1} and $\sqrt{s} = 13$ TeV in each reconstructed event category, shown separately for each Stage-0 production bin. The ggF and *bbH* contributions are shown separately but both contribute to the same (ggF) production bin. Statistical and systematic uncertainties are added in quadrature.

Reconstructed	SM Higgs boson production mode				
event category	ggF	VBF	*VH*	*ttH*	*bbH*
$0j$	25.9 ± 2.5	0.29 ± 0.09	0.253 ± 0.025	0.00025 ± 0.00019	0.29 ± 0.14
$1j$-$p_{\mathrm{T}}^{4\ell}$-Low	8.0 ± 1.1	0.514 ± 0.034	0.230 ± 0.018	0.0007 ± 0.0005	0.09 ± 0.05
$1j$-$p_{\mathrm{T}}^{4\ell}$-Med	4.5 ± 0.7	0.64 ± 0.09	0.227 ± 0.019	0.0010 ± 0.0005	0.026 ± 0.013
$1j$-$p_{\mathrm{T}}^{4\ell}$-High	1.10 ± 0.24	0.27 ± 0.04	0.095 ± 0.007	0.00080 ± 0.00024	0.0036 ± 0.0018
VBF-enriched-p_{T}^{j}-Low	3.9 ± 0.8	2.03 ± 0.19	0.285 ± 0.024	0.065 ± 0.009	0.045 ± 0.023
VBF-enriched-p_{T}^{j}-High	0.33 ± 0.09	0.185 ± 0.024	0.050 ± 0.004	0.0159 ± 0.0027	0.00058 ± 0.00029
VH-Had-enriched-$p_{\mathrm{T}}^{4\ell}$-Low	2.3 ± 0.5	0.169 ± 0.014	0.418 ± 0.023	0.022 ± 0.004	0.025 ± 0.013
VH-Had-enriched-$p_{\mathrm{T}}^{4\ell}$-High	0.42 ± 0.09	0.048 ± 0.008	0.162 ± 0.005	0.0090 ± 0.0015	< 0.0001
VH-Lep-enriched	0.0129 ± 0.0018	0.00310 ± 0.00021	0.263 ± 0.018	0.038 ± 0.005	0.0009 ± 0.0005
ttH-enriched	0.050 ± 0.016	0.010 ± 0.006	0.0196 ± 0.0031	0.301 ± 0.032	0.0064 ± 0.0035
Total	47 ± 4	4.16 ± 0.23	2.00 ± 0.11	0.45 ± 0.05	0.49 ± 0.24

5.4 Additional discriminating observables

In order to further increase the sensitivity of the cross-section measurements in the production bins (Section 3.1), BDT discriminants are introduced in reconstructed event categories with a sufficiently high number of events. The BDTs are trained on simulated samples to distinguish a particular Higgs boson production process from either the background or the other production processes, based on several discriminating observables as summarized in Table 3. It is assumed for the training that all input distributions are governed by the SM predictions.

A BDT discriminant in the $0j$ category is built to separate the Higgs boson signal from the non-resonant ZZ^* background, relying on the four-lepton transverse momentum and rapidity as well as on the kinematic discriminant D_{ZZ^*} [11], defined as the difference between the logarithms of the signal and background matrix elements squared. In the two 1-jet categories with $p_{\mathrm{T}}^{4\ell}$ below 120 GeV, a BDT discriminant combining information about the jet transverse momentum (p_{T}^{j}), rapidity (η_j) and angular separation

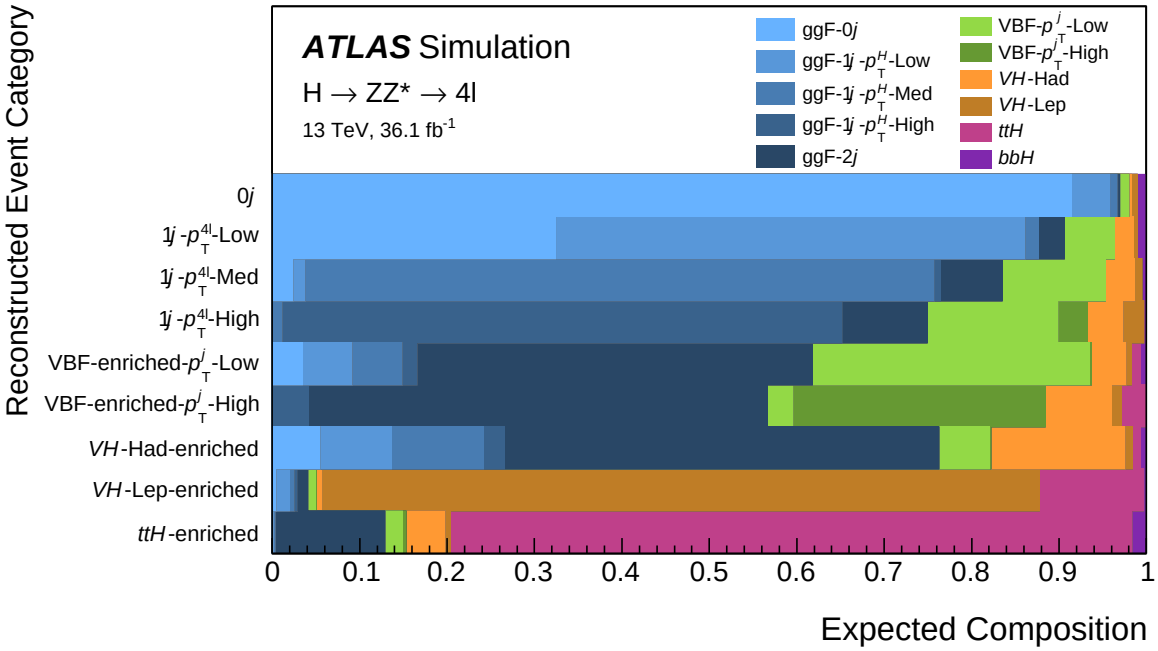

Figure 2: Signal composition in terms of the reduced Stage-1 production bins in each reconstructed event category. The ggF and *bbH* contributions are shown separately but both contribute to the same (ggF) production bin.

Table 3: The BDT discriminants and their corresponding input variables used for the measurement of cross sections per production bin. The jets are denoted by "j". See the text for variable definitions.

Reconstructed event category	BDT discriminant	Input variables
$0j$	$\mathrm{BDT}_{\mathrm{ggF}}$	$p_{\mathrm{T}}^{4\ell}$, $\eta_{4\ell}$, D_{ZZ^*}
$1j$-$p_{\mathrm{T}}^{4\ell}$-Low	$\mathrm{BDT}_{\mathrm{VBF}}^{1j\text{-}p_{\mathrm{T}}^{4\ell}\text{-Low}}$	p_{T}^{j}, η_j, $\Delta R(j, 4\ell)$
$1j$-$p_{\mathrm{T}}^{4\ell}$-Med	$\mathrm{BDT}_{\mathrm{VBF}}^{1j\text{-}p_{\mathrm{T}}^{4\ell}\text{-Med}}$	p_{T}^{j}, η_j, $\Delta R(j, 4\ell)$
$1j$-$p_{\mathrm{T}}^{4\ell}$-High	-	-
VBF-enriched-p_{T}^{j}-Low	$\mathrm{BDT}_{\mathrm{VBF}}$	m_{jj}, $\Delta\eta_{jj}$, p_{T}^{j1}, p_{T}^{j2}, $\eta_{4\ell}^{*}$, $\Delta R_{jZ}^{\mathrm{min}}$, $(p_{\mathrm{T}}^{4\ell jj})_{\mathrm{constrained}}$
VBF-enriched-p_{T}^{j}-High	-	-
VH-Had-enriched	$\mathrm{BDT}_{VH\text{-Had}}$	m_{jj}, $\Delta\eta_{jj}$, p_{T}^{j1}, p_{T}^{j2}, $\eta_{4\ell}^{*}$, $\Delta R_{jZ}^{\mathrm{min}}$, η_{j1}
VH-Lep-enriched	-	-
ttH-enriched	-	-

between the jet and the four-lepton system ($\Delta R(j, 4\ell)$) is introduced to distinguish between ggF and VBF Higgs boson production. In the VBF-enriched-p_{T}^{j}-Low (VH-Had-enriched) category, the separation of the VBF (VH) from ggF (ggF and VBF) production mechanism is achieved by means of the following input variables: m_{jj}, pseudorapidity separation ($\Delta\eta_{jj}$) and transverse momenta of the two leading jets (p_{T}^{j1} and p_{T}^{j2}), the difference between the pseudorapidity of the four-lepton system and the average pseudorapidity of the two leading jets ($\eta^{*}_{4\ell}$), as well as the minimum angular separation between the leading lepton pair and the two leading jets ($\Delta R^{\mathrm{min}}_{jZ}$). In addition, the pseudorapidity of the leading jet (η_{j1}) is used as an input in the VH-Had-enriched category, while the constrained transverse momentum of the Higgs–dijet system, defined as $(p_{\mathrm{T}}^{4\ell jj})_{\mathrm{constrained}} = p_{\mathrm{T}}^{4\ell jj}$ (50 GeV) for $p_{\mathrm{T}}^{4\ell jj} > 50$ GeV ($p_{\mathrm{T}}^{4\ell jj} < 50$ GeV) is employed for the VBF-enriched category. The transverse momentum $p_{\mathrm{T}}^{4\ell jj}$ of the Higgs–dijet system below 50 GeV is replaced by the minimum value of $p_{\mathrm{T}}^{4\ell jj} = 50$ GeV in order to reduce the QCD scale variation uncertainty.

The BDT discriminants improve the expected cross-section measurement statistical uncertainties by 15%, 35% and 25% for the ggF, VBF and VH Stage-0 production bins, respectively.

6 Signal modelling

The observables used for the measurements of the cross sections in the production bins introduced in Section 3 are BDT discriminants for five of the selected reconstructed event categories, described in Section 5.4, together with event yields for the remaining four event categories. For the SM Higgs boson signal, the shapes of the BDT distributions and the fractions of events in each category are predicted using simulation.

No BDT discriminants are used for the measurement of the tensor structure of the Higgs boson couplings. This measurement is based on event yields in the ten event categories introduced in Section 5. A dedicated signal model is introduced to describe the impact of BSM contributions. The model is based on a morphing technique [100] which provides a parameterization to evaluate the signal response as a function of the BSM coupling parameters. The expected number of signal events $n_{\mathrm{S}}(\vec{\kappa}_{\mathrm{target}})$ at a given target point in the BSM parameter space, defined by a set of BSM coupling values $\vec{\kappa}_{\mathrm{target}} \equiv \{\kappa_{\mathrm{SM}}, \kappa_{\mathrm{BSM\_1}}, .., \kappa_{\mathrm{BSM\_}n}\}$, is obtained by

$$n_{\mathrm{S}}(\vec{\kappa}_{\mathrm{target}}) = \sum_{i} w_i(\vec{\kappa}_{\mathrm{target}}, \vec{\kappa}_i) \cdot n_{\mathrm{S}}(\vec{\kappa}_i).$$

This corresponds to a linear weighted ($w_i(\vec{\kappa}_{\mathrm{target}}, \vec{\kappa}_i)$) combination of a minimal set of base inputs $n_{\mathrm{S}}(\vec{\kappa}_i)$, with coupling values $\vec{\kappa}_i = \{\kappa^i_{\mathrm{SM}}, \kappa^i_{\mathrm{BSM\_1}}, .., \kappa^i_{\mathrm{BSM\_}n}\}$ for each input i selected in such a way as to span the full coupling parameter space. The functional form of the weight w_i and the value assigned to each input is defined by the coupling structure of the BSM signal matrix element as described in Ref. [100]. The inputs for the ggF, VBF and VH production processes are obtained from the simulation samples described in Section 4. The values κ_i for each input sample are chosen to cover most parts of the interesting BSM parameter space and to therefore ensure a reasonably small statistical uncertainty for any target point in the BSM parameter space within the range of coupling values under study. These samples are then used to predict the expected variations of event yields in each reconstructed event category relative to the SM prediction. The limited number of events in the simulated BSM samples is estimated to impact the measurement results by less than 5%. In combination with all other systematic uncertainties, the impact on the final result is negligible in the couplings range under study. Therefore, this uncertainty is not taken into account in the results presented in Section 9. Since the BSM input samples were generated with the

SM value Γ_{SM} for the total decay width of the Higgs boson, an additional correction corresponding to ratio of the total width with BSM to the SM width is applied to the $\sigma \cdot \mathcal{B}(H \to ZZ)$ value for the samples with non-vanishing BSM coupling parameters. The correction is of the order of -11% for $\kappa_{Agg} = \pm 0.8$, -2% for $\kappa_{AVV} = \pm 8$ and about $+14\%$ (-17%) for $\kappa_{HVV} = -8$ (+8).

The *ttH* and *bbH* BSM processes are not simulated. Since the Higgs boson coupling to top or bottom quarks in the effective coupling to gluons is included in κ_{Hgg} and κ_{Agg}, and there is little sensitivity to *ttH* production in the $H \to ZZ^* \to 4\ell$ channel, it is assumed that the production vertex of the *ttH* and *bbH* processes is not affected by the BSM parameters. The impact of the BSM parameters on the Higgs boson decay is accounted for by scaling the corresponding decay branching ratio. The BSM parameters also affect $\mathcal{B}(H \to Z\gamma)$ and $\mathcal{B}(H \to \gamma\gamma)$ but the impact on the signal model predictions is found to be negligible and is not considered in the analyses.

7 Background contributions

The main source of background in the $H \to ZZ^* \to 4\ell$ decay channel is non-resonant ZZ^* production with the same final state as the signal. This process, as well as a minor contribution from $t\bar{t}V$ and triboson production, is modelled using simulation normalized to the highest-order SM prediction available. Additional reducible background sources are the Z+jets, $t\bar{t}$ and WZ processes whose contributions in the signal region (SR) are estimated using dedicated signal-depleted control regions (CRs) in data, separately for events with different flavours of the subleading lepton pair (i.e. $\ell\ell + \mu\mu$ or $\ell\ell + ee$, where $\ell\ell$ denotes the leading and $\mu\mu$ or ee the subleading lepton pair). No requirement is imposed on the four-lepton invariant mass in the control data. The backgrounds are first estimated for the inclusive event selection, i.e. prior to event categorization, and then divided into separate contributions in each reconstructed event category.

7.1 Background estimation for the inclusive selection

The reducible $\ell\ell + \mu\mu$ background with at least one jet containing a muon from secondary decays of pions/kaons or heavy-flavour hadrons originates from Z+jets, $t\bar{t}$ and WZ production. The Z+jets background comprises a heavy-flavour (Z+HF) component containing jets with b- or c-quark content and a light-flavour (Z+LF) component from pion or kaon decays. These components of the Z+jets background and the $t\bar{t}$ contribution are extracted using orthogonal CRs formed by relaxing the χ^2 requirement on the vertex fit, and by inverting or relaxing isolation and/or impact parameter requirements on the subleading muon pair. In these regions an unbinned maximum-likelihood fit to m_{12} is performed. The numbers of $t\bar{t}$, Z+HF and Z+LF events estimated in these CRs are each extrapolated to the SR using a simulation-based transfer factor which depends on the efficiency of the isolation and impact parameter selection criteria. The contribution from WZ production is estimated using simulation.

The reducible $\ell\ell + ee$ background originating mainly from the Z+jets, $t\bar{t}$ and WZ production is classified into processes with misidentified jets faking an electron (f), electrons from photon conversions (γ) and electrons from semileptonic decays of heavy quarks (q). The contribution of the q component is obtained from simulation, while the f and the γ components are obtained from the $3\ell + X$ CR containing $2\mu 2e$ and $4e$ final states. In this CR, three leptons pass the full analysis selection, while the most probable candidate for a fake electron, the lowest-E_{T} electron (denoted by X) in the subleading electron pair, has only the track hit requirement of the electron identification applied. In order to suppress the ZZ^*

contribution, only electrons with same-sign charge are considered for the subleading electron pair in this CR. A template fit to the number of track hits (n_{InnerPix}) in the innermost or next-to-innermost[2] pixel layer for the associated track is used to separate the γ and f background components. The templates for the γ and f background contributions are obtained from simulated $Z + X$ events with an on-shell Z boson decay candidate accompanied by an electron X selected using the same criteria as in the $3\ell + X$ CR. The simulated $Z + X$ events are also used to obtain the efficiencies needed to extrapolate the f and γ background contributions from the CR to the SR, after correcting the simulation to match the data in dedicated control samples of $Z + X$ events.

7.2 Background estimation per reconstructed event category

The background event yields and BDT output distributions are determined separately for each event category. The reducible $\ell\ell + ee$ background normalization is obtained by applying the data-driven approach described above for the inclusive sample in each separate category. The fraction of the reducible $\ell\ell + \mu\mu$ background per category with respect to the inclusive yield is obtained from simulation, separately for the Z+jets and $t\bar{t}$ background. The $\ell\ell + \mu\mu$ simulation was checked against data in CRs with relaxed selection criteria and is found to predict the fraction of reducible background events in each category well within the statistical uncertainty.

Since the data-driven background estimates provide the event yields for the full $m_{4\ell}$ range, the effect of the $m_{4\ell}$ mass window requirement has to be taken into account. For this purpose, the $m_{4\ell}$ distributions of reducible backgrounds in each category are smoothed with the kernel density estimation method [101] and then integrated to obtain the fraction of events within the mass window. The yields of the backgrounds in each category are shown in Table 4, together with the associated systematic uncertainties. Three sources of uncertainty are considered. First, the systematic uncertainty of the inclusive background estimate from the determination of the selection efficiencies related to the lepton identification, isolation and impact parameter significance. This uncertainty is evaluated by comparing data with an on-shell Z boson decay candidate accompanied by an electron or a muon to the simulation. Second, the inclusive background estimate has also a relatively small (4%) statistical uncertainty from the control data. The total uncertainty of the inclusive reducible background estimate from both of these sources is considered as correlated across the experimental categories. Third, there is an additional uncorrelated uncertainty in the fraction of the reducible background in each experimental category due to the statistical precision of the simulated samples.

The shapes of the BDT discriminant distributions for the reducible background are determined from simulation by combining the simulated $t\bar{t}$ and Z+jets distributions according to the relative fractions measured in data. To increase the statistical precision of the simulated samples, the isolation requirements and $m_{4\ell}$ range are relaxed. The mass window requirement is relaxed in the $0j$ category to $115 < m_{4\ell} < 130$ GeV and to $110 < m_{4\ell} < 200$ GeV for all other categories. Instead of both leptons, at least one lepton in the subleading pair is required to meet the isolation criteria. These looser selection criteria have no impact on the shape of the BDT distributions. The statistical precision of the simulated samples and the uncertainty in the relative fractions of Z+jets and $t\bar{t}$ contributions are taken into account as systematic shape variations.

[2] A hit in the next-to-innermost pixel layer is used when the electron falls in a region that is either not instrumented with an IBL module or the IBL module is not operating.

Table 4: Estimates of reducible background yields in each reconstructed event category in the signal region for 36.1 fb^{-1} at $\sqrt{s}$ = 13 TeV, together with the associated correlated and uncorrelated systematic uncertainties. The total error in each category is composed of the combined statistical and systematic uncertainty of the inclusive background estimate, as well as an additional statistical uncertainty in the fraction of the reducible background in each category. The uncertainty due to the inclusive background estimate is considered as correlated (penultimate column), while the statistical uncertainty due to the event categorization (last column) is uncorrelated across the reconstructed event categories.

Reconstructed	Reducible background			Uncertainty	
event category	$\ell\ell$+$\mu\mu$	$\ell\ell$+ee	Total	Corr.	Uncorr.
$0j$	0.96 ± 0.21	1.25 ± 0.23	2.21 ± 0.33	±13%	±7%
$1j$-$p_{\mathrm{T}}^{4\ell}$-Low	0.21 ± 0.05	0.30 ± 0.06	0.52 ± 0.08	±13%	±10%
$1j$-$p_{\mathrm{T}}^{4\ell}$-Med	0.19 ± 0.12	0.16 ± 0.04	0.35 ± 0.13	±13%	±40%
$1j$-$p_{\mathrm{T}}^{4\ell}$-High	0.0049 ± 0.0025	0.036 ± 0.008	0.041 ± 0.009	±13%	±18%
VBF-enriched-p_{T}^{j}-Low	0.14 ± 0.04	0.128 ± 0.025	0.27 ± 0.05	±13%	±15%
VBF-enriched-p_{T}^{j}-High	0.019 ± 0.010	0.018 ± 0.004	0.037 ± 0.009	±13%	±28%
VH-Had-enriched-$p_{\mathrm{T}}^{4\ell}$-Low	0.057 ± 0.015	0.067 ± 0.015	0.124 ± 0.021	±13%	±14%
VH-Had-enriched-$p_{\mathrm{T}}^{4\ell}$-High	0.0035 ± 0.0023	0.011 ± 0.004	0.015 ± 0.004	±13%	±34%
VH-Lep-enriched	0.003 ± 0.004	0.0005 ± 0.0008	0.0031 ± 0.0031	±13%	±100%
ttH-enriched	0.009 ± 0.004	0.022 ± 0.005	0.031 ± 0.007	±13%	±22%

8 Systematic uncertainties

The systematic uncertainties in this analysis are grouped into experimental and theoretical uncertainties. The first category includes uncertainties in the modelling of lepton and jet reconstruction, identification efficiencies, energy resolution and scale, and in the total integrated luminosity. Uncertainties from the procedure used to derive the data-driven background estimates are also included in this category. The second category includes uncertainties in the theoretical modelling of the signal and the background processes.

The uncertainties can affect the signal acceptance, efficiency and discriminant distributions as well as the background estimates. The dominant sources of uncertainty and their effect are described in the following subsections. The impact of these uncertainties on the cross-section measurements in different production bins is summarized in Table 5.

8.1 Experimental uncertainties

The uncertainty in the combined 2015+2016 integrated luminosity is 3.2%. It is derived, following a methodology similar to the one described in Ref. [102], from a preliminary calibration of the luminosity scale using x–y beam-separation scans performed in August 2015 and May 2016.

The uncertainty in the predicted yields due to pile-up modelling is about 2% and is derived by varying the average number of pile-up events in the simulation to cover the uncertainty in the ratio of the predicted to measured inelastic cross sections [103].

Table 5: Impact of the dominant systematic uncertainties (in percent) on the measured inclusive and the Stage-0 production mode cross sections $\sigma \cdot B(H \to ZZ^*)$. Signal theory uncertainties include only acceptance effects and no uncertainty in predicted cross sections.

Production bin	Experimental uncertainties [%]					Theory uncertainties [%]			
	Lumi	e, μ, pile-up	Jets, flavour tagging	Higgs mass	Reducible backgr.	ZZ^* backgr.	PDF	Signal theory QCD scale	Shower
Inclusive cross section									
	4.1	3.1	0.7	0.8	0.9	1.9	0.3	0.8	1.2
Stage-0 production bin cross sections									
ggF	4.3	3.4	1.1	1.2	1.1	1.8	0.5	1.8	1.4
VBF	2.6	2.7	10	1.3	0.9	2.2	1.6	11	5.3
VH	3.0	2.7	11	1.6	1.7	5.9	2.1	12	3.7
ttH	3.6	2.9	19	< 0.1	2.4	1.9	3.3	7.9	2.1

The electron (muon) reconstruction and identification efficiencies, and the energy (momentum) scale and resolution are derived from data using large samples of $J/\psi \to \ell\ell$ and $Z \to \ell\ell$ decays [91–93]. Typical uncertainties in the predicted yield due to the identification efficiencies are in the range 0.5–1.0% for muons and 1.0–1.3% for electrons. The uncertainty in the expected yields coming from the muon and electron isolation efficiencies are also taken into account, with the typical size being 2%. The uncertainties in the electron and muon energy scale and resolution are small and have a negligible impact on the measurements presented in Section 9.

The uncertainties in the jet energy scale and resolution are in the range of 3–7% and 2–4%, respectively [104, 105]. Given the analysis categories, the impact of these uncertainties are more relevant for the *VH*, VBF and *ttH* production modes cross-section measurements (10–20%) and for all the reduced Stage-1 cross-section measurements, including the ggF process split into the different *n-jet* exclusive production bins (5–20%), while they are negligible for the inclusive and the ggF (Stage-0) cross-section measurements.

The uncertainties associated with the efficiency of the b-tagging algorithm, which are derived from $t\bar{t}$ events, are at the level of a few percent over most of the jet p_{T} range [97]. This uncertainty is only relevant in the *ttH*-enriched category, with its expected impact being approximately 5% in the *ttH* cross-section measurement.

The impact of the precision of the Higgs boson mass measurement, $m_H = 125.09 \pm 0.24$ GeV [16], on the signal acceptance due to the mass window requirement defining the signal region is negligible. A small dependency of the $\mathrm{BDT}_{\mathrm{ggF}}$ shape on m_H is observed for the signal (below 2% in the highest BDT bins) and is included in the signal model. This uncertainty affects the measurement of ggF production, as well as the measurements in other production bins with large ggF contamination.

The uncertainties from the data-driven measurement of reducible background contributions are detailed in Section 7. Their impact on the cross-section measurements is also summarized in Table 5.

8.2 Theoretical uncertainties

The theoretical modelling of the signal and background processes is affected by uncertainties from QCD scale variations, modelling of parton showers and multiple-particle interactions, and PDF uncertainties.

The impact of the theory systematic uncertainties on the signal depends on the kind of measurement that is performed. For the signal strength measurements and the tensor structure analysis, each source of theory uncertainty affects both the fiducial acceptance and the predicted SM cross section. For the cross-section measurements, only effects on the acceptance need to be considered.

One of the dominant sources of theoretical uncertainty is the prediction of the ggF process in the different n-jet categories. The ggF process is the major background in the 2-jet categories that are used to measure the cross section of the VBF and VH production modes. To estimate the QCD scale variation and migration effects on the n-jet ggF cross sections, the approach described in Ref. [15] is used, which exploits the latest predictions for the inclusive jet cross sections and the exclusive jet bin fractions. In particular, the uncertainty from the choice of the factorization and renormalization scales, the choice of resummation scales, and the migrations between the 0-jet and 1-jet phase-space bins or between the 1-jet and $\geq$ 2-jet bins are considered. The impact of QCD scale variations on the Higgs boson p_{T} distribution is taken into account as an additional uncertainty. The uncertainty in the Higgs boson p_{T} at higher order originating from the assumption of infinite top and bottom quark masses in the heavy-quark loop is also taken into account by comparing the p_{T} distribution predictions to finite-mass calculations. An additional uncertainty in the acceptance of the ggF process in VBF topologies due to missing higher orders in QCD in the calculation is estimated by variations of the resummation and factorization scales using fixed-order calculations with MCFM [106]. For the other production modes, the QCD scale uncertainties are obtained by varying the scale by factors of two. The configuration with the largest impact is chosen to define the uncertainty in each experimental category as the relative difference between the prediction in this and the nominal configuration. QCD scale uncertainties are treated as uncorrelated among the different production modes.

The uncertainties in the acceptances due to the modelling of parton showers and multiple-parton interactions are estimated with AZNLO tune eigenvector variations and by comparing the acceptance using the parton showering algorithm from PYTHIA 8 with HERWIG7 for the ggF, VBF and VH processes, while HERWIG++ is compared with PYTHIA 8 for the ttH process. The uncertainty due to each AZNLO tune variation is taken as correlated among the different production modes while the difference between the parton showering algorithms is treated as an uncorrelated uncertainty. Uncertainties due to the modelling of the ggF production in association with b-quarks affect the measurement in the ttH production bin only negligibly compared to the statistical precision. They are therefore not taken into account for the final result.

The impact of the PDF uncertainties is estimated with the eigenvector variations of the PDF4LHC_NLO_30 Hessian PDF set. The modification of the predictions for each eigenvector variation is added as a separate source of uncertainty in the model. The same procedure is applied for the ggF, VBF and VH processes, enabling correlations to be taken into account in the fit model.

The same procedure is used to estimate the impact of the sources of theoretical uncertainty described above on the shape of BDT discriminants. In addition, for VBF Higgs production, the changes in the $\Delta\eta_{jj}$ distribution as predicted at NNLO compared to NLO in QCD [107] are considered and shown to have a negligible impact on the BDT distributions. For ggF production, a further cross-check is performed by comparing the $\mathrm{BDT}_{\mathrm{VBF}}^{1j\text{-}p_{\mathrm{T}}^{4\ell}\text{-Low}}$, $\mathrm{BDT}_{\mathrm{VBF}}^{1j\text{-}p_{\mathrm{T}}^{4\ell}\text{-Med}}$, $\mathrm{BDT}_{\mathrm{VBF}}$ and $\mathrm{BDT}_{VH\text{-Had}}$ shapes in the corresponding

categories as predicted by POWHEG NNLOPS and MADGRAPH5_aMC@NLO (with the FxFx merging scheme). The BDT shapes from the two generators agree within the statistical uncertainties and, therefore, no additional shape uncertainty is included.

For BSM interactions parameterized via the effective Lagrangian terms, the theoretical uncertainties in the PDF set and the missing higher-order QCD and EW corrections are generally assumed to factorize with respect to the new physics. However, it has been shown [108] that the K-factors corresponding to the NLO to LO cross-section ratio, as well as several kinematic quantities that affect the categorization of reconstructed events, such as the jet transverse momenta, receive higher-order corrections that can differ from those computed for the SM process and depend on the value of the BSM couplings. Therefore, an uncertainty is assigned to the K-factor obtained from the SM samples. For this purpose, the K-factor for a given VBF and VH BSM process is evaluated as the ratio of NLO to LO event yields in simulated BSM samples, separately for each reconstructed event category. The uncertainty in the SM K-factor is then defined as the relative difference of the K-factors computed for the BSM and SM processes. The obtained uncertainties range from 10% to 40% depending on the category and are considered as being correlated across all categories. This is one of the dominant sources of uncertainty for the tensor structure measurements. No such uncertainty is considered for the ggF BSM samples as these are simulated at NLO.

The dominant theoretical uncertainty in the expected ZZ^* background yield in the signal mass window is obtained by varying the factorization and renormalization QCD scales by factors of two. The configuration with the largest impact is chosen to define the uncertainty in each experimental category as the relative difference between the prediction in this and the nominal configuration. This uncertainty is about 4% for the inclusive event yield and is as large as 30% for the categories where additional jets are required. The impact of the QCD scale uncertainty on the BDT discriminant shapes is approximately 1–2%. The PDF uncertainty on the ZZ^* event yield in each category and on the BDT distributions, obtained using the MC replicas of the NNPDF3.0 PDF set, was found to be approximately 1–2%. The impact of the parton shower modelling uncertainty on the ZZ^* event yield is estimated to be approximately 1–5%, with the largest value reached in the categories where the presence of one or more jets is required. In addition, the event yield and BDT discriminant shapes in each event category are compared to the data in a sideband around the signal region ($m_{4l} < 115$ GeV or 130 GeV$< m_{4l} <$ 170 GeV). Good agreement between the SHERPA predictions and the data is found.

9 Results

The expected and observed four-lepton invariant mass distribution of the selected Higgs boson candidates after the event selection with a constrained Z boson mass is shown in Figure 3. The corresponding expected and observed numbers of events are shown in Table 6 separately for each of the four decay channels. The predicted event yields are in reasonable agreement with the data. The observed and expected distributions of the jet multiplicity, the dijet invariant mass, as well as the leading jet and the four-lepton transverse momenta, which are used for the categorization of reconstructed events, are shown in Figure 4 for different stages of the event categorization. As shown in figures 4(c) and 4(d) there is an excess of events observed in the sample with ≥ 2 jets (shown as a dijet invariant mass distribution) and also in the subset with $m_{jj} > 120$ GeV (shown as the jet p_{T} distribution) in comparison with the expectations. All other distributions are in good agreement with the data. The expected numbers of signal and background events in each reconstructed event category (including the splitting of the VH-enriched category for the tensor

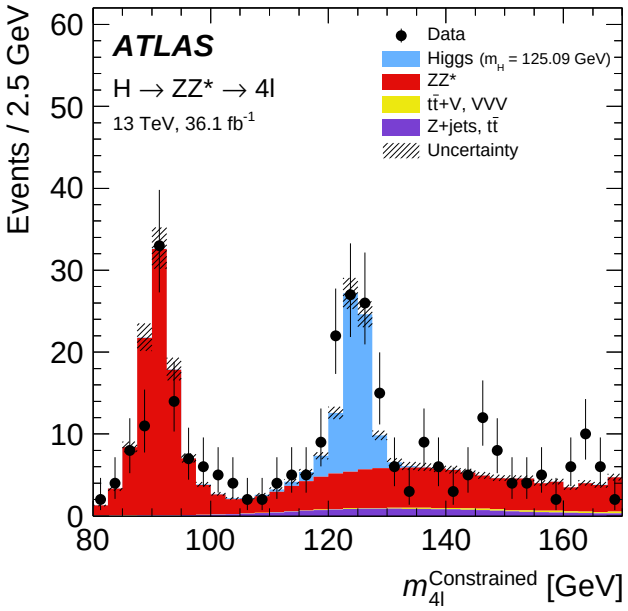

Figure 3: The expected and observed four-lepton invariant mass distribution for the selected Higgs boson candidates with a constrained Z boson mass, shown for an integrated luminosity of 36.1 fb^{-1} and at $\sqrt{s}$ = 13 TeV assuming the SM Higgs boson signal with a mass m_H = 125.09 GeV.

Table 6: The expected and observed numbers of signal and background events in the four-lepton decay channels for an integrated luminosity of 36.1 fb^{-1} and at $\sqrt{s}$ = 13 TeV, assuming the SM Higgs boson signal with a mass m_H = 125.09 GeV. The second column shows the expected number of signal events for the full mass range while the subsequent columns correspond to the mass range of $118 < m_{4\ell} < 129$ GeV. In addition to the ZZ^* background, the contribution of other backgrounds is shown, comprising the data-driven estimate from Table 4 and the simulation-based estimate of contributions from rare triboson and $t\bar{t}V$ processes. Statistical and systematic uncertainties are added in quadrature.

Decay channel	Signal (full mass range)	Signal	ZZ^* background	Other backgrounds	Total expected	Observed
4μ	21.0 ± 1.7	19.7 ± 1.6	7.5 ± 0.6	1.00 ± 0.21	28.1 ± 1.7	32
$2e2\mu$	15.0 ± 1.2	13.5 ± 1.0	5.4 ± 0.4	0.78 ± 0.17	19.7 ± 1.1	30
$2\mu2e$	11.4 ± 1.1	10.4 ± 1.0	3.57 ± 0.35	1.09 ± 0.19	15.1 ± 1.0	18
$4e$	11.3 ± 1.1	9.9 ± 1.0	3.35 ± 0.32	1.01 ± 0.17	14.3 ± 1.0	15
Total	59 ± 5	54 ± 4	19.7 ± 1.5	3.9 ± 0.5	77 ± 4	95

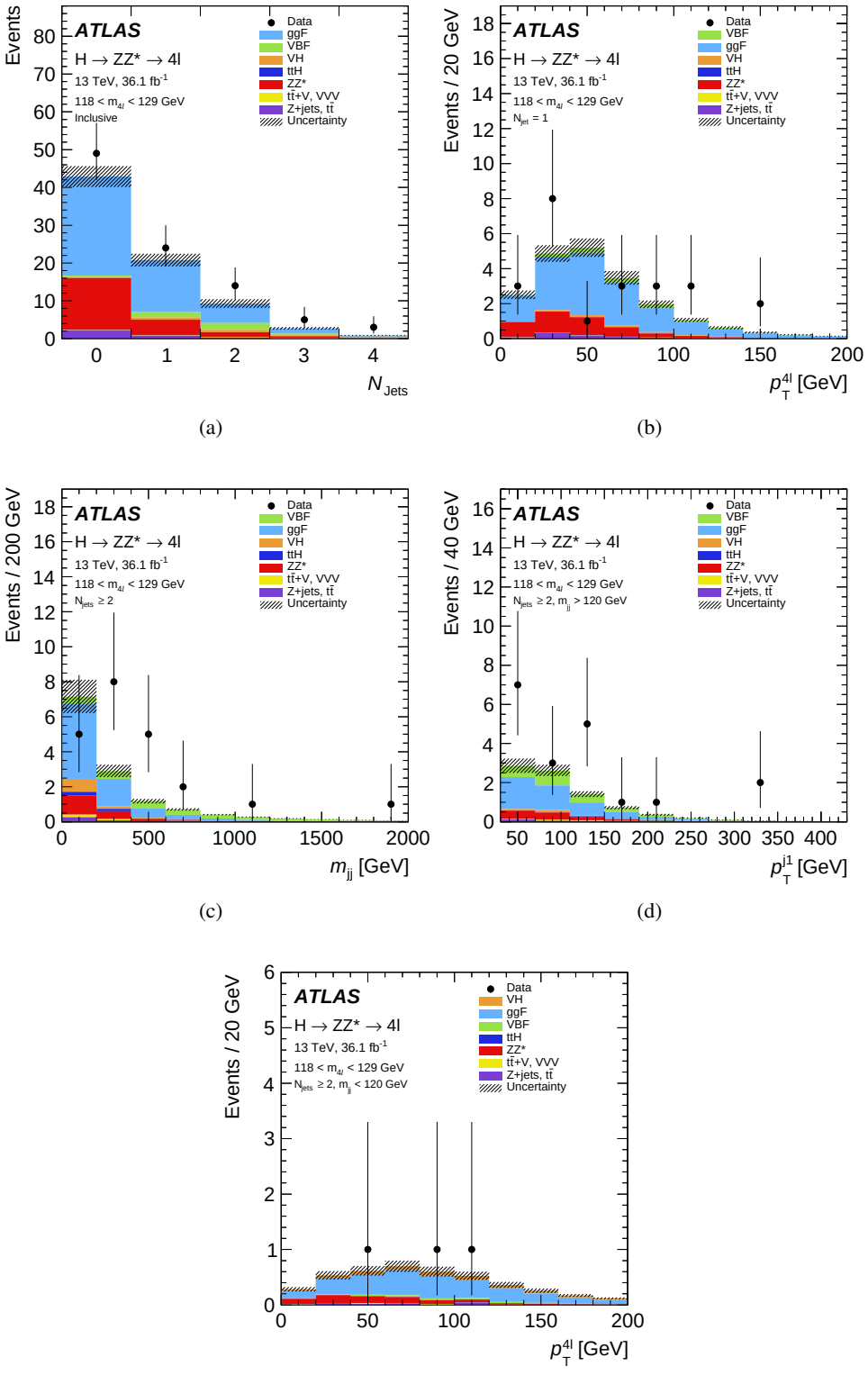

Figure 4: The observed and expected distributions of (a) N_{jet} after the inclusive selection, (b) p_{T}^{4l} in the 1-jet categories, (c) m_{jj} in the 2-jet categories, (d) p_{T}^{j1} in the VBF-enriched categories and (e) p_{T}^{4l} in the VH-Had-enriched categories for an integrated luminosity of 36.1 fb^{-1} collected at $\sqrt{s}$ = 13 TeV assuming the SM Higgs boson signal with a mass m_H = 125.09 GeV.

structure measurement) are shown in Table 7 together with the corresponding observed number of events. The expected event yields are in reasonable agreement with the observed ones. The largest differences

Table 7: The expected and observed numbers of signal and background events in the mass range $118 < m_{4\ell} < 129$ GeV for an integrated luminosity of 36.1 fb^{-1} and at $\sqrt{s} = 13$ TeV in each reconstructed event category (including the splitting of the VH-enriched category for the tensor structure measurement), assuming the SM Higgs boson signal with a mass $m_H = 125.09$ GeV. In addition to the ZZ^* background, the contribution of other backgrounds is shown, comprising the data-driven estimate from Table 4 and the simulation-based estimate of contributions from rare triboson and $t\bar{t}V$ processes. Statistical and systematic uncertainties are added in quadrature.

Reconstructed event category	Signal	ZZ^* background	Other backgrounds	Total expected	Observed
$0j$	26.8 ± 2.5	13.7 ± 1.0	2.23 ± 0.31	42.7 ± 2.7	49
$1j$-$p_{\mathrm{T}}^{4\ell}$-Low	8.8 ± 1.1	3.1 ± 0.4	0.53 ± 0.07	12.5 ± 1.2	12
$1j$-$p_{\mathrm{T}}^{4\ell}$-Med	5.4 ± 0.7	0.88 ± 0.12	0.38 ± 0.05	6.7 ± 0.7	9
$1j$-$p_{\mathrm{T}}^{4\ell}$-High	1.47 ± 0.24	0.139 ± 0.022	0.045 ± 0.007	1.65 ± 0.24	3
VBF-enriched-p_{T}^{j}-Low	6.3 ± 0.8	1.08 ± 0.32	0.40 ± 0.04	7.7 ± 0.9	16
VBF-enriched-p_{T}^{j}-High	0.58 ± 0.10	0.093 ± 0.032	0.054 ± 0.006	0.72 ± 0.10	3
VH-Had-enriched-$p_{\mathrm{T}}^{4\ell}$-Low	2.9 ± 0.5	0.63 ± 0.16	0.169 ± 0.021	3.7 ± 0.5	3
VH-Had-enriched-$p_{\mathrm{T}}^{4\ell}$-High	0.64 ± 0.09	0.029 ± 0.008	0.0182 ± 0.0022	0.69 ± 0.09	0
VH-Lep-enriched	0.318 ± 0.019	0.049 ± 0.008	0.0137 ± 0.0019	0.380 ± 0.020	0
ttH-enriched	0.39 ± 0.04	0.014 ± 0.006	0.07 ± 0.04	0.47 ± 0.05	0
Total	54 ± 4	19.7 ± 1.5	3.9 ± 0.5	77 ± 4	95

are again observed in the two VBF-enriched categories. The expected and observed distributions of the BDT discriminants introduced in Section 5.4 are shown in Figure 5, where a small excess is observed at larger values of the VBF BDT. All other distributions are in good agreement with the data. Based on these results, the measurements of the Higgs boson production cross sections and of its tensor coupling structure are performed. The profile likelihood ratio [109] is used for the interpretation of data with the effects of systematic uncertainties included as constrained nuisance parameters. If the same source of uncertainty affects two or more processes (e.g. the error in the integrated luminosity can affect the signal yield and the MC-based background estimates), the same nuisance parameter is assigned to each of these processes.

9.1 Cross-section measurement by production modes

In order to measure the Higgs boson production cross section times branching ratio for $H \to ZZ^*$ decay for each Stage-0 or reduced Stage-1 production bin, a fit to the data is performed using the likelihood function $\mathcal{L}(\vec{\sigma}, \vec{\theta})$ that depends on the Higgs boson production cross section $\vec{\sigma} = \{\sigma_1, \sigma_2, \ldots, \sigma_N\}$ in each production bin and the nuisance parameters $\vec{\theta}$ accounting for the systematic uncertainties. The likelihood function is defined as a product of conditional probabilities P over binned distributions of the discriminating observables in each reconstructed event category j,

$$\mathcal{L}(\vec{\sigma}, \vec{\theta}) = \prod_{j}^{N_{\text{categories}}} \prod_{i}^{N_{\text{bins}}} P\left(N_{i,j} \mid L \cdot \vec{\sigma} \cdot \vec{A}_{i,j}(\vec{\theta}) + B_{i,j}(\vec{\theta})\right) \times \prod_{m}^{N_{\text{nuisance}}} C_m(\vec{\theta}),$$

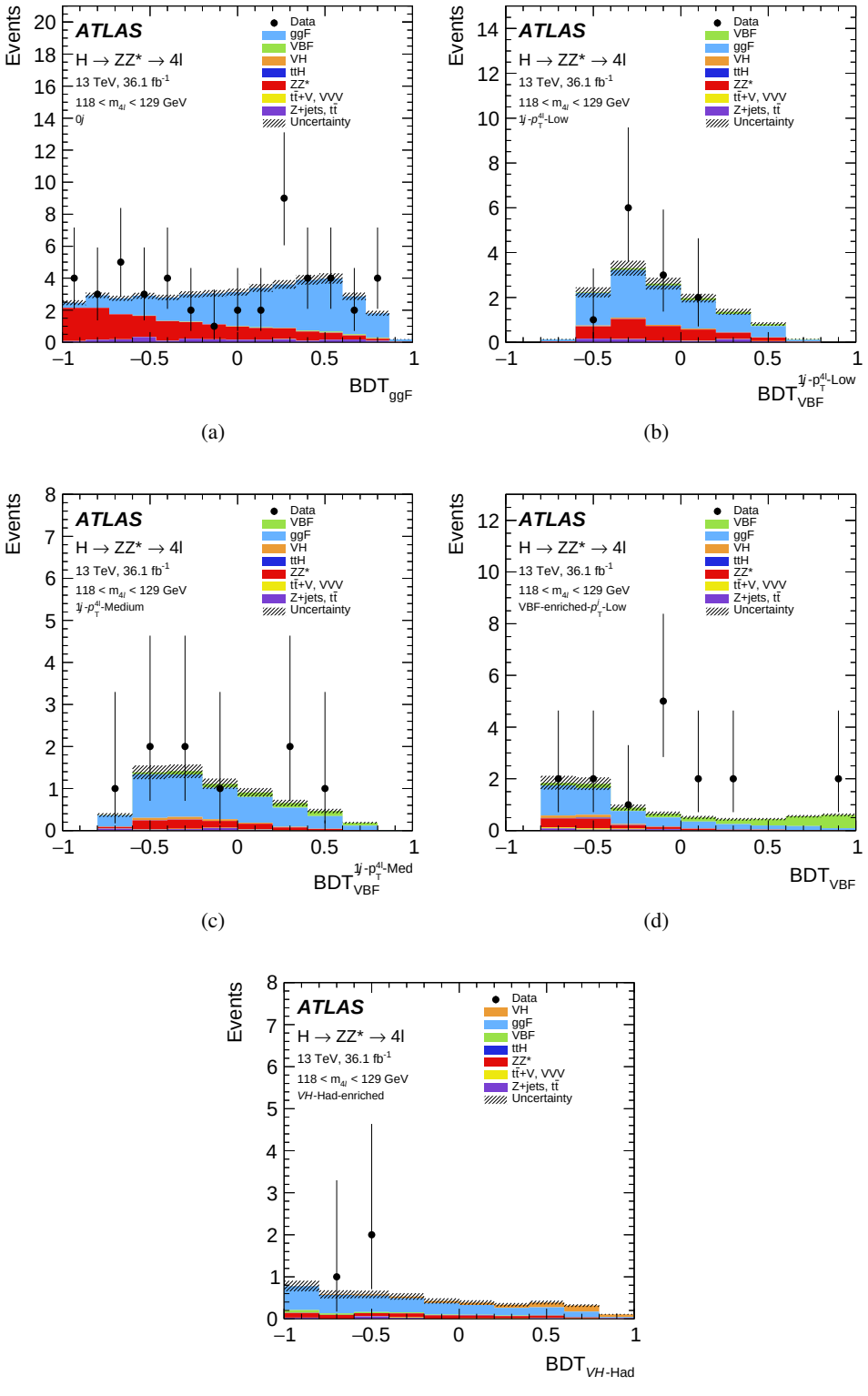

Figure 5: The observed and expected BDT output distributions in the (a) $0j$, (b) $1j$-$p_{\mathrm{T}}^{4\ell}$-Low, (c) $1j$-$p_{\mathrm{T}}^{4\ell}$-Med, (d) VBF-enriched-p_{T}^{j}-Low and (e) VH-Had-enriched categories for an integrated luminosity of 36.1 fb^{-1} and at $\sqrt{s}$ = 13 TeV assuming the SM Higgs boson signal with a mass m_H = 125.09 GeV.

with Poisson distributions P corresponding to the observation of $N_{i,j}$ events in each bin i of the discriminating observable given the expectations for the background, $B_{i,j}(\vec{\theta})$, and for the signal, $S_{i,j}(\vec{\theta}) = L \cdot \vec{\sigma} \cdot \vec{A}_{i,j}(\vec{\theta})$, where L is the integrated luminosity and $\vec{A}_{i,j}(\vec{\theta})$ the signal acceptance in each production bin. The signal acceptance is defined as the number of simulated signal events satisfying the event selection criteria in a given reconstructed event category divided by the total number of events generated in the phase space defined by the production bin. Constraints on the nuisance parameters corresponding to systematic uncertainties described in Section 8 are represented by the functions $C_m(\vec{\theta})$. The cross sections are treated as independent parameters for each production bin and correlated among the different categories. The test statistic used to compare the probabilities of different hypotheses is the ratio of profile likelihoods [109],

$$q = -2 \ln \frac{\mathcal{L}(\vec{\sigma}, \hat{\hat{\vec{\theta}}}(\vec{\sigma}))}{\mathcal{L}(\hat{\vec{\sigma}}, \hat{\hat{\vec{\theta}}})} = -2 \ln \lambda(\vec{\sigma}) \,,$$

where $\vec{\sigma}$ represents only the cross section(s) considered as parameter(s) of interest in the given fit, while the likelihood is maximized with respect to all remaining cross sections and nuisance parameters. In the denominator the likelihood is maximized with respect to all other cross sections and nuisance parameters as well as the parameters of interest, which are fixed to hypothetical values in the numerator. The parameter of interest σ in each production bin is alternatively replaced by $\mu \cdot \sigma_{\mathrm{SM}}(\vec{\theta})$, allowing an interpretation in terms of the signal strength μ relative to the SM prediction $\sigma_{\mathrm{SM}}(\vec{\theta})$. In addition, the number of signal events is extracted from a simultaneous fit of the signal templates in all reconstructed event categories, using a coarser BDT binning with several bins merged into one and considering only the background systematic uncertainties in the fit.

The expected and observed numbers N_{S} of signal events are shown in Table 8 together with the signal acceptances for the Stage-0 production bins.

Assuming that the relative signal fractions in each production bin are given by the predictions for the SM Higgs boson, the inclusive production cross section of

$$\sigma \cdot B \equiv \sigma \cdot B(H \to ZZ^*) = 1.73^{+0.24}_{-0.23}(\mathrm{stat.})^{+0.10}_{-0.08}(\mathrm{exp.}) \pm 0.04(\mathrm{th.})\ \mathrm{pb} = 1.73^{+0.26}_{-0.24}\ \mathrm{pb}$$

is measured in the rapidity range $|y_H| < 2.5$, compared to the SM prediction of $(\sigma \cdot B)_{\mathrm{SM}} \equiv (\sigma \cdot B(H \to ZZ^*))_{\mathrm{SM}} = 1.34 \pm 0.09$ pb. The data are also interpreted in terms of the global signal strength, yielding

$$\mu = 1.28^{+0.18}_{-0.17}(\mathrm{stat.})^{+0.08}_{-0.06}(\mathrm{exp.})^{+0.08}_{-0.06}(\mathrm{th.}) = 1.28^{+0.21}_{-0.19}.$$

The measured cross section and signal strength agree with the SM prediction at the level of 1.7σ and 1.6σ, respectively. The corresponding likelihood scans are shown in Figure 6. The dominant systematic uncertainty of the cross-section measurement is the experimental uncertainty in the integrated luminosity and lepton efficiency measurements. The signal strength measurement is also equally affected by the theoretical uncertainty of the ggF signal yield due to QCD scale variations. This theory uncertainty in the predicted signal yield cancels out when expressing the results in terms of the ratio of the observed to expected cross section times the branching ratio $(\sigma \cdot B)/(\sigma \cdot B)_{\mathrm{SM}} = 1.29^{+0.20}_{-0.18}$, with no uncertainty assigned to the denominator.

Table 8: The expected and observed numbers of signal events in reconstructed event categories for an integrated luminosity of 36.1 fb^{-1} at $\sqrt{s}$ = 13 TeV, together with signal acceptances for each Stage-0 production mode. Results are obtained in bins of BDT discriminants using coarse binning with several bins merged into one. The symbol – represents the cases in which the acceptance is < 0.01%.

Reconstructed	N_S		Acceptance [%]				
event category	Expected	Observed	ggF	VBF	*VH*	*ttH*	*bbH*
$0j$, BDT-Bin 0-4	5^{+4}_{-3}	10^{+5}_{-4}	2.40 ± 0.23	0.178 ± 0.029	0.20 ± 0.05	–	2.0 ± 1.0
$0j$, BDT-Bin 5-9	11 ± 4	11 ± 4	5.4 ± 0.5	0.64 ± 0.12	0.74 ± 0.11	–	6.3 ± 3.2
$0j$, BDT-Bin 10-14	11^{+4}_{-3}	12^{+4}_{-3}	5.2 ± 0.6	1.03 ± 0.28	1.89 ± 0.27	–	5.6 ± 2.8
$1j$-$p_{\mathrm{T}}^{4\ell}$-Low, BDT-Bin 0-4	$5.8^{+3.2}_{-2.6}$	$7.6^{+3.5}_{-2.9}$	2.7 ± 0.4	1.25 ± 0.10	1.72 ± 0.19	–	3.1 ± 1.6
$1j$-$p_{\mathrm{T}}^{4\ell}$-Low, BDT-Bin 5-9	$3.1^{+2.4}_{-1.8}$	$0.8^{+1.8}$	1.33 ± 0.20	2.02 ± 0.12	0.85 ± 0.09	–	1.4 ± 0.7
$1j$-$p_{\mathrm{T}}^{4\ell}$-Med, BDT-Bin 0-4	$3.5^{+2.5}_{-1.8}$	$5.1^{+2.8}_{-2.1}$	1.53 ± 0.25	1.41 ± 0.23	2.09 ± 0.25	–	1.0 ± 0.5
$1j$-$p_{\mathrm{T}}^{4\ell}$-Med, BDT-Bin 5-9	$2.0^{+1.9}_{-1.2}$	$2.6^{+2.1}_{-1.4}$	0.74 ± 0.11	2.68 ± 0.27	0.49 ± 0.05	–	0.27 ± 0.14
$1j$-$p_{\mathrm{T}}^{4\ell}$-High	$1.5^{+1.7}_{-1.0}$	$2.8^{+2.1}_{-1.4}$	0.56 ± 0.12	1.74 ± 0.24	1.06 ± 0.10	–	0.17 ± 0.09
VBF-enriched-p_{T}^{j}-Low, BDT-Bin 0-4	$4.0^{+2.7}_{-2.0}$	$8.7^{+3.5}_{-2.8}$	1.53 ± 0.30	3.33 ± 0.32	2.83 ± 0.32	2.8 ± 0.4	1.9 ± 1.0
VBF-enriched-p_{T}^{j}-Low, BDT-Bin 5-9	$2.4^{+2.0}_{-1.3}$	$5.7^{+2.8}_{-2.1}$	0.43 ± 0.11	9.6 ± 0.9	0.27 ± 0.04	0.153 ± 0.028	0.32 ± 0.17
VBF-enriched-p_{T}^{j}-High	$0.6^{+1.3}_{-0.6}$	$2.8^{+2.1}_{-1.4}$	0.16 ± 0.05	1.18 ± 0.11	0.51 ± 0.06	0.71 ± 0.09	–
VH-Had-enriched, BDT-Bin 0-4	$2.4^{+2.1}_{-1.4}$	$2.4^{+2.1}_{-1.4}$	1.00 ± 0.23	1.08 ± 0.13	1.52 ± 0.17	0.33 ± 0.07	0.9 ± 0.5
VH-Had-enriched, BDT-Bin 5-9	$1.3^{+1.6}_{-0.9}$	0	0.37 ± 0.07	0.29 ± 0.06	5.0 ± 0.5	1.06 ± 0.19	0.29 ± 0.15
VH-Lep-enriched	$0.3^{+1.0}$	0	–	–	2.94 ± 0.24	1.70 ± 0.19	–
ttH-enriched	$0.4^{+1.1}$	0	–	–	0.19 ± 0.04	13.5 ± 2.9	0.31 ± 0.17
Combined acceptance			23.5 ± 1.9	26.4 ± 1.4	22.3 ± 1.9	20.3 ± 2.0	24 ± 12

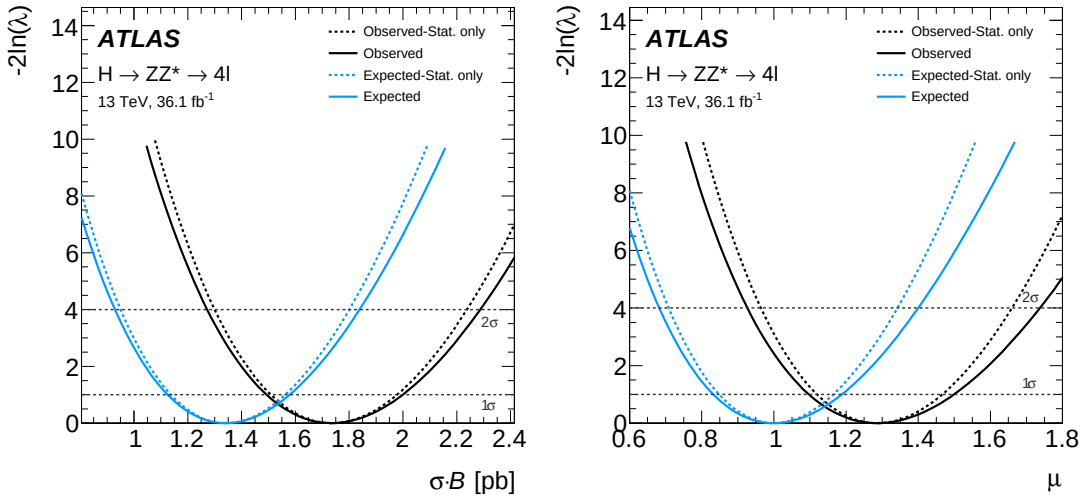

(a) (b)

Figure 6: The profile likelihood as a function of (a) $\sigma \cdot B(H \rightarrow ZZ^*)$ and (b) the inclusive signal strength μ; the scans are shown both with (solid line) and without (dashed line) systematic uncertainties.

The SM expected cross section, the observed values of $\sigma \cdot B(H \rightarrow ZZ^*)$ and their ratio for the inclusive production and in each Stage-0 and reduced Stage-1 production bin are shown in Table 9. The corresponding values are summarized in Figure 7. The *bbH* production process is treated as a part of the ggF production bins. In the ratio calculation uncertainties on the SM expectation are not taken into account.

All measured Stage-0 and reduced Stage-1 ggF measurements agree with the predictions for the SM Higgs boson within 1σ. Somewhat worse agreement is obtained for the VBF bins due to the observed excess of events in the two VBF-enriched reconstructed event categories. The largest deviation of 2.2σ is observed for the Stage-0 VBF production bin due to an observed excess of events characterized by the presence of at least two jets and a dijet invariant mass above 120 GeV. Due to the limited number of events in the *VH*- and *ttH*-enriched categories, only upper limits are set on the cross sections and signal strengths for these production modes. The limits are based on the CL_s prescription [110] and derived using pseudo-experiments. The *VH* and *ttH* parameters of interest are constrained to positive values to avoid the fit's prediction of negative total event yields in the *VH*-Lep-enriched and *ttH*-enriched categories and provide a stable fit configuration. It was found that the impact of this constraint on the final fit results is negligible.

The dominant contribution to the measurement uncertainty in the Stage-0 ggF production bin originates from the same sources as in the inclusive measurement. In the remaining three Stage-0 production bins, similar sources of uncertainty are relevant for both the cross section and the signal strength measurements: the jet energy scale or resolution uncertainties in all production bins and, additionally, jet bin migrations for the VBF and *VH* processes. For the reduced Stage-1 categories the dominant cross-section uncertainties are the integrated luminosity and lepton efficiency measurements for the ggF-0j and *VH*-Lep bins and the jet energy scale or resolution for all other categories. The VBF-p_{T}^{j}-Low bin is additionally affected by parton shower uncertainties, while the effects of the finite top quark mass have a dominant impact on the VBF-p_{T}^{j}-High bin, together with migrations between transverse momentum bins. The signal strength

Table 9: The SM expected cross section $(\sigma \cdot B)_{\mathrm{SM}}$, the observed values of $\sigma \cdot B(H \to ZZ^*)$, and their ratio $(\sigma \cdot B)/(\sigma \cdot B)_{\mathrm{SM}}$ for the inclusive production and in each Stage-0 and reduced Stage-1 production bin for an integrated luminosity of 36.1 fb^{-1} and at $\sqrt{s}$ = 13 TeV. The *bbH* contribution is considered as a part of the ggF production bins. The upper limits correspond to the 95% CL obtained with pseudo-experiments using the $\mathrm{CL_s}$ method. The uncertainties are given as (stat.)+(exp.)+(th.) for Stage 0 and as (stat.)+(syst.) for reduced Stage 1.

Production bin	Cross section $(\sigma \cdot B)$ [pb]		$(\sigma \cdot B)/(\sigma \cdot B)_{\mathrm{SM}}$
	SM expected	Observed	Observed
Inclusive production, $\lvert y_H \rvert < 2.5$			
	1.34 ± 0.09	$1.73^{+0.24+0.10}_{-0.23-0.08} \pm 0.04$	$1.29^{+0.18+0.07}_{-0.17-0.06} \pm 0.03$
Stage-0 production bins, $\lvert y_H \rvert < 2.5$			
ggF	1.18 ± 0.08	$1.31^{+0.26+0.09}_{-0.24-0.07} \pm 0.05$	$1.11^{+0.22+0.07}_{-0.20-0.06} \pm 0.04$
VBF	0.0928 ± 0.0028	$0.37^{+0.15}_{-0.13} \pm 0.03 \pm 0.03$	$4.0^{+1.7}_{-1.4} \pm 0.3 \pm 0.3$
VH	$0.053^{+0.003}_{-0.005}$	< 0.20	< 3.7
ttH	$0.0154^{+0.0011}_{-0.0016}$	< 0.12	< 7.5
Reduced Stage-1 production bins, $\lvert y_H \rvert < 2.5$			
ggF-0j	0.73 ± 0.05	$0.88^{+0.22+0.09}_{-0.20-0.07}$	$1.22^{+0.30+0.13}_{-0.27-0.09}$
ggF-1j-p_{T}^{H}-Low	0.174 ± 0.025	$0.08^{+0.15+0.04}_{-0.12-0.06}$	$0.5^{+0.8+0.3}_{-0.7-0.4}$
ggF-1j-p_{T}^{H}-Med	0.120 ± 0.018	$0.16^{+0.11+0.03}_{-0.09-0.01}$	$1.3^{+0.9}_{-0.7} \pm 0.2$
ggF-1j-p_{T}^{H}-High	0.024 ± 0.005	$0.03^{+0.05}_{-0.04} \pm 0.01$	$1.2^{+2.3}_{-1.7} \pm 0.3$
ggF-2j	0.137 ± 0.029	$0.20^{+0.16}_{-0.14} \pm 0.03$	$1.4^{+1.2}_{-1.0} \pm 0.2$
VBF-p_{T}^{j}-Low	0.0886 ± 0.0027	$0.26^{+0.18+0.03}_{-0.14-0.02}$	$3.0^{+2.0+0.4}_{-1.6-0.2}$
VBF-p_{T}^{j}-High	$0.0042^{+0.0004}_{-0.0002}$	$0.06^{+0.05}_{-0.04} \pm 0.01$	$13^{+12}_{-8} \pm 1$
VH-Had	$0.0362^{+0.0019}_{-0.0033}$	< 0.20	< 5.6
VH-Lep	$0.0166^{+0.0008}_{-0.0014}$	< 0.16	< 9.3
ttH	$0.0154^{+0.0011}_{-0.0016}$	< 0.11	< 7.1

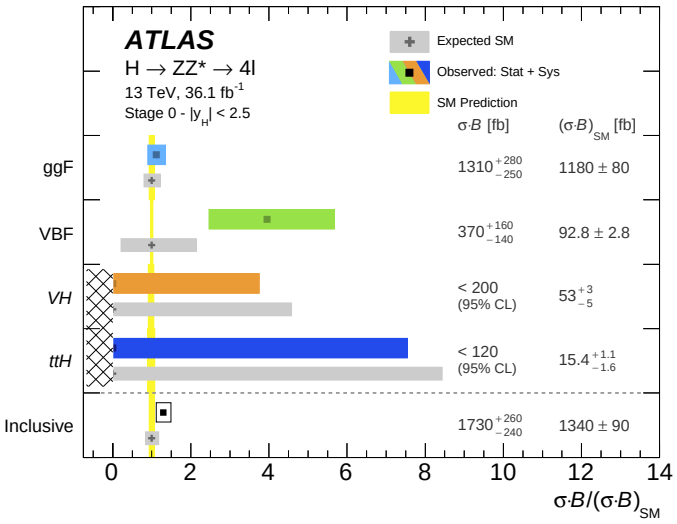

(a)

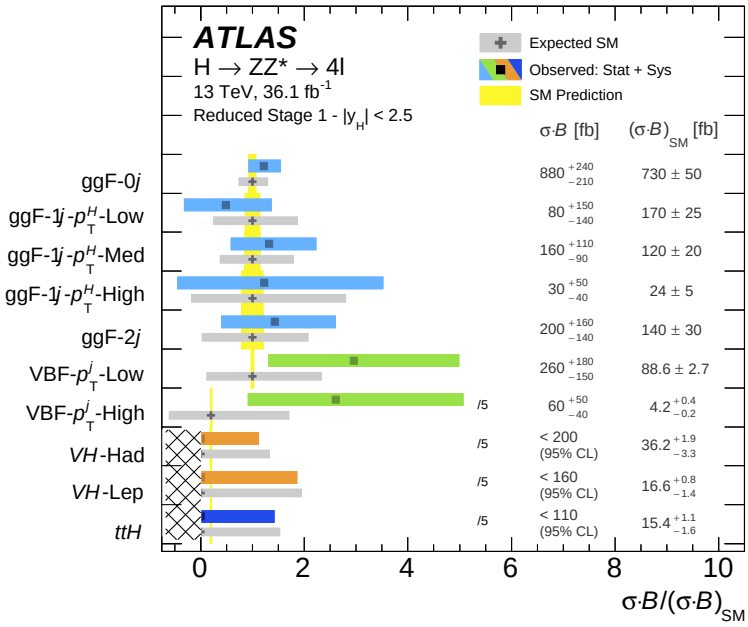

(b)

Figure 7: The observed and expected SM values of the cross-section ratios $\sigma \cdot B$ normalized by the SM expectation $(\sigma \cdot B)_{\mathrm{SM}}$ for the inclusive production and in the (a) Stage-0 and (b) reduced Stage-1 production bins for an integrated luminosity of 36.1 fb^{-1} at $\sqrt{s}$ = 13 TeV. Different colors for the observed results indicate different Higgs boson production modes. The hatched area indicates that the *VH* and *ttH* parameters of interest are constrained to positive values. For visualization purposes, the VBF-p_{T}^{j}-High value and the limits for the three reduced Stage-1 production bins *VH*-Had, *VH*-Lep and *ttH* are divided by a factor of five when shown normalized to $(\sigma \cdot B)_{\mathrm{SM}}$. The yellow vertical band represents the theory uncertainty in the signal prediction, while the horizontal grey bands represent the expected measurement uncertainty.

measurement of the reduced Stage-1 ggF processes is also strongly affected by the theory uncertainties from event migrations between different jet multiplicity and Higgs boson transverse momentum bins, while parton shower and QCD scale uncertainties affect the remaining reduced Stage-1 production bins.

Figure 8(a) shows the likelihood contours in the ($\sigma_{\mathrm{ggF}} \cdot B$, $\sigma_{\mathrm{VBF}} \cdot B$) plane. The VH and ttH cross section parameters are left free in the fit, i.e. they are not treated as parameters of interest. The compatibility with respect to the Standard Model expectation is at the level of 2.3σ, due to the discrepancies observed in the VBF-related distributions in Figures 4 and 5. The cross-section results by production mode (Stage 0) can also be interpreted in the κ framework [14, 15] in which coupling modifiers, κ_i, are introduced to parameterize possible deviations from the SM predictions of the Higgs boson couplings to SM bosons and fermions. One interesting benchmark allows two different Higgs boson coupling strength modifiers to fermions and bosons, reflecting the different structure of the interactions of the SM Higgs sector with gauge bosons and fermions. The universal coupling-strength scale factors κ_F for all fermions and κ_V for all vector bosons are defined as $\kappa_V = \kappa_W = \kappa_Z$ and $\kappa_F = \kappa_t = \kappa_b = \kappa_c = \kappa_\tau = \kappa_\mu = \kappa_g$. It is assumed that there are no undetected or invisible Higgs boson decays. The observed likelihood contours in the $\kappa_V - \kappa_F$ plane are shown in Figure 8(b) (only the quadrant $\kappa_F > 0$ and $\kappa_V > 0$ is shown since this channel is not sensitive to the relative sign of the two coupling modifiers). The compatibility with the Standard Model expectation is at the level of 1.4σ. Better agreement is observed here compared to the likelihood contours for the cross-section ratios, since the VH production is fixed to the SM expectation and the lower observed yield in the VH-Lep-enriched categories compared with SM expectations compensates for the observed excess in the VBF categories.

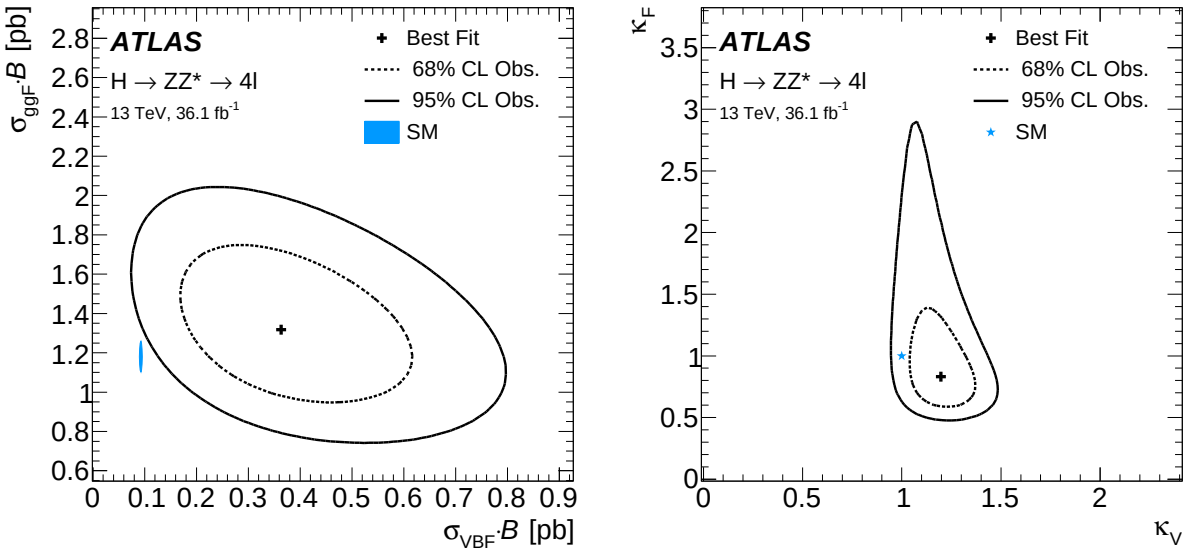

(a) (b)

Figure 8: (a) Likelihood contours at 68% CL (dashed line) and 95% CL (solid line) in the ($\sigma_{\mathrm{ggF}} \cdot B$, $\sigma_{\mathrm{VBF}} \cdot B$) plane and (b) likelihood contours in the κ_V–κ_F plane. The best fits to the data (solid cross) and the SM predictions are also indicated. In (a), the SM prediction is shown together with its theory uncertainty (filled blue elipse), while in (b) only the central value of the SM prediction (solid blue star) is shown.

Table 10: Expected and observed confidence intervals at 95% CL on the κ_{Agg}, κ_{HVV} and κ_{AVV} coupling parameters, their best-fit values and corresponding compatibility with the SM expectation, as obtained from the negative log-likelihood scans performed with 36.1 fb^{-1} of data at $\sqrt{s}$ = 13 TeV. The coupling κ_{Hgg} is fixed to the SM value of one in the fit, while the coupling κ_{SM} is either fixed to the SM value of one or left as a free parameter of the fit.

BSM coupling κ_{BSM}	Fit configuration	Expected conf. inter.	Observed conf. inter.	Best-fit $\hat{\kappa}_{BSM}$	Best-fit $\hat{\kappa}_{SM}$	Deviation from SM
κ_{Agg}	(κ_{Hgg} = 1, κ_{SM} = 1)	[−0.47, 0.47]	[−0.68, 0.68]	±0.43	-	1.8σ
κ_{HVV}	(κ_{Hgg} = 1, κ_{SM} = 1)	[−2.9, 3.2]	[0.8, 4.5]	2.9	-	2.3σ
κ_{HVV}	(κ_{Hgg} = 1, κ_{SM} free)	[−3.1, 4.0]	[−0.6, 4.2]	2.2	1.2	1.7σ
κ_{AVV}	(κ_{Hgg} = 1, κ_{SM} = 1)	[−3.5, 3.5]	[−5.2, 5.2]	±2.9	-	1.4σ
κ_{AVV}	(κ_{Hgg} = 1, κ_{SM} free)	[−4.0, 4.0]	[−4.4, 4.4]	±1.5	1.2	0.5σ

9.2 Tensor structure of Higgs boson couplings to vector bosons

In order to probe the tensor structure of the Higgs boson couplings to vector bosons, a likelihood function is constructed as a product of conditional probabilities over the event yield N_j in each reconstructed event category j,

$$\mathcal{L}(\vec{\kappa},\vec{\theta}) = \prod_{j}^{N_{\text{categories}}} P\left(N_j \,|S_j^{(\vec{\kappa})}(\vec{\theta}) + B_j(\vec{\theta})\right) \times \prod_{m}^{N_{\text{nuisance}}} C_m(\vec{\theta}),$$

with the set of coupling parameters $\vec{\kappa}$ representing the parameters of interest for a specific hypothesis test. The expected number of signal events $S_j^{(\vec{\kappa})}(\vec{\theta})$ is parameterized in terms of the SM and BSM couplings using the signal modelling described in Section 6, while the expected background event yields $B_j(\vec{\theta})$ are given by the background estimates detailed in Section 7. As in the case of the cross-section measurements, the test statistic is based on a profile likelihood ratio,

$$q = -2\ln\frac{\mathcal{L}(\vec{\kappa},\hat{\hat{\vec{\theta}}}(\vec{\kappa}))}{\mathcal{L}(\hat{\vec{\kappa}},\hat{\hat{\vec{\theta}}}(\hat{\vec{\kappa}}))} = -2\ln\lambda(\vec{\kappa}),$$

with the conditional and the unconditional maximum-likelihood estimators in the numerator and the denominator, respectively. The coupling parameter κ_{Agg} is measured assuming that all other BSM couplings are equal to zero. The coupling parameters κ_{HVV} and κ_{AVV} are probed both simultaneously and one at a time assuming that all other BSM couplings vanish. If not stated otherwise, the SM couplings κ_{SM} and κ_{Hgg} described in Section 3.2 are fixed to the SM value of one. The BSM changes in the Higgs sector are assumed not to affect the SM background processes.

Figure 9 shows the observed negative log-likelihood as function of one BSM coupling at a time, together with the expectation for the SM Higgs boson. The corresponding exclusion limits at a 95% confidence level (CL), the best-fit values and the size of the deviation from the SM are summarized in Table 10. The event yields measured in the introduced reconstructed event categories do not provide any sensitivity to the sign of the κ_{Agg} and κ_{AVV} coupling parameters. On the other hand, event yields are expected to be larger for positive κ_{HVV} values compared to the negative ones due to large interference effects with the CP-even SM coupling interactions. Due to the larger number of events observed compared with expectation in the

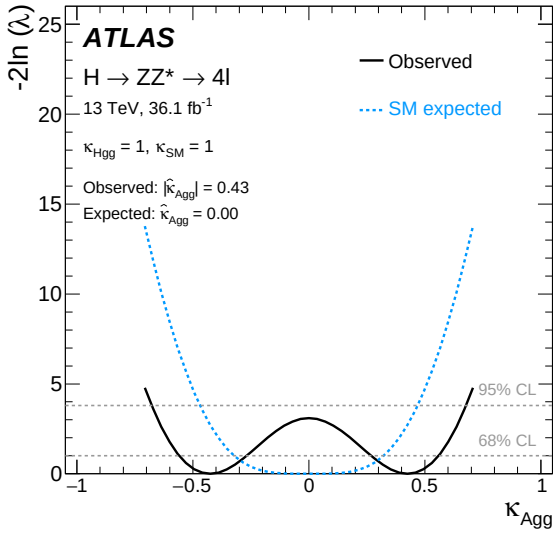

(a)

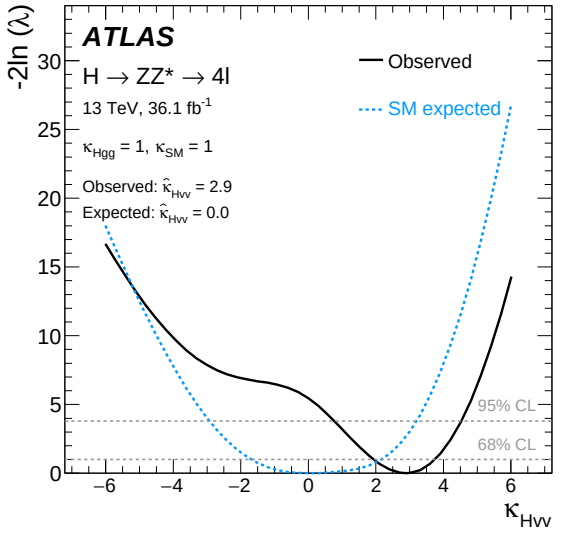

(b)

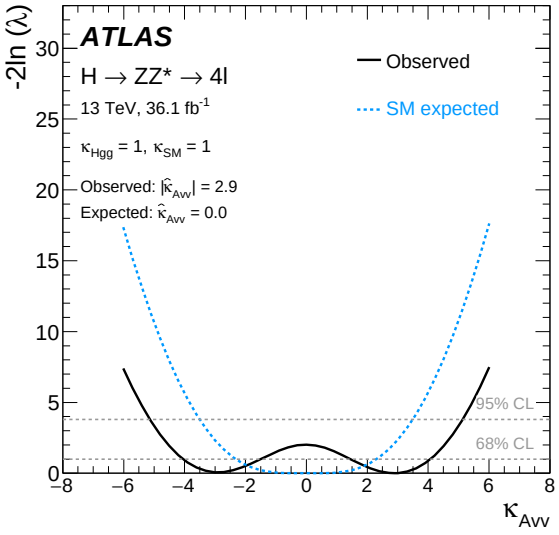

(c)

Figure 9: Observed (solid black line) and SM expected (dashed blue line) negative log-likelihood scans for (a) κ_{Agg}, (b) κ_{HVV} and (c) κ_{AVV} coupling parameters using 36.1 fb^{-1} of data at $\sqrt{s}$ = 13 TeV. The horizontal lines indicate the value of the profile likelihood ratio corresponding to the 68% and 95% CL intervals for the parameter of interest, assuming the asymptotic χ^2 distribution of the test statistic.

reconstructed VBF-enriched event categories, the best-fit values for the coupling parameters κ_{Agg}, κ_{HVV} and κ_{AVV} differ from zero and deviate from the SM expectation at the level of 1.8σ, 2.3σ and 1.4σ, respectively. If the coupling parameter κ_{SM} of the SM interaction is left free in the fit, the expected limits on the BSM HVV and AVV couplings decrease by up to 10%. The observed deviation from the SM hypothesis decreases to below 2σ (1σ) for the BSM HVV (AVV) coupling, since the observed excess of events is at least partially absorbed by a 20% increase of the SM coupling parameter κ_{SM}. The best-fit κ_{HVV} and κ_{AVV} values decrease correspondingly. Due to the mentioned interference effects for CP-even couplings, the expected yields decrease more steeply with decreasing κ_{HVV}, so that the increasing κ_{SM} value cannot fully compensate for the observed excess. The best-fit κ_{HVV} value therefore decreases less than the best-fit κ_{AVV} value compared to the fit configuration with $\kappa_{\mathrm{SM}} = 1$.

The CP-even and CP-odd BSM couplings to heavy vector bosons are also probed simultaneously in a two-dimensional contour analysis of the negative log-likelihood. The results are shown in Figure 10 and summarized in Table 11.

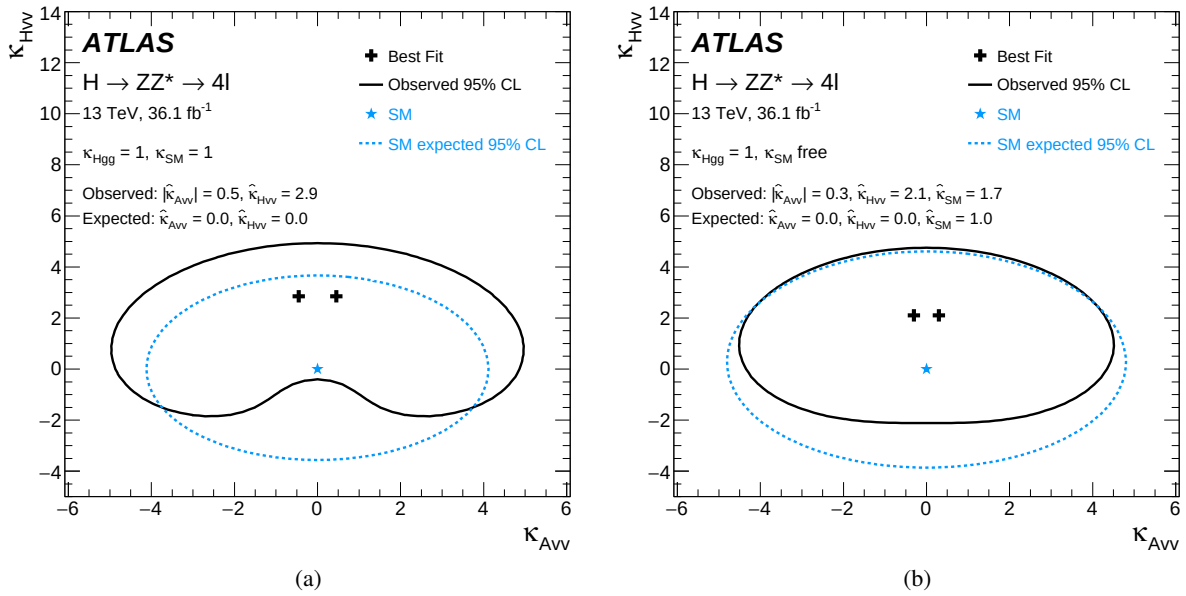

(a) (b)

Figure 10: Observed (black) and SM expected (blue) contours of the two-dimensional negative log-likelihood at 95% CL for the κ_{HVV} and κ_{AVV} coupling parameters with 36.1 fb^{-1} of data at $\sqrt{s}$ = 13 TeV. The coupling κ_{Hgg} is fixed to the SM value of one in the fit. The coupling κ_{SM} is (a) fixed to the SM value of one or (b) left as a free parameter of the fit (b).

Table 11: The best-fit coupling values and corresponding deviation from the SM expectation, as obtained from the two-dimensional $\kappa_{HVV} - \kappa_{AVV}$ negative log-likelihood scans performed with 36.1 fb^{-1} of data at $\sqrt{s}$ = 13 TeV.

Fit configuration	Best-fit $\hat{\kappa}_{HVV}$	Best-fit $\hat{\kappa}_{AVV}$	Best-fit $\hat{\kappa}_{\mathrm{SM}}$	Deviation from SM
$\kappa_{Hgg} = 1$, $\kappa_{\mathrm{SM}} = 1$	2.9	±0.5	-	1.9σ
$\kappa_{Hgg} = 1$, κ_{SM} free	2.1	±0.3	1.7	1.2σ

The best-fit value $\hat{\kappa}_{HVV}$ obtained from the two-dimensional scan is similar to the one obtained in the

one-dimensional scan. The value of $\hat{\kappa}_{AVV}$ from the two-dimensional scan is closer to the SM expectation than the corresponding value from the one-dimensional scan. The obtained result is compatible with the SM prediction within 2σ.

The coupling parameter κ_{Agg} is also probed directly by the cross sections measured in the reduced Stage-1 production bins. The largest sensitivity to this coupling is obtained from the ggF-0j production bin. Here one can neglect the impact of the BSM gluon coupling on the $\mathrm{BDT}_{\mathrm{ggF}}$ observable that is based solely on the Higgs boson decay topology. The cross-section dependence on the BSM coupling is parameterized using simulated MadGraph5_aMC@NLO samples and fitted to the measured values. The fit results agree with those presented in Table 10.

10 Summary

The coupling properties of the Higgs boson are studied in the four-lepton decay channel using 36.1 fb^{-1} of LHC pp collision data at $\sqrt{s}$ =13 TeV collected by the ATLAS experiment. The Higgs boson candidate events are categorized into several topologies, providing sensitivity to different production modes in various regions of phase space. Additional BDT discriminants are used to further improve the sensitivity in reconstructed event categories with a sufficiently large number of events.

The cross sections times branching ratio for $H \to ZZ^*$ decay measured in dedicated production bins are in agreement with the SM predictions. The largest deviation of 2.2σ is observed for the VBF production due to an observed excess of events characterized by the presence of at least two jets and a dijet invariant mass above 120 GeV. The inclusive cross section in the Higgs boson rapidity range of $|y_H| < 2.5$ is measured to be $\sigma \cdot B(H \to ZZ^*) = 1.73^{+0.26}_{-0.24}$ pb compared to the SM prediction of 1.34 ± 0.09 pb. Results are also interpreted within the κ framework with coupling modifiers κ_V and κ_F, showing compatibility with the SM. Based on event yields observed in each reconstructed event category, constraints are placed on possible BSM interactions of the Higgs boson within the framework of an effective Lagrangian extension of the SM. The data are shown to be consistent with the SM hypothesis, with the largest deviations of about 2σ due to the excess of observed events in the VBF categories. Exclusion limits are set on the CP-even and CP-odd BSM couplings of the Higgs boson to vector bosons and on the CP-odd BSM Higgs boson coupling to gluons.

Acknowledgements

We thank CERN for the very successful operation of the LHC, as well as the support staff from our institutions without whom ATLAS could not be operated efficiently.

We acknowledge the support of ANPCyT, Argentina; YerPhI, Armenia; ARC, Australia; BMWFW and FWF, Austria; ANAS, Azerbaijan; SSTC, Belarus; CNPq and FAPESP, Brazil; NSERC, NRC and CFI, Canada; CERN; CONICYT, Chile; CAS, MOST and NSFC, China; COLCIENCIAS, Colombia; MSMT CR, MPO CR and VSC CR, Czech Republic; DNRF and DNSRC, Denmark; IN2P3-CNRS, CEA-DRF/IRFU, France; SRNSF, Georgia; BMBF, HGF, and MPG, Germany; GSRT, Greece; RGC, Hong Kong SAR, China; ISF, I-CORE and Benoziyo Center, Israel; INFN, Italy; MEXT and JSPS, Japan; CNRST, Morocco; NWO, Netherlands; RCN, Norway; MNiSW and NCN, Poland; FCT, Portugal; MNE/IFA, Romania; MES of Russia and NRC KI, Russian Federation; JINR; MESTD, Serbia; MSSR,

Slovakia; ARRS and MIZŠ, Slovenia; DST/NRF, South Africa; MINECO, Spain; SRC and Wallenberg Foundation, Sweden; SERI, SNSF and Cantons of Bern and Geneva, Switzerland; MOST, Taiwan; TAEK, Turkey; STFC, United Kingdom; DOE and NSF, United States of America. In addition, individual groups and members have received support from BCKDF, the Canada Council, CANARIE, CRC, Compute Canada, FQRNT, and the Ontario Innovation Trust, Canada; EPLANET, ERC, ERDF, FP7, Horizon 2020 and Marie Skłodowska-Curie Actions, European Union; Investissements d'Avenir Labex and Idex, ANR, Région Auvergne and Fondation Partager le Savoir, France; DFG and AvH Foundation, Germany; Herakleitos, Thales and Aristeia programmes co-financed by EU-ESF and the Greek NSRF; BSF, GIF and Minerva, Israel; BRF, Norway; CERCA Programme Generalitat de Catalunya, Generalitat Valenciana, Spain; the Royal Society and Leverhulme Trust, United Kingdom.

The crucial computing support from all WLCG partners is acknowledged gratefully, in particular from CERN, the ATLAS Tier-1 facilities at TRIUMF (Canada), NDGF (Denmark, Norway, Sweden), CC-IN2P3 (France), KIT/GridKA (Germany), INFN-CNAF (Italy), NL-T1 (Netherlands), PIC (Spain), ASGC (Taiwan), RAL (UK) and BNL (USA), the Tier-2 facilities worldwide and large non-WLCG resource providers. Major contributors of computing resources are listed in Ref. [111].

References

[1] ATLAS Collaboration, *Observation of a new particle in the search for the Standard Model Higgs boson with the ATLAS detector at the LHC*, Phys. Lett. B **716** (2012) 1, arXiv: 1207.7214 [hep-ex].

[2] CMS Collaboration, *Observation of a new boson at a mass of 125 GeV with the CMS experiment at the LHC*, Phys. Lett. B **716** (2012) 30, arXiv: 1207.7235 [hep-ex].

[3] F. Englert and R. Brout, *Broken symmetry and the mass of gauge vector mesons*, Phys. Rev. Lett. **13** (1964) 321.

[4] P. W. Higgs, *Broken symmetries and the masses of gauge bosons*, Phys. Rev. Lett. **13** (1964) 508.

[5] G. Guralnik, C. Hagen and T. Kibble, *Global conservation laws and massless particles*, Phys. Rev. Lett. **13** (1964) 585.

[6] ATLAS Collaboration, *Study of the spin and parity of the Higgs boson in diboson decays with the ATLAS detector*, Eur. Phys. J. C **75** (2015) 476, arXiv: 1506.05669 [hep-ex].

[7] CMS Collaboration, *Constraints on the spin-parity and anomalous HVV couplings of the Higgs boson in proton collisions at* 7 *and* 8 *TeV*, Phys. Rev. D **92** (2015) 012004, arXiv: 1411.3441 [hep-ex].

[8] ATLAS Collaboration, *Measurements of the Higgs boson production and decay rates and coupling strengths using pp collision data at* $\sqrt{s} = 7$ *and* 8 *TeV in the ATLAS experiment*, Eur. Phys. J. C **76** (2016) 6, arXiv: 1507.04548 [hep-ex].

[9] CMS Collaboration, *Precise determination of the mass of the Higgs boson and tests of compatibility of its couplings with the standard model predictions using proton collisions at* 7 *and* 8 *TeV*, Eur. Phys. J. C **75** (2015) 212, arXiv: 1412.8662 [hep-ex].

[10] ATLAS and CMS Collaborations, *Measurements of the Higgs boson production and decay rates and constraints on its couplings from a combined ATLAS and CMS analysis of the LHC pp collision data at* $\sqrt{s} = 7$ *and* 8 *TeV*, JHEP **08** (2016) 045, arXiv: 1606.02266 [hep-ex].

[11] ATLAS Collaboration, *Measurements of Higgs boson production and couplings in the four-lepton channel in pp collisions at center-of-mass energies of* 7 *and* 8 *TeV with the ATLAS detector*, Phys. Rev. D **91** (2015) 012006, arXiv: 1408.5191 [hep-ex].

[12] CMS Collaboration, *Combined search for anomalous pseudoscalar HVV couplings in* $VH(H \to b\bar{b})$ *production and* $H \to VV$ *decay*, Phys. Lett. B **759** (2016) 672, arXiv: 1602.04305 [hep-ex].

[13] CMS Collaboration, *Measurement of the properties of a Higgs boson in the four-lepton final state*, Phys. Rev. D **89** (2014) 092007, arXiv: 1312.5353 [hep-ex].

[14] LHC Higgs Cross Section Working Group, S. Heinemeyer et al., *Handbook of LHC Higgs Cross Sections: 3. Higgs Properties*, CERN-2013-004 (CERN, Geneva, 2013), arXiv: 1307.1347 [hep-ph].

[15] LHC Higgs Cross Section Working Group, D. de Florian et al.,
Handbook of LHC Higgs Cross Sections: 4. Deciphering the nature of the Higgs sector,
CERN-2017-002-M (CERN, Geneva, 2016), arXiv: 1610.07922 [hep-ph].

[16] ATLAS and CMS Collaborations, *Combined Measurement of the Higgs Boson Mass in pp Collisions at $\sqrt{s} = 7$ and 8 TeV with the ATLAS and CMS Experiments*,
Phys. Rev. Lett. **114** (2015) 191803, arXiv: 1503.07589 [hep-ex].

[17] ATLAS Collaboration, *The ATLAS Experiment at the CERN Large Hadron Collider*,
JINST **3** (2008) S08003.

[18] ATLAS Collaboration, *ATLAS Insertable B-Layer Technical Design Report*, ATLAS-TDR-19, 2010, URL: https://cds.cern.ch/record/1291633,
ATLAS Insertable B-Layer Technical Design Report Addendum, ATLAS-TDR-19-ADD-1, 2012, URL: https://cds.cern.ch/record/1451888.

[19] A. Hoecker et al., *TMVA: Toolkit for Multivariate Data Analysis*, 2007,
arXiv: physics/0703039 [physics.data-an].

[20] M. Cacciari, G. P. Salam and G. Soyez, *The anti-k_t jet clustering algorithm*,
JHEP **04** (2008) 063, arXiv: 0802.1189 [hep-ph].

[21] M. Cacciari, G. P. Salam and G. Soyez, *FastJet User Manual*, Eur. Phys. J. C **72** (2012) 1896,
arXiv: 1111.6097 [hep-ph].

[22] P. Artoisenet, P. de Aquino, F. Demartin, R. Frederix, S. Frixione et al.,
A framework for Higgs characterisation, JHEP **11** (2013) 043, arXiv: 1306.6464 [hep-ph].

[23] P. Nason and C. Oleari,
NLO Higgs boson production via vector-boson fusion matched with shower in POWHEG,
JHEP **02** (2010) 037, arXiv: 0911.5299 [hep-ph].

[24] G. Luisoni, P. Nason, C. Oleari and F. Tramontano, *$HW^{\pm}/HZ + 0$ and 1 jet at NLO with the POWHEG BOX interfaced to GoSam and their merging within MiNLO*, JHEP **10** (2013) 083,
arXiv: 1306.2542 [hep-ph].

[25] D. J. Lange, *The EvtGen particle decay simulation package*,
Nucl. Instrum. Meth. **A462** (2001) 152.

[26] J. Butterworth et al., *PDF4LHC recommendations for LHC Run II*, J. Phys. G **43** (2016) 023001,
arXiv: 1510.03865 [hep-ph].

[27] K. Hamilton, P. Nason, E. Re and G. Zanderighi,
NNLOPS simulation of Higgs boson production, JHEP **10** (2013) 222,
arXiv: 1309.0017 [hep-ph].

[28] S. Catani and M. Grazzini, *An NNLO subtraction formalism in hadron collisions and its application to Higgs boson production at the LHC*, Phys. Rev. Lett. **98** (2007) 222002,
arXiv: hep-ph/0703012.

[29] M. Grazzini, *NNLO predictions for the Higgs boson signal in the $H \to WW \to \ell\nu\ell\nu$ and $H \to ZZ \to 4\ell$ decay channels*, JHEP **02** (2008) 043, arXiv: 0801.3232 [hep-ph].

[30] K. Hamilton, P. Nason, C. Oleari and G. Zanderighi, *Merging H/W/Z + 0 and 1 jet at NLO with no merging scale: a path to parton shower + NNLO matching*, JHEP **05** (2013) 082,
arXiv: 1212.4504 [hep-ph].

[31] J. Alwall et al., *The automated computation of tree-level and next-to-leading order differential cross sections, and their matching to parton shower simulations*, JHEP **07** (2014) 079, arXiv: 1405.0301 [hep-ph].

[32] M. Wiesemann et al., *Higgs production in association with bottom quarks*, JHEP **02** (2015) 132, arXiv: 1409.5301 [hep-ph].

[33] H.-L. Lai, M. Guzzi, J. Huston, Z. Li, P. M. Nadolsky et al., *New parton distributions for collider physics*, Phys. Rev. D **82** (2010) 074024, arXiv: 1007.2241 [hep-ph].

[34] R. D. Ball et al., *Parton distributions for the LHC Run II*, JHEP **04** (2015) 040, arXiv: 1410.8849 [hep-ph].

[35] T. Sjöstrand, S. Mrenna and P. Z. Skands, *A brief introduction to PYTHIA 8.1*, Comput. Phys. Commun. **178** (2008) 852, arXiv: 0710.3820 [hep-ph].

[36] ATLAS Collaboration, *Measurement of the Z/γ^* boson transverse momentum distribution in pp collisions at $\sqrt{s} = 7$ TeV with the ATLAS detector*, JHEP **09** (2014) 145, arXiv: 1406.3660 [hep-ex].

[37] M. Bahr et al., *Herwig++ physics and manual*, Eur. Phys. J. C **58** (2008) 639, arXiv: 0803.0883 [hep-ph].

[38] M. H. Seymour and A. Siodmok, *Constraining MPI models using σ_{eff} and recent Tevatron and LHC Underlying Event data*, JHEP **10** (2013) 113, arXiv: 1307.5015 [hep-ph].

[39] LHC Higgs Cross Section Working Group, S. Dittmaier et al., *Handbook of LHC Higgs Cross Sections: 1. Inclusive Observables*, CERN-2011-002 (CERN, Geneva, 2011), arXiv: 1101.0593 [hep-ph].

[40] LHC Higgs Cross Section Working Group, S. Dittmaier et al., *Handbook of LHC Higgs Cross Sections: 2. Differential Distributions*, CERN-2012-002 (CERN, Geneva, 2012), arXiv: 1201.3084 [hep-ph].

[41] C. Anastasiou, C. Duhr, F. Dulat, F. Herzog and B. Mistlberger, *Higgs Boson Gluon-Fusion Production in QCD at Three Loops*, Phys. Rev. Lett. **114** (2015) 212001, arXiv: 1503.06056 [hep-ph].

[42] C. Anastasiou et al., *High precision determination of the gluon fusion Higgs boson cross-section at the LHC*, JHEP **05** (2016) 058, arXiv: 1602.00695 [hep-ph].

[43] S. Actis, G. Passarino, C. Sturm and S. Uccirati, *NLO electroweak corrections to Higgs boson production at hadron colliders*, Phys. Lett. B **670** (2008) 12, arXiv: 0809.1301 [hep-ph].

[44] C. Anastasiou, R. Boughezal and F. Petriello, *Mixed QCD-electroweak corrections to Higgs boson production in gluon fusion*, JHEP **04** (2009) 003, arXiv: 0811.3458 [hep-ph].

[45] M. Grazzini and H. Sargsyan, *Heavy-quark mass effects in Higgs boson production at the LHC*, JHEP **09** (2013) 129, arXiv: 1306.4581 [hep-ph].

[46] I. W. Stewart and F. J. Tackmann, *Theory uncertainties for Higgs and other searches using jet bins*, Phys. Rev. D **85** (2012) 034011, arXiv: 1107.2117 [hep-ph].

[47] M. Ciccolini, A. Denner and S. Dittmaier, *Strong and electroweak corrections to the production of Higgs + 2-jets via weak interactions at the LHC*, Phys. Rev. Lett. **99** (2007) 161803, arXiv: 0707.0381 [hep-ph].

[48] M. Ciccolini, A. Denner and S. Dittmaier, *Electroweak and QCD corrections to Higgs production via vector-boson fusion at the LHC*, Phys. Rev. D **77** (2008) 013002, arXiv: 0710.4749 [hep-ph].

[49] P. Bolzoni, F. Maltoni, S.-O. Moch and M. Zaro, *Higgs production via vector-boson fusion at NNLO in QCD*, Phys. Rev. Lett. **105** (2010) 011801, arXiv: 1003.4451 [hep-ph].

[50] O. Brein, A. Djouadi and R. Harlander, *NNLO QCD corrections to the Higgs-strahlung processes at hadron colliders*, Phys. Lett. B **579** (2004) 149, arXiv: hep-ph/0307206.

[51] A. Denner, S. Dittmaier, S. Kallweit and A. Mück, *Electroweak corrections to Higgs-strahlung off W/Z bosons at the Tevatron and the LHC with HAWK*, JHEP **03** (2012) 075, arXiv: 1112.5142 [hep-ph].

[52] L. Altenkamp, S. Dittmaier, R. V. Harlander, H. Rzehak and T. J. E. Zirke, *Gluon-induced Higgs-strahlung at next-to-leading order QCD*, JHEP **02** (2013) 078, arXiv: 1211.5015 [hep-ph].

[53] W. Beenakker et al., *NLO QCD corrections to $t\bar{t}H$ production in hadron collisions*, Nucl. Phys. B **653** (2003) 151, arXiv: hep-ph/0211352.

[54] S. Dawson, C. Jackson, L. Orr, L. Reina and D. Wackeroth, *Associated Higgs production with top quarks at the large hadron collider: NLO QCD corrections*, Phys. Rev. D **68** (2003) 034022, arXiv: hep-ph/0305087.

[55] Y. Zhang, W.-G. Ma, R.-Y. Zhang, C. Chen and L. Guo, *QCD NLO and EW NLO corrections to $t\bar{t}H$ production with top quark decays at hadron collider*, Phys. Lett. B **738** (2014) 1, arXiv: 1407.1110 [hep-ph].

[56] S. Frixione, V. Hirschi, D. Pagani, H.-S. Shao and M. Zaro, *Electroweak and QCD corrections to top-pair hadroproduction in association with heavy bosons*, JHEP **06** (2015) 184, arXiv: 1504.03446 [hep-ph].

[57] S. Dawson, C. Jackson, L. Reina and D. Wackeroth, *Exclusive Higgs boson production with bottom quarks at hadron colliders*, Phys. Rev. D **69** (2004) 074027, arXiv: hep-ph/0311067.

[58] S. Dittmaier, M. Krämer and M. Spira, *Higgs radiation off bottom quarks at the Tevatron and the CERN LHC*, Phys. Rev. D **70** (2004) 074010, arXiv: hep-ph/0309204.

[59] R. V. Harlander and W. B. Kilgore, *Higgs boson production in bottom quark fusion at next-to-next-to leading order*, Phys. Rev. D **68** (2003) 013001, arXiv: hep-ph/0304035.

[60] A. Djouadi, J. Kalinowski and M. Spira, *HDECAY: A Program for Higgs boson decays in the Standard Model and its supersymmetric extension*, Comput. Phys. Commun. **108** (1998) 56, arXiv: hep-ph/9704448.

[61] A. Djouadi, M. M. Mühlleitner and M. Spira, *Decays of supersymmetric particles: The Program SUSY-HIT (SUspect-SdecaY-Hdecay-InTerface)*, Acta Phys. Polon. B **38** (2007) 635, arXiv: hep-ph/0609292.

[62] A. Bredenstein, A. Denner, S. Dittmaier and M. Weber, *Precise predictions for the Higgs-boson decay $H \to WW/ZZ \to 4$ leptons*, Phys. Rev. D **74** (2006) 013004, arXiv: hep-ph/0604011.

[63] A. Bredenstein, A. Denner, S. Dittmaier and M. Weber, *Radiative corrections to the semileptonic and hadronic Higgs-boson decays $H \to WW/ZZ \to 4$ fermions*, JHEP **02** (2007) 080, arXiv: hep-ph/0611234.

[64] S. Boselli, C. M. Carloni Calame, G. Montagna, O. Nicrosini and F. Piccinini, *Higgs boson decay into four leptons at NLOPS electroweak accuracy*, JHEP **06** (2015) 023, arXiv: 1503.07394 [hep-ph].

[65] S. Dulat et al., *New parton distribution functions from a global analysis of quantum chromodynamics*, Phys. Rev. D **93** (2016) 033006, arXiv: 1506.07443 [hep-ph].

[66] L. A. Harland-Lang, A. D. Martin, P. Motylinski and R. S. Thorne, *Parton distributions in the LHC era: MMHT 2014 PDFs*, Eur. Phys. J. C **75** (2015) 204, arXiv: 1412.3989 [hep-ph].

[67] R. Frederix and S. Frixione, *Merging meets matching in MC@NLO*, JHEP **12** (2012) 061, arXiv: 1209.6215 [hep-ph].

[68] T. Gleisberg et al., *Event generation with SHERPA 1.1*, JHEP **02** (2009) 007, arXiv: 0811.4622 [hep-ph].

[69] T. Gleisberg and S. Höche, *Comix, a new matrix element generator*, JHEP **12** (2008) 039, arXiv: 0808.3674 [hep-ph].

[70] F. Cascioli, P. Maierhofer and S. Pozzorini, *Scattering Amplitudes with Open Loops*, Phys. Rev. Lett. **108** (2012) 111601, arXiv: 1111.5206 [hep-ph].

[71] S. Schumann and F. Krauss, *A Parton shower algorithm based on Catani-Seymour dipole factorisation*, JHEP **03** (2008) 038, arXiv: 0709.1027 [hep-ph].

[72] S. Höche, F. Krauss, M. Schönherr and F. Siegert, *QCD matrix elements + parton showers: The NLO case*, JHEP **04** (2013) 027, arXiv: 1207.5030 [hep-ph].

[73] B. Biedermann, A. Denner, S. Dittmaier, L. Hofer and B. Jäger, *Electroweak corrections to $pp \to \mu^+\mu^- e^+ e^- + X$ at the LHC: a Higgs background study*, Phys. Rev. Lett. **116** (2016) 161803, arXiv: 1601.07787 [hep-ph].

[74] B. Biedermann, A. Denner, S. Dittmaier, L. Hofer and B. Jager, *Next-to-leading-order electroweak corrections to the production of four charged leptons at the LHC*, JHEP **01** (2017) 033, arXiv: 1611.05338 [hep-ph].

[75] N. Kauer, C. O'Brien and E. Vryonidou, *Interference effects for $H \to W\,W \to \ell\nu q\overline{q}'$ and $H \to ZZ \to \ell\bar{\ell}q\overline{q}$ searches in gluon fusion at the LHC*, JHEP **10** (2015) 074, arXiv: 1506.01694 [hep-ph].

[76] F. Caola, K. Melnikov, R. Röntsch and L. Tancredi,
QCD corrections to ZZ production in gluon fusion at the LHC, Phys. Rev. D **92** (2015) 094028, arXiv: 1509.06734 [hep-ph].

[77] F. Caola, K. Melnikov, R. Röntsch and L. Tancredi,
QCD corrections to W^+W^- production through gluon fusion, Phys. Lett. B **754** (2016) 275, arXiv: 1511.08617 [hep-ph].

[78] J. M. Campbell, R. K. Ellis, M. Czakon and S. Kirchner,
Two Loop Correction to Interference in $gg \to ZZ$, JHEP **08** (2016) 011, arXiv: 1605.01380 [hep-ph].

[79] K. Melnikov and M. Dowling,
Production of two Z-bosons in gluon fusion in the heavy top quark approximation, Phys. Lett. B **744** (2015) 43, arXiv: 1503.01274 [hep-ph].

[80] M. Bonvini, F. Caola, S. Forte, K. Melnikov and G. Ridolfi,
Signal-background interference effects for $gg \to H \to W^+W^-$ beyond leading order, Phys. Rev. D **88** (2013) 034032, arXiv: 1304.3053 [hep-ph].

[81] C. S. Li, H. T. Li, D. Y. Shao and J. Wang,
Soft gluon resummation in the signal-background interference process of $gg(\to h^*) \to ZZ$, JHEP **08** (2015) 065, arXiv: 1504.02388 [hep-ph].

[82] K. Melnikov and F. Petriello,
Electroweak gauge boson production at hadron colliders through $O(\alpha_S^2)$, Phys. Rev. D **74** (2006) 114017, arXiv: hep-ph/0609070.

[83] C. Anastasiou, L. J. Dixon, K. Melnikov and F. Petriello, *High precision QCD at hadron colliders: Electroweak gauge boson rapidity distributions at NNLO*, Phys. Rev. D **69** (2004) 094008, arXiv: hep-ph/0312266.

[84] T. Sjöstrand, S. Mrenna and P. Z. Skands, *PYTHIA 6.4 physics and manual*, JHEP **05** (2006) 026, arXiv: hep-ph/0603175.

[85] ATLAS Collaboration, *The ATLAS Simulation Infrastructure*, Eur. Phys. J. C **70** (2010) 823, arXiv: 1005.4568 [hep-ex].

[86] S. Agostinelli et al., *GEANT4: a simulation toolkit*, Nucl. Instrum. Meth. **A 506** (2003) 250.

[87] *Summary of ATLAS Pythia 8 tunes*, (2012).

[88] A. Martin, W. Stirling, R. Thorne and G. Watt, *Parton distributions for the LHC*, Eur. Phys. J. C **63** (2009) 189, arXiv: 0901.0002 [hep-ph].

[89] ATLAS Collaboration, *Study of the Higgs boson properties and search for high-mass scalar resonances in the $H \to ZZ^* \to 4\ell$ decay channel at $\sqrt{s} = 13$ TeV with the ATLAS detector*, ATLAS-CONF-2016-079, 2016, URL: https://cds.cern.ch/record/2206253.

[90] ATLAS Collaboration, *Electron identification measurements in ATLAS using $\sqrt{s} = 13$ TeV data with 50 ns bunch spacing*, ATL-PHYS-PUB-2015-041, 2015, URL: https://cds.cern.ch/record/2048202.

[91] ATLAS Collaboration, *Electron efficiency measurements with the ATLAS detector using the 2012 LHC proton–proton collision data*, ATLAS-CONF-2014-032, 2014, URL: https://cds.cern.ch/record/1706245.

[92] ATLAS Collaboration,
Electron and photon energy calibration with the ATLAS detector using LHC Run 1 data,
Eur. Phys. J. C **74** (2014) 3071, arXiv: 1407.5063 [hep-ex].

[93] ATLAS Collaboration, *Muon reconstruction performance of the ATLAS detector in proton–proton collision data at* $\sqrt{s} = 13$ *TeV*, Eur. Phys. J. C **76** (2016) 292,
arXiv: 1603.05598 [hep-ex].

[94] ATLAS Collaboration,
Topological cell clustering in the ATLAS calorimeters and its performance in LHC Run 1,
Eur. Phys. J. C **77** (2017) 490, arXiv: 1603.02934 [hep-ex].

[95] ATLAS Collaboration, *Tagging and suppression of pileup jets with the ATLAS detector*,
ATLAS-CONF-2014-018, 2014, URL: https://cds.cern.ch/record/1700870.

[96] ATLAS Collaboration, *Performance of pile-up mitigation techniques for jets in pp collisions at* $\sqrt{s} = 8$ *TeV using the ATLAS detector*, Eur. Phys. J. C **76** (2016) 581,
arXiv: 1510.03823 [hep-ex].

[97] ATLAS Collaboration, *Performance of b-jet identification in the ATLAS experiment*,
JINST **11** (2016) P04008, arXiv: 1512.01094 [hep-ex].

[98] ATLAS Collaboration, *Expected performance of the ATLAS b-tagging algorithms in Run-2*,
ATL-PHYS-PUB-2015-022, 2015, URL: https://cds.cern.ch/record/2037697.

[99] ATLAS Collaboration, *Measurements of Higgs boson production and couplings in diboson final states with the ATLAS detector at the LHC*, Phys. Lett. B **726** (2013) 88,
arXiv: 1307.1427 [hep-ex].

[100] ATLAS Collaboration,
A morphing technique for signal modelling in a multidimensional space of coupling parameters,
ATL-PHYS-PUB-2015-047, 2015, URL: https://cds.cern.ch/record/2066980.

[101] K. S. Cranmer, *Kernel estimation in high-energy physics*,
Comput. Phys. Commun. **136** (2001) 198, arXiv: hep-ex/0011057.

[102] ATLAS Collaboration,
Luminosity determination in pp collisions at $\sqrt{s} = 8$ *TeV using the ATLAS detector at the LHC*,
Eur. Phys. J. C **76** (2016) 653, arXiv: 1608.03953 [hep-ex].

[103] ATLAS Collaboration, *Measurement of the Inelastic Proton–Proton Cross Section at* $\sqrt{s} = 13$ *TeV with the ATLAS Detector at the LHC*, Phys. Rev. Lett. **117** (2016) 182002,
arXiv: 1606.02625 [hep-ex].

[104] ATLAS Collaboration,
Jet energy measurement with the ATLAS detector in proton–proton collisions at $\sqrt{s} = 7$ *TeV*,
Eur. Phys. J. C **73** (2013) 2304, arXiv: 1112.6426 [hep-ex].

[105] ATLAS Collaboration, *Jet Calibration and Systematic Uncertainties for Jets Reconstructed in the ATLAS Detector at* $\sqrt{s} = 13$ *TeV*, ATL-PHYS-PUB-2015-015, 2015,
URL: https://cds.cern.ch/record/2037613.

[106] Campbell, J. M. and Ellis, R. K. and Williams, C., *Vector boson pair production at the LHC*,
JHEP **07** (2011) 018, arXiv: 1105.0020 [hep-ph].

[107] M. Cacciari, F. A. Dreyer, A. Karlberg, G. P. Salam and G. Zanderighi,
Fully Differential Vector-Boson-Fusion Higgs Production at Next-to-Next-to-Leading Order,
Phys. Rev. Lett. **115** (2015) 082002, arXiv: 1506.02660 [hep-ph].

[108] F. Maltoni, K. Mawatari and M. Zaro, *Higgs characterisation via vector-boson fusion and associated production: NLO and parton-shower effects*, Eur. Phys. J. C **74** (2014) 2710, arXiv: 1311.1829 [hep-ph].

[109] G. Cowan, K. Cranmer, E. Gross and O. Vitells, *Asymptotic formulae for likelihood-based tests of new physics*, Eur. Phys. J. C **71** (2011) 1554, arXiv: 1007.1727 [hep-ex], Erratum: Eur. Phys. J. C **73** (2013) 2501.

[110] A. L. Read, *Presentation of the search results: the CLs technique*, J. Phys. G **28** (2002) 2693.

[111] ATLAS Collaboration, *ATLAS Computing Acknowledgements 2016–2017*, ATL-GEN-PUB-2016-002, URL: https://cds.cern.ch/record/2202407.

The ATLAS Collaboration

M. Aaboud[137d], G. Aad[88], B. Abbott[115], O. Abdinov[12,*], B. Abeloos[119], S.H. Abidi[161], O.S. AbouZeid[139], N.L. Abraham[151], H. Abramowicz[155], H. Abreu[154], R. Abreu[118], Y. Abulaiti[148a,148b], B.S. Acharya[167a,167b,a], S. Adachi[157], L. Adamczyk[41a], J. Adelman[110], M. Adersberger[102], T. Adye[133], A.A. Affolder[139], Y. Afik[154], T. Agatonovic-Jovin[14], C. Agheorghiesei[28c], J.A. Aguilar-Saavedra[128a,128f], S.P. Ahlen[24], F. Ahmadov[68,b], G. Aielli[135a,135b], S. Akatsuka[71], H. Akerstedt[148a,148b], T.P.A. Åkesson[84], E. Akilli[52], A.V. Akimov[98], G.L. Alberghi[22a,22b], J. Albert[172], P. Albicocco[50], M.J. Alconada Verzini[74], S.C. Alderweireldt[108], M. Aleksa[32], I.N. Aleksandrov[68], C. Alexa[28b], G. Alexander[155], T. Alexopoulos[10], M. Alhroob[115], B. Ali[130], M. Aliev[76a,76b], G. Alimonti[94a], J. Alison[33], S.P. Alkire[38], B.M.M. Allbrooke[151], B.W. Allen[118], P.P. Allport[19], A. Aloisio[106a,106b], A. Alonso[39], F. Alonso[74], C. Alpigiani[140], A.A. Alshehri[56], M.I. Alstaty[88], B. Alvarez Gonzalez[32], D. Álvarez Piqueras[170], M.G. Alviggi[106a,106b], B.T. Amadio[16], Y. Amaral Coutinho[26a], C. Amelung[25], D. Amidei[92], S.P. Amor Dos Santos[128a,128c], S. Amoroso[32], G. Amundsen[25], C. Anastopoulos[141], L.S. Ancu[52], N. Andari[19], T. Andeen[11], C.F. Anders[60b], J.K. Anders[77], K.J. Anderson[33], A. Andreazza[94a,94b], V. Andrei[60a], S. Angelidakis[37], I. Angelozzi[109], A. Angerami[38], A.V. Anisenkov[111,c], N. Anjos[13], A. Annovi[126a,126b], C. Antel[60a], M. Antonelli[50], A. Antonov[100,*], D.J. Antrim[166], F. Anulli[134a], M. Aoki[69], L. Aperio Bella[32], G. Arabidze[93], Y. Arai[69], J.P. Araque[128a], V. Araujo Ferraz[26a], A.T.H. Arce[48], R.E. Ardell[80], F.A. Arduh[74], J-F. Arguin[97], S. Argyropoulos[66], M. Arik[20a], A.J. Armbruster[32], L.J. Armitage[79], O. Arnaez[161], H. Arnold[51], M. Arratia[30], O. Arslan[23], A. Artamonov[99,*], G. Artoni[122], S. Artz[86], S. Asai[157], N. Asbah[45], A. Ashkenazi[155], L. Asquith[151], K. Assamagan[27], R. Astalos[146a], M. Atkinson[169], N.B. Atlay[143], K. Augsten[130], G. Avolio[32], B. Axen[16], M.K. Ayoub[35a], G. Azuelos[97,d], A.E. Baas[60a], M.J. Baca[19], H. Bachacou[138], K. Bachas[76a,76b], M. Backes[122], P. Bagnaia[134a,134b], M. Bahmani[42], H. Bahrasemani[144], J.T. Baines[133], M. Bajic[39], O.K. Baker[179], P.J. Bakker[109], E.M. Baldin[111,c], P. Balek[175], F. Balli[138], W.K. Balunas[124], E. Banas[42], A. Bandyopadhyay[23], Sw. Banerjee[176,e], A.A.E. Bannoura[178], L. Barak[155], E.L. Barberio[91], D. Barberis[53a,53b], M. Barbero[88], T. Barillari[103], M-S Barisits[32], J.T. Barkeloo[118], T. Barklow[145], N. Barlow[30], S.L. Barnes[36c], B.M. Barnett[133], R.M. Barnett[16], Z. Barnovska-Blenessy[36a], A. Baroncelli[136a], G. Barone[25], A.J. Barr[122], L. Barranco Navarro[170], F. Barreiro[85], J. Barreiro Guimarães da Costa[35a], R. Bartoldus[145], A.E. Barton[75], P. Bartos[146a], A. Basalaev[125], A. Bassalat[119,f], R.L. Bates[56], S.J. Batista[161], J.R. Batley[30], M. Battaglia[139], M. Bauce[134a,134b], F. Bauer[138], H.S. Bawa[145,g], J.B. Beacham[113], M.D. Beattie[75], T. Beau[83], P.H. Beauchemin[165], P. Bechtle[23], H.P. Beck[18,h], H.C. Beck[57], K. Becker[122], M. Becker[86], C. Becot[112], A.J. Beddall[20e], A. Beddall[20b], V.A. Bednyakov[68], M. Bedognetti[109], C.P. Bee[150], T.A. Beermann[32], M. Begalli[26a], M. Begel[27], J.K. Behr[45], A.S. Bell[81], G. Bella[155], L. Bellagamba[22a], A. Bellerive[31], M. Bellomo[154], K. Belotskiy[100], O. Beltramello[32], N.L. Belyaev[100], O. Benary[155,*], D. Benchekroun[137a], M. Bender[102], N. Benekos[10], Y. Benhammou[155], E. Benhar Noccioli[179], J. Benitez[66], D.P. Benjamin[48], M. Benoit[52], J.R. Bensinger[25], S. Bentvelsen[109], L. Beresford[122], M. Beretta[50], D. Berge[109], E. Bergeaas Kuutmann[168], N. Berger[5], L.J. Bergsten[25], J. Beringer[16], S. Berlendis[58], N.R. Bernard[89], G. Bernardi[83], C. Bernius[145], F.U. Bernlochner[23], T. Berry[80], P. Berta[86], C. Bertella[35a], G. Bertoli[148a,148b], I.A. Bertram[75], C. Bertsche[45], G.J. Besjes[39], O. Bessidskaia Bylund[148a,148b], M. Bessner[45], N. Besson[138], A. Bethani[87], S. Bethke[103], A. Betti[23], A.J. Bevan[79], J. Beyer[103], R.M. Bianchi[127], O. Biebel[102], D. Biedermann[17], R. Bielski[87], K. Bierwagen[86], N.V. Biesuz[126a,126b], M. Biglietti[136a], T.R.V. Billoud[97], H. Bilokon[50], M. Bindi[57], A. Bingul[20b], C. Bini[134a,134b], S. Biondi[22a,22b], T. Bisanz[57], C. Bittrich[47], D.M. Bjergaard[48], J.E. Black[145], K.M. Black[24], R.E. Blair[6], T. Blazek[146a], I. Bloch[45], C. Blocker[25], A. Blue[56], U. Blumenschein[79], S. Blunier[34a], G.J. Bobbink[109], V.S. Bobrovnikov[111,c], S.S. Bocchetta[84], A. Bocci[48],

C. Bock[102], M. Boehler[51], D. Boerner[178], D. Bogavac[102], A.G. Bogdanchikov[111], C. Bohm[148a], V. Boisvert[80], P. Bokan[168,i], T. Bold[41a], A.S. Boldyrev[101], A.E. Bolz[60b], M. Bomben[83], M. Bona[79], M. Boonekamp[138], A. Borisov[132], G. Borissov[75], J. Bortfeldt[32], D. Bortoletto[122], V. Bortolotto[62a], D. Boscherini[22a], M. Bosman[13], J.D. Bossio Sola[29], J. Boudreau[127], E.V. Bouhova-Thacker[75], D. Boumediene[37], C. Bourdarios[119], S.K. Boutle[56], A. Boveia[113], J. Boyd[32], I.R. Boyko[68], A.J. Bozson[80], J. Bracinik[19], A. Brandt[8], G. Brandt[57], O. Brandt[60a], F. Braren[45], U. Bratzler[158], B. Brau[89], J.E. Brau[118], W.D. Breaden Madden[56], K. Brendlinger[45], A.J. Brennan[91], L. Brenner[109], R. Brenner[168], S. Bressler[175], D.L. Briglin[19], T.M. Bristow[49], D. Britton[56], D. Britzger[45], F.M. Brochu[30], I. Brock[23], R. Brock[93], G. Brooijmans[38], T. Brooks[80], W.K. Brooks[34b], J. Brosamer[16], E. Brost[110], J.H Broughton[19], P.A. Bruckman de Renstrom[42], D. Bruncko[146b], A. Bruni[22a], G. Bruni[22a], L.S. Bruni[109], S. Bruno[135a,135b], BH Brunt[30], M. Bruschi[22a], N. Bruscino[127], P. Bryant[33], L. Bryngemark[45], T. Buanes[15], Q. Buat[144], P. Buchholz[143], A.G. Buckley[56], I.A. Budagov[68], F. Buehrer[51], M.K. Bugge[121], O. Bulekov[100], D. Bullock[8], T.J. Burch[110], S. Burdin[77], C.D. Burgard[109], A.M. Burger[5], B. Burghgrave[110], K. Burka[42], S. Burke[133], I. Burmeister[46], J.T.P. Burr[122], D. Büscher[51], V. Büscher[86], P. Bussey[56], J.M. Butler[24], C.M. Buttar[56], J.M. Butterworth[81], P. Butti[32], W. Buttinger[27], A. Buzatu[153], A.R. Buzykaev[111,c], Changqiao C.-Q.[36a], S. Cabrera Urbán[170], D. Caforio[130], H. Cai[169], V.M. Cairo[40a,40b], O. Cakir[4a], N. Calace[52], P. Calafiura[16], A. Calandri[88], G. Calderini[83], P. Calfayan[64], G. Callea[40a,40b], L.P. Caloba[26a], S. Calvente Lopez[85], D. Calvet[37], S. Calvet[37], T.P. Calvet[88], R. Camacho Toro[33], S. Camarda[32], P. Camarri[135a,135b], D. Cameron[121], R. Caminal Armadans[169], C. Camincher[58], S. Campana[32], M. Campanelli[81], A. Camplani[94a,94b], A. Campoverde[143], V. Canale[106a,106b], M. Cano Bret[36c], J. Cantero[116], T. Cao[155], M.D.M. Capeans Garrido[32], I. Caprini[28b], M. Caprini[28b], M. Capua[40a,40b], R.M. Carbone[38], R. Cardarelli[135a], F. Cardillo[51], I. Carli[131], T. Carli[32], G. Carlino[106a], B.T. Carlson[127], L. Carminati[94a,94b], R.M.D. Carney[148a,148b], S. Caron[108], E. Carquin[34b], S. Carrá[94a,94b], G.D. Carrillo-Montoya[32], D. Casadei[19], M.P. Casado[13,j], A.F. Casha[161], M. Casolino[13], D.W. Casper[166], R. Castelijn[109], V. Castillo Gimenez[170], N.F. Castro[128a,k], A. Catinaccio[32], J.R. Catmore[121], A. Cattai[32], J. Caudron[23], V. Cavaliere[169], E. Cavallaro[13], D. Cavalli[94a], M. Cavalli-Sforza[13], V. Cavasinni[126a,126b], E. Celebi[20d], F. Ceradini[136a,136b], L. Cerda Alberich[170], A.S. Cerqueira[26b], A. Cerri[151], L. Cerrito[135a,135b], F. Cerutti[16], A. Cervelli[22a,22b], S.A. Cetin[20d], A. Chafaq[137a], D. Chakraborty[110], S.K. Chan[59], W.S. Chan[109], Y.L. Chan[62a], P. Chang[169], J.D. Chapman[30], D.G. Charlton[19], C.C. Chau[31], C.A. Chavez Barajas[151], S. Che[113], S. Cheatham[167a,167c], A. Chegwidden[93], S. Chekanov[6], S.V. Chekulaev[163a], G.A. Chelkov[68,l], M.A. Chelstowska[32], C. Chen[36a], C. Chen[67], H. Chen[27], J. Chen[36a], S. Chen[35b], S. Chen[157], X. Chen[35c,m], Y. Chen[70], H.C. Cheng[92], H.J. Cheng[35a,35d], A. Cheplakov[68], E. Cheremushkina[132], R. Cherkaoui El Moursli[137e], E. Cheu[7], K. Cheung[63], L. Chevalier[138], V. Chiarella[50], G. Chiarelli[126a,126b], G. Chiodini[76a], A.S. Chisholm[32], A. Chitan[28b], Y.H. Chiu[172], M.V. Chizhov[68], K. Choi[64], A.R. Chomont[37], S. Chouridou[156], Y.S. Chow[62a], V. Christodoulou[81], M.C. Chu[62a], J. Chudoba[129], A.J. Chuinard[90], J.J. Chwastowski[42], L. Chytka[117], A.K. Ciftci[4a], D. Cinca[46], V. Cindro[78], I.A. Cioara[23], A. Ciocio[16], F. Cirotto[106a,106b], Z.H. Citron[175], M. Citterio[94a], M. Ciubancan[28b], A. Clark[52], B.L. Clark[59], M.R. Clark[38], P.J. Clark[49], R.N. Clarke[16], C. Clement[148a,148b], Y. Coadou[88], M. Cobal[167a,167c], A. Coccaro[52], J. Cochran[67], L. Colasurdo[108], B. Cole[38], A.P. Colijn[109], J. Collot[58], T. Colombo[166], P. Conde Muiño[128a,128b], E. Coniavitis[51], S.H. Connell[147b], I.A. Connelly[87], S. Constantinescu[28b], G. Conti[32], F. Conventi[106a,n], M. Cooke[16], A.M. Cooper-Sarkar[122], F. Cormier[171], K.J.R. Cormier[161], M. Corradi[134a,134b], F. Corriveau[90,o], A. Cortes-Gonzalez[32], G. Costa[94a], M.J. Costa[170], D. Costanzo[141], G. Cottin[30], G. Cowan[80], B.E. Cox[87], K. Cranmer[112], S.J. Crawley[56], R.A. Creager[124], G. Cree[31], S. Crépé-Renaudin[58], F. Crescioli[83], W.A. Cribbs[148a,148b], M. Cristinziani[23], V. Croft[112], G. Crosetti[40a,40b], A. Cueto[85], T. Cuhadar Donszelmann[141], A.R. Cukierman[145], J. Cummings[179], M. Curatolo[50], J. Cúth[86], S. Czekierda[42], P. Czodrowski[32], G. D'amen[22a,22b], S. D'Auria[56],

L. D'eramo[83], M. D'Onofrio[77], M.J. Da Cunha Sargedas De Sousa[128a,128b], C. Da Via[87], W. Dabrowski[41a], T. Dado[146a], T. Dai[92], O. Dale[15], F. Dallaire[97], C. Dallapiccola[89], M. Dam[39], J.R. Dandoy[124], M.F. Daneri[29], N.P. Dang[176], A.C. Daniells[19], N.S. Dann[87], M. Danninger[171], M. Dano Hoffmann[138], V. Dao[150], G. Darbo[53a], S. Darmora[8], J. Dassoulas[3], A. Dattagupta[118], T. Daubney[45], W. Davey[23], C. David[45], T. Davidek[131], D.R. Davis[48], P. Davison[81], E. Dawe[91], I. Dawson[141], K. De[8], R. de Asmundis[106a], A. De Benedetti[115], S. De Castro[22a,22b], S. De Cecco[83], N. De Groot[108], P. de Jong[109], H. De la Torre[93], F. De Lorenzi[67], A. De Maria[57], D. De Pedis[134a], A. De Salvo[134a], U. De Sanctis[135a,135b], A. De Santo[151], K. De Vasconcelos Corga[88], J.B. De Vivie De Regie[119], R. Debbe[27], C. Debenedetti[139], D.V. Dedovich[68], N. Dehghanian[3], I. Deigaard[109], M. Del Gaudio[40a,40b], J. Del Peso[85], D. Delgove[119], F. Deliot[138], C.M. Delitzsch[7], A. Dell'Acqua[32], L. Dell'Asta[24], M. Dell'Orso[126a,126b], M. Della Pietra[106a,106b], D. della Volpe[52], M. Delmastro[5], C. Delporte[119], P.A. Delsart[58], D.A. DeMarco[161], S. Demers[179], M. Demichev[68], A. Demilly[83], S.P. Denisov[132], D. Denysiuk[138], D. Derendarz[42], J.E. Derkaoui[137d], F. Derue[83], P. Dervan[77], K. Desch[23], C. Deterre[45], K. Dette[161], M.R. Devesa[29], P.O. Deviveiros[32], A. Dewhurst[133], S. Dhaliwal[25], F.A. Di Bello[52], A. Di Ciaccio[135a,135b], L. Di Ciaccio[5], W.K. Di Clemente[124], C. Di Donato[106a,106b], A. Di Girolamo[32], B. Di Girolamo[32], B. Di Micco[136a,136b], R. Di Nardo[32], K.F. Di Petrillo[59], A. Di Simone[51], R. Di Sipio[161], D. Di Valentino[31], C. Diaconu[88], M. Diamond[161], F.A. Dias[39], M.A. Diaz[34a], E.B. Diehl[92], J. Dietrich[17], S. Díez Cornell[45], A. Dimitrievska[14], J. Dingfelder[23], P. Dita[28b], S. Dita[28b], F. Dittus[32], F. Djama[88], T. Djobava[54b], J.I. Djuvsland[60a], M.A.B. do Vale[26c], D. Dobos[32], M. Dobre[28b], D. Dodsworth[25], C. Doglioni[84], J. Dolejsi[131], Z. Dolezal[131], M. Donadelli[26d], S. Donati[126a,126b], P. Dondero[123a,123b], J. Donini[37], J. Dopke[133], A. Doria[106a], M.T. Dova[74], A.T. Doyle[56], E. Drechsler[57], M. Dris[10], Y. Du[36b], J. Duarte-Campderros[155], F. Dubinin[98], A. Dubreuil[52], E. Duchovni[175], G. Duckeck[102], A. Ducourthial[83], O.A. Ducu[97,p], D. Duda[109], A. Dudarev[32], A.Chr. Dudder[86], E.M. Duffield[16], L. Duflot[119], M. Dührssen[32], C. Dulsen[178], M. Dumancic[175], A.E. Dumitriu[28b], A.K. Duncan[56], M. Dunford[60a], A. Duperrin[88], H. Duran Yildiz[4a], M. Düren[55], A. Durglishvili[54b], D. Duschinger[47], B. Dutta[45], D. Duvnjak[1], M. Dyndal[45], B.S. Dziedzic[42], C. Eckardt[45], K.M. Ecker[103], R.C. Edgar[92], T. Eifert[32], G. Eigen[15], K. Einsweiler[16], T. Ekelof[168], M. El Kacimi[137c], R. El Kosseifi[88], V. Ellajosyula[88], M. Ellert[168], S. Elles[5], F. Ellinghaus[178], A.A. Elliot[172], N. Ellis[32], J. Elmsheuser[27], M. Elsing[32], D. Emeliyanov[133], Y. Enari[157], J.S. Ennis[173], M.B. Epland[48], J. Erdmann[46], A. Ereditato[18], M. Ernst[27], S. Errede[169], M. Escalier[119], C. Escobar[170], B. Esposito[50], O. Estrada Pastor[170], A.I. Etienvre[138], E. Etzion[155], H. Evans[64], A. Ezhilov[125], M. Ezzi[137e], F. Fabbri[22a,22b], L. Fabbri[22a,22b], V. Fabiani[108], G. Facini[81], R.M. Fakhrutdinov[132], S. Falciano[134a], R.J. Falla[81], J. Faltova[32], Y. Fang[35a], M. Fanti[94a,94b], A. Farbin[8], A. Farilla[136a], C. Farina[127], E.M. Farina[123a,123b], T. Farooque[93], S. Farrell[16], S.M. Farrington[173], P. Farthouat[32], F. Fassi[137e], P. Fassnacht[32], D. Fassouliotis[9], M. Faucci Giannelli[49], A. Favareto[53a,53b], W.J. Fawcett[122], L. Fayard[119], O.L. Fedin[125,q], W. Fedorko[171], S. Feigl[121], L. Feligioni[88], C. Feng[36b], E.J. Feng[32], M.J. Fenton[56], A.B. Fenyuk[132], L. Feremenga[8], P. Fernandez Martinez[170], J. Ferrando[45], A. Ferrari[168], P. Ferrari[109], R. Ferrari[123a], D.E. Ferreira de Lima[60b], A. Ferrer[170], D. Ferrere[52], C. Ferretti[92], F. Fiedler[86], A. Filipčič[78], M. Filipuzzi[45], F. Filthaut[108], M. Fincke-Keeler[172], K.D. Finelli[24], M.C.N. Fiolhais[128a,128c,r], L. Fiorini[170], A. Fischer[2], C. Fischer[13], J. Fischer[178], W.C. Fisher[93], N. Flaschel[45], I. Fleck[143], P. Fleischmann[92], R.R.M. Fletcher[124], T. Flick[178], B.M. Flierl[102], L.R. Flores Castillo[62a], M.J. Flowerdew[103], G.T. Forcolin[87], A. Formica[138], F.A. Förster[13], A. Forti[87], A.G. Foster[19], D. Fournier[119], H. Fox[75], S. Fracchia[141], P. Francavilla[126a,126b], M. Franchini[22a,22b], S. Franchino[60a], D. Francis[32], L. Franconi[121], M. Franklin[59], M. Frate[166], M. Fraternali[123a,123b], D. Freeborn[81], S.M. Fressard-Batraneanu[32], B. Freund[97], D. Froidevaux[32], J.A. Frost[122], C. Fukunaga[158], T. Fusayasu[104], J. Fuster[170], O. Gabizon[154], A. Gabrielli[22a,22b], A. Gabrielli[16], G.P. Gach[41a], S. Gadatsch[32], S. Gadomski[80], G. Gagliardi[53a,53b], L.G. Gagnon[97],

C. Galea[108], B. Galhardo[128a,128c], E.J. Gallas[122], B.J. Gallop[133], P. Gallus[130], G. Galster[39], K.K. Gan[113], S. Ganguly[37], Y. Gao[77], Y.S. Gao[145,g], F.M. Garay Walls[34a], C. García[170], J.E. García Navarro[170], J.A. García Pascual[35a], M. Garcia-Sciveres[16], R.W. Gardner[33], N. Garelli[145], V. Garonne[121], A. Gascon Bravo[45], K. Gasnikova[45], C. Gatti[50], A. Gaudiello[53a,53b], G. Gaudio[123a], I.L. Gavrilenko[98], C. Gay[171], G. Gaycken[23], E.N. Gazis[10], C.N.P. Gee[133], J. Geisen[57], M. Geisen[86], M.P. Geisler[60a], K. Gellerstedt[148a,148b], C. Gemme[53a], M.H. Genest[58], C. Geng[92], S. Gentile[134a,134b], C. Gentsos[156], S. George[80], D. Gerbaudo[13], G. Geßner[46], S. Ghasemi[143], M. Ghneimat[23], B. Giacobbe[22a], S. Giagu[134a,134b], N. Giangiacomi[22a,22b], P. Giannetti[126a,126b], S.M. Gibson[80], M. Gignac[171], M. Gilchriese[16], D. Gillberg[31], G. Gilles[178], D.M. Gingrich[3,d], M.P. Giordani[167a,167c], F.M. Giorgi[22a], P.F. Giraud[138], P. Giromini[59], G. Giugliarelli[167a,167c], D. Giugni[94a], F. Giuli[122], C. Giuliani[103], M. Giulini[60b], B.K. Gjelsten[121], S. Gkaitatzis[156], I. Gkialas[9,s], E.L. Gkougkousis[13], P. Gkountoumis[10], L.K. Gladilin[101], C. Glasman[85], J. Glatzer[13], P.C.F. Glaysher[45], A. Glazov[45], M. Goblirsch-Kolb[25], J. Godlewski[42], S. Goldfarb[91], T. Golling[52], D. Golubkov[132], A. Gomes[128a,128b,128d], R. Gonçalo[128a], R. Goncalves Gama[26a], J. Goncalves Pinto Firmino Da Costa[138], G. Gonella[51], L. Gonella[19], A. Gongadze[68], J.L. Gonski[59], S. González de la Hoz[170], S. Gonzalez-Sevilla[52], L. Goossens[32], P.A. Gorbounov[99], H.A. Gordon[27], I. Gorelov[107], B. Gorini[32], E. Gorini[76a,76b], A. Gorišek[78], A.T. Goshaw[48], C. Gössling[46], M.I. Gostkin[68], C.A. Gottardo[23], C.R. Goudet[119], D. Goujdami[137c], A.G. Goussiou[140], N. Govender[147b,t], E. Gozani[154], I. Grabowska-Bold[41a], P.O.J. Gradin[168], J. Gramling[166], E. Gramstad[121], S. Grancagnolo[17], V. Gratchev[125], P.M. Gravila[28f], C. Gray[56], H.M. Gray[16], Z.D. Greenwood[82,u], C. Grefe[23], K. Gregersen[81], I.M. Gregor[45], P. Grenier[145], K. Grevtsov[5], J. Griffiths[8], A.A. Grillo[139], K. Grimm[75], S. Grinstein[13,v], Ph. Gris[37], J.-F. Grivaz[119], S. Groh[86], E. Gross[175], J. Grosse-Knetter[57], G.C. Grossi[82], Z.J. Grout[81], A. Grummer[107], L. Guan[92], W. Guan[176], J. Guenther[32], F. Guescini[163a], D. Guest[166], O. Gueta[155], B. Gui[113], E. Guido[53a,53b], T. Guillemin[5], S. Guindon[32], U. Gul[56], C. Gumpert[32], J. Guo[36c], W. Guo[92], Y. Guo[36a,w], R. Gupta[43], S. Gurbuz[20a], G. Gustavino[115], B.J. Gutelman[154], P. Gutierrez[115], N.G. Gutierrez Ortiz[81], C. Gutschow[81], C. Guyot[138], M.P. Guzik[41a], C. Gwenlan[122], C.B. Gwilliam[77], A. Haas[112], C. Haber[16], H.K. Hadavand[8], N. Haddad[137e], A. Hadef[88], S. Hageböck[23], M. Hagihara[164], H. Hakobyan[180,*], M. Haleem[45], J. Haley[116], G. Halladjian[93], G.D. Hallewell[88], K. Hamacher[178], P. Hamal[117], K. Hamano[172], A. Hamilton[147a], G.N. Hamity[141], P.G. Hamnett[45], L. Han[36a], S. Han[35a,35d], K. Hanagaki[69,x], K. Hanawa[157], M. Hance[139], D.M. Handl[102], B. Haney[124], P. Hanke[60a], J.B. Hansen[39], J.D. Hansen[39], M.C. Hansen[23], P.H. Hansen[39], K. Hara[164], A.S. Hard[176], T. Harenberg[178], F. Hariri[119], S. Harkusha[95], P.F. Harrison[173], N.M. Hartmann[102], Y. Hasegawa[142], A. Hasib[49], S. Hassani[138], S. Haug[18], R. Hauser[93], L. Hauswald[47], L.B. Havener[38], M. Havranek[130], C.M. Hawkes[19], R.J. Hawkings[32], D. Hayakawa[159], D. Hayden[93], C.P. Hays[122], J.M. Hays[79], H.S. Hayward[77], S.J. Haywood[133], S.J. Head[19], T. Heck[86], V. Hedberg[84], L. Heelan[8], S. Heer[23], K.K. Heidegger[51], S. Heim[45], T. Heim[16], B. Heinemann[45,y], J.J. Heinrich[102], L. Heinrich[112], C. Heinz[55], J. Hejbal[129], L. Helary[32], A. Held[171], S. Hellman[148a,148b], C. Helsens[32], R.C.W. Henderson[75], Y. Heng[176], S. Henkelmann[171], A.M. Henriques Correia[32], S. Henrot-Versille[119], G.H. Herbert[17], H. Herde[25], V. Herget[177], Y. Hernández Jiménez[147c], H. Herr[86], G. Herten[51], R. Hertenberger[102], L. Hervas[32], T.C. Herwig[124], G.G. Hesketh[81], N.P. Hessey[163a], J.W. Hetherly[43], S. Higashino[69], E. Higón-Rodriguez[170], K. Hildebrand[33], E. Hill[172], J.C. Hill[30], K.H. Hiller[45], S.J. Hillier[19], M. Hils[47], I. Hinchliffe[16], M. Hirose[51], D. Hirschbuehl[178], B. Hiti[78], O. Hladik[129], D.R. Hlaluku[147c], X. Hoad[49], J. Hobbs[150], N. Hod[163a], M.C. Hodgkinson[141], P. Hodgson[141], A. Hoecker[32], M.R. Hoeferkamp[107], F. Hoenig[102], D. Hohn[23], T.R. Holmes[33], M. Homann[46], S. Honda[164], T. Honda[69], T.M. Hong[127], B.H. Hooberman[169], W.H. Hopkins[118], Y. Horii[105], A.J. Horton[144], J-Y. Hostachy[58], A. Hostiuc[140], S. Hou[153], A. Hoummada[137a], J. Howarth[87], J. Hoya[74], M. Hrabovsky[117], J. Hrdinka[32], I. Hristova[17], J. Hrivnac[119], T. Hryn'ova[5], A. Hrynevich[96], P.J. Hsu[63], S.-C. Hsu[140], Q. Hu[27], S. Hu[36c], Y. Huang[35a],

Z. Hubacek[130], F. Hubaut[88], F. Huegging[23], T.B. Huffman[122], E.W. Hughes[38], M. Huhtinen[32], R.F.H. Hunter[31], P. Huo[150], N. Huseynov[68,b], J. Huston[93], J. Huth[59], R. Hyneman[92], G. Iacobucci[52], G. Iakovidis[27], I. Ibragimov[143], L. Iconomidou-Fayard[119], Z. Idrissi[137e], P. Iengo[32], O. Igonkina[109,z], T. Iizawa[174], Y. Ikegami[69], M. Ikeno[69], Y. Ilchenko[11,aa], D. Iliadis[156], N. Ilic[145], F. Iltzsche[47], G. Introzzi[123a,123b], P. Ioannou[9,*], M. Iodice[136a], K. Iordanidou[38], V. Ippolito[59], M.F. Isacson[168], N. Ishijima[120], M. Ishino[157], M. Ishitsuka[159], C. Issever[122], S. Istin[20a], F. Ito[164], J.M. Iturbe Ponce[62a], R. Iuppa[162a,162b], H. Iwasaki[69], J.M. Izen[44], V. Izzo[106a], S. Jabbar[3], P. Jackson[1], R.M. Jacobs[23], V. Jain[2], K.B. Jakobi[86], K. Jakobs[51], S. Jakobsen[65], T. Jakoubek[129], D.O. Jamin[116], D.K. Jana[82], R. Jansky[52], J. Janssen[23], M. Janus[57], P.A. Janus[41a], G. Jarlskog[84], N. Javadov[68,b], T. Javůrek[51], M. Javurkova[51], F. Jeanneau[138], L. Jeanty[16], J. Jejelava[54a,ab], A. Jelinskas[173], P. Jenni[51,ac], C. Jeske[173], S. Jézéquel[5], H. Ji[176], J. Jia[150], H. Jiang[67], Y. Jiang[36a], Z. Jiang[145], S. Jiggins[81], J. Jimenez Pena[170], S. Jin[35b], A. Jinaru[28b], O. Jinnouchi[159], H. Jivan[147c], P. Johansson[141], K.A. Johns[7], C.A. Johnson[64], W.J. Johnson[140], K. Jon-And[148a,148b], R.W.L. Jones[75], S.D. Jones[151], S. Jones[7], T.J. Jones[77], J. Jongmanns[60a], P.M. Jorge[128a,128b], J. Jovicevic[163a], X. Ju[176], A. Juste Rozas[13,v], M.K. Köhler[175], A. Kaczmarska[42], M. Kado[119], H. Kagan[113], M. Kagan[145], S.J. Kahn[88], T. Kaji[174], E. Kajomovitz[154], C.W. Kalderon[84], A. Kaluza[86], S. Kama[43], A. Kamenshchikov[132], N. Kanaya[157], L. Kanjir[78], V.A. Kantserov[100], J. Kanzaki[69], B. Kaplan[112], L.S. Kaplan[176], D. Kar[147c], K. Karakostas[10], N. Karastathis[10], M.J. Kareem[163b], E. Karentzos[10], S.N. Karpov[68], Z.M. Karpova[68], K. Karthik[112], V. Kartvelishvili[75], A.N. Karyukhin[132], K. Kasahara[164], L. Kashif[176], R.D. Kass[113], A. Kastanas[149], Y. Kataoka[157], C. Kato[157], A. Katre[52], J. Katzy[45], K. Kawade[70], K. Kawagoe[73], T. Kawamoto[157], G. Kawamura[57], E.F. Kay[77], V.F. Kazanin[111,c], R. Keeler[172], R. Kehoe[43], J.S. Keller[31], E. Kellermann[84], J.J. Kempster[80], J Kendrick[19], H. Keoshkerian[161], O. Kepka[129], B.P. Kerševan[78], S. Kersten[178], R.A. Keyes[90], M. Khader[169], F. Khalil-zada[12], A. Khanov[116], A.G. Kharlamov[111,c], T. Kharlamova[111,c], A. Khodinov[160], T.J. Khoo[52], V. Khovanskiy[99,*], E. Khramov[68], J. Khubua[54b,ad], S. Kido[70], C.R. Kilby[80], H.Y. Kim[8], S.H. Kim[164], Y.K. Kim[33], N. Kimura[156], O.M. Kind[17], B.T. King[77], D. Kirchmeier[47], J. Kirk[133], A.E. Kiryunin[103], T. Kishimoto[157], D. Kisielewska[41a], V. Kitali[45], O. Kivernyk[5], E. Kladiva[146b], T. Klapdor-Kleingrothaus[51], M.H. Klein[92], M. Klein[77], U. Klein[77], K. Kleinknecht[86], P. Klimek[110], A. Klimentov[27], R. Klingenberg[46,*], T. Klingl[23], T. Klioutchnikova[32], F.F. Klitzner[102], E.-E. Kluge[60a], P. Kluit[109], S. Kluth[103], E. Kneringer[65], E.B.F.G. Knoops[88], A. Knue[103], A. Kobayashi[157], D. Kobayashi[73], T. Kobayashi[157], M. Kobel[47], M. Kocian[145], P. Kodys[131], T. Koffas[31], E. Koffeman[109], N.M. Köhler[103], T. Koi[145], M. Kolb[60b], I. Koletsou[5], A.A. Komar[98,*], T. Kondo[69], N. Kondrashova[36c], K. Köneke[51], A.C. König[108], T. Kono[69,ae], R. Konoplich[112,af], N. Konstantinidis[81], B. Konya[84], R. Kopeliansky[64], S. Koperny[41a], A.K. Kopp[51], K. Korcyl[42], K. Kordas[156], A. Korn[81], A.A. Korol[111,c], I. Korolkov[13], E.V. Korolkova[141], O. Kortner[103], S. Kortner[103], T. Kosek[131], V.V. Kostyukhin[23], A. Kotwal[48], A. Koulouris[10], A. Kourkoumeli-Charalampidi[123a,123b], C. Kourkoumelis[9], E. Kourlitis[141], V. Kouskoura[27], A.B. Kowalewska[42], R. Kowalewski[172], T.Z. Kowalski[41a], C. Kozakai[157], W. Kozanecki[138], A.S. Kozhin[132], V.A. Kramarenko[101], G. Kramberger[78], D. Krasnopevtsev[100], M.W. Krasny[83], A. Krasznahorkay[32], D. Krauss[103], J.A. Kremer[41a], J. Kretzschmar[77], K. Kreutzfeldt[55], P. Krieger[161], K. Krizka[16], K. Kroeninger[46], H. Kroha[103], J. Kroll[129], J. Kroll[124], J. Kroseberg[23], J. Krstic[14], U. Kruchonak[68], H. Krüger[23], N. Krumnack[67], M.C. Kruse[48], T. Kubota[91], H. Kucuk[81], S. Kuday[4b], J.T. Kuechler[178], S. Kuehn[32], A. Kugel[60a], F. Kuger[177], T. Kuhl[45], V. Kukhtin[68], R. Kukla[88], Y. Kulchitsky[95], S. Kuleshov[34b], Y.P. Kulinich[169], M. Kuna[134a,134b], T. Kunigo[71], A. Kupco[129], T. Kupfer[46], O. Kuprash[155], H. Kurashige[70], L.L. Kurchaninov[163a], Y.A. Kurochkin[95], M.G. Kurth[35a,35d], E.S. Kuwertz[172], M. Kuze[159], J. Kvita[117], T. Kwan[172], D. Kyriazopoulos[141], A. La Rosa[103], J.L. La Rosa Navarro[26d], L. La Rotonda[40a,40b], F. La Ruffa[40a,40b], C. Lacasta[170], F. Lacava[134a,134b], J. Lacey[45], D.P.J. Lack[87], H. Lacker[17], D. Lacour[83], E. Ladygin[68], R. Lafaye[5], B. Laforge[83], T. Lagouri[179], S. Lai[57], S. Lammers[64],

W. Lampl[7], E. Lançon[27], U. Landgraf[51], M.P.J. Landon[79], M.C. Lanfermann[52], V.S. Lang[45], J.C. Lange[13], R.J. Langenberg[32], A.J. Lankford[166], F. Lanni[27], K. Lantzsch[23], A. Lanza[123a], A. Lapertosa[53a,53b], S. Laplace[83], J.F. Laporte[138], T. Lari[94a], F. Lasagni Manghi[22a,22b], M. Lassnig[32], T.S. Lau[62a], A. Laudrain[119], P. Laurelli[50], W. Lavrijsen[16], A.T. Law[139], P. Laycock[77], T. Lazovich[59], M. Lazzaroni[94a,94b], B. Le[91], O. Le Dortz[83], E. Le Guirriec[88], E.P. Le Quilleuc[138], M. LeBlanc[172], T. LeCompte[6], F. Ledroit-Guillon[58], C.A. Lee[27], G.R. Lee[34a], S.C. Lee[153], L. Lee[59], B. Lefebvre[90], G. Lefebvre[83], M. Lefebvre[172], F. Legger[102], C. Leggett[16], G. Lehmann Miotto[32], X. Lei[7], W.A. Leight[45], M.A.L. Leite[26d], R. Leitner[131], D. Lellouch[175], B. Lemmer[57], K.J.C. Leney[81], T. Lenz[23], B. Lenzi[32], R. Leone[7], S. Leone[126a,126b], C. Leonidopoulos[49], G. Lerner[151], C. Leroy[97], R. Les[161], A.A.J. Lesage[138], C.G. Lester[30], M. Levchenko[125], J. Levêque[5], D. Levin[92], L.J. Levinson[175], M. Levy[19], D. Lewis[79], B. Li[36a,w], H. Li[150], L. Li[36c], Q. Li[35a,35d], Q. Li[36a], S. Li[48], X. Li[36c], Y. Li[143], Z. Liang[35a], B. Liberti[135a], A. Liblong[161], K. Lie[62c], J. Liebal[23], W. Liebig[15], A. Limosani[152], C.Y. Lin[30], K. Lin[93], S.C. Lin[182], T.H. Lin[86], R.A. Linck[64], B.E. Lindquist[150], A.E. Lionti[52], E. Lipeles[124], A. Lipniacka[15], M. Lisovyi[60b], T.M. Liss[169,ag], A. Lister[171], A.M. Litke[139], B. Liu[67], H. Liu[92], H. Liu[27], J.K.K. Liu[122], J. Liu[36b], J.B. Liu[36a], K. Liu[88], L. Liu[169], M. Liu[36a], Y.L. Liu[36a], Y. Liu[36a], M. Livan[123a,123b], A. Lleres[58], J. Llorente Merino[35a], S.L. Lloyd[79], C.Y. Lo[62b], F. Lo Sterzo[43], E.M. Lobodzinska[45], P. Loch[7], F.K. Loebinger[87], A. Loesle[51], K.M. Loew[25], T. Lohse[17], K. Lohwasser[141], M. Lokajicek[129], B.A. Long[24], J.D. Long[169], R.E. Long[75], L. Longo[76a,76b], K.A. Looper[113], J.A. Lopez[34b], I. Lopez Paz[13], A. Lopez Solis[83], J. Lorenz[102], N. Lorenzo Martinez[5], M. Losada[21], P.J. Lösel[102], X. Lou[35a], A. Lounis[119], J. Love[6], P.A. Love[75], H. Lu[62a], N. Lu[92], Y.J. Lu[63], H.J. Lubatti[140], C. Luci[134a,134b], A. Lucotte[58], C. Luedtke[51], F. Luehring[64], W. Lukas[65], L. Luminari[134a], O. Lundberg[148a,148b], B. Lund-Jensen[149], M.S. Lutz[89], P.M. Luzi[83], D. Lynn[27], R. Lysak[129], E. Lytken[84], F. Lyu[35a], V. Lyubushkin[68], H. Ma[27], L.L. Ma[36b], Y. Ma[36b], G. Maccarrone[50], A. Macchiolo[103], C.M. Macdonald[141], B. Maček[78], J. Machado Miguens[124,128b], D. Madaffari[170], R. Madar[37], W.F. Mader[47], A. Madsen[45], N. Madysa[47], J. Maeda[70], S. Maeland[15], T. Maeno[27], A.S. Maevskiy[101], V. Magerl[51], C. Maiani[119], C. Maidantchik[26a], T. Maier[102], A. Maio[128a,128b,128d], O. Majersky[146a], S. Majewski[118], Y. Makida[69], N. Makovec[119], B. Malaescu[83], Pa. Malecki[42], V.P. Maleev[125], F. Malek[58], U. Mallik[66], D. Malon[6], C. Malone[30], S. Maltezos[10], S. Malyukov[32], J. Mamuzic[170], G. Mancini[50], I. Mandić[78], J. Maneira[128a,128b], L. Manhaes de Andrade Filho[26b], J. Manjarres Ramos[47], K.H. Mankinen[84], A. Mann[102], A. Manousos[32], B. Mansoulie[138], J.D. Mansour[35a], R. Mantifel[90], M. Mantoani[57], S. Manzoni[94a,94b], L. Mapelli[32], G. Marceca[29], L. March[52], L. Marchese[122], G. Marchiori[83], M. Marcisovsky[129], C.A. Marin Tobon[32], M. Marjanovic[37], D.E. Marley[92], F. Marroquim[26a], S.P. Marsden[87], Z. Marshall[16], M.U.F Martensson[168], S. Marti-Garcia[170], C.B. Martin[113], T.A. Martin[173], V.J. Martin[49], B. Martin dit Latour[15], M. Martinez[13,v], V.I. Martinez Outschoorn[169], S. Martin-Haugh[133], V.S. Martoiu[28b], A.C. Martyniuk[81], A. Marzin[32], L. Masetti[86], T. Mashimo[157], R. Mashinistov[98], J. Masik[87], A.L. Maslennikov[111,c], L.H. Mason[91], L. Massa[135a,135b], P. Mastrandrea[5], A. Mastroberardino[40a,40b], T. Masubuchi[157], P. Mättig[178], J. Maurer[28b], S.J. Maxfield[77], D.A. Maximov[111,c], R. Mazini[153], I. Maznas[156], S.M. Mazza[94a,94b], N.C. Mc Fadden[107], G. Mc Goldrick[161], S.P. Mc Kee[92], A. McCarn[92], R.L. McCarthy[150], T.G. McCarthy[103], L.I. McClymont[81], E.F. McDonald[91], J.A. Mcfayden[32], G. Mchedlidze[57], M.A. McKay[43], S.J. McMahon[133], P.C. McNamara[91], C.J. McNicol[173], R.A. McPherson[172,o], S. Meehan[140], T.J. Megy[51], S. Mehlhase[102], A. Mehta[77], T. Meideck[58], K. Meier[60a], B. Meirose[44], D. Melini[170,ah], B.R. Mellado Garcia[147c], J.D. Mellenthin[57], M. Melo[146a], F. Meloni[18], A. Melzer[23], S.B. Menary[87], L. Meng[77], X.T. Meng[92], A. Mengarelli[22a,22b], S. Menke[103], E. Meoni[40a,40b], S. Mergelmeyer[17], C. Merlassino[18], P. Mermod[52], L. Merola[106a,106b], C. Meroni[94a], F.S. Merritt[33], A. Messina[134a,134b], J. Metcalfe[6], A.S. Mete[166], C. Meyer[124], J-P. Meyer[138], J. Meyer[109], H. Meyer Zu Theenhausen[60a], F. Miano[151], R.P. Middleton[133], S. Miglioranzi[53a,53b], L. Mijović[49],

G. Mikenberg[175], M. Mikestikova[129], M. Mikuž[78], M. Milesi[91], A. Milic[161], D.A. Millar[79], D.W. Miller[33], C. Mills[49], A. Milov[175], D.A. Milstead[148a,148b], A.A. Minaenko[132], Y. Minami[157], I.A. Minashvili[54b], A.I. Mincer[112], B. Mindur[41a], M. Mineev[68], Y. Minegishi[157], Y. Ming[176], L.M. Mir[13], A. Mirto[76a,76b], K.P. Mistry[124], T. Mitani[174], J. Mitrevski[102], V.A. Mitsou[170], A. Miucci[18], P.S. Miyagawa[141], A. Mizukami[69], J.U. Mjörnmark[84], T. Mkrtchyan[180], M. Mlynarikova[131], T. Moa[148a,148b], K. Mochizuki[97], P. Mogg[51], S. Mohapatra[38], S. Molander[148a,148b], R. Moles-Valls[23], M.C. Mondragon[93], K. Mönig[45], J. Monk[39], E. Monnier[88], A. Montalbano[150], J. Montejo Berlingen[32], F. Monticelli[74], S. Monzani[94a,94b], R.W. Moore[3], N. Morange[119], D. Moreno[21], M. Moreno Llácer[32], P. Morettini[53a], S. Morgenstern[32], D. Mori[144], T. Mori[157], M. Morii[59], M. Morinaga[174], V. Morisbak[121], A.K. Morley[32], G. Mornacchi[32], J.D. Morris[79], L. Morvaj[150], P. Moschovakos[10], M. Mosidze[54b], H.J. Moss[141], J. Moss[145,ai], K. Motohashi[159], R. Mount[145], E. Mountricha[27], E.J.W. Moyse[89], S. Muanza[88], F. Mueller[103], J. Mueller[127], R.S.P. Mueller[102], D. Muenstermann[75], P. Mullen[56], G.A. Mullier[18], F.J. Munoz Sanchez[87], W.J. Murray[173,133], H. Musheghyan[32], M. Muškinja[78], A.G. Myagkov[132,aj], M. Myska[130], B.P. Nachman[16], O. Nackenhorst[52], K. Nagai[122], R. Nagai[69,ae], K. Nagano[69], Y. Nagasaka[61], K. Nagata[164], M. Nagel[51], E. Nagy[88], A.M. Nairz[32], Y. Nakahama[105], K. Nakamura[69], T. Nakamura[157], I. Nakano[114], R.F. Naranjo Garcia[45], R. Narayan[11], D.I. Narrias Villar[60a], I. Naryshkin[125], T. Naumann[45], G. Navarro[21], R. Nayyar[7], H.A. Neal[92], P.Yu. Nechaeva[98], T.J. Neep[138], A. Negri[123a,123b], M. Negrini[22a], S. Nektarijevic[108], C. Nellist[57], A. Nelson[166], M.E. Nelson[122], S. Nemecek[129], P. Nemethy[112], M. Nessi[32,ak], M.S. Neubauer[169], M. Neumann[178], P.R. Newman[19], T.Y. Ng[62c], Y.S. Ng[17], T. Nguyen Manh[97], R.B. Nickerson[122], R. Nicolaidou[138], J. Nielsen[139], N. Nikiforou[11], V. Nikolaenko[132,aj], I. Nikolic-Audit[83], K. Nikolopoulos[19], P. Nilsson[27], Y. Ninomiya[69], A. Nisati[134a], N. Nishu[36c], R. Nisius[103], I. Nitsche[46], T. Nitta[174], T. Nobe[157], Y. Noguchi[71], M. Nomachi[120], I. Nomidis[31], M.A. Nomura[27], T. Nooney[79], M. Nordberg[32], N. Norjoharuddeen[122], O. Novgorodova[47], M. Nozaki[69], L. Nozka[117], K. Ntekas[166], E. Nurse[81], F. Nuti[91], K. O'connor[25], D.C. O'Neil[144], A.A. O'Rourke[45], V. O'Shea[56], F.G. Oakham[31,d], H. Oberlack[103], T. Obermann[23], J. Ocariz[83], A. Ochi[70], I. Ochoa[38], J.P. Ochoa-Ricoux[34a], S. Oda[73], S. Odaka[69], A. Oh[87], S.H. Oh[48], C.C. Ohm[149], H. Ohman[168], H. Oide[53a,53b], H. Okawa[164], Y. Okumura[157], T. Okuyama[69], A. Olariu[28b], L.F. Oleiro Seabra[128a], S.A. Olivares Pino[34a], D. Oliveira Damazio[27], M.J.R. Olsson[33], A. Olszewski[42], J. Olszowska[42], A. Onofre[128a,128e], K. Onogi[105], P.U.E. Onyisi[11,aa], H. Oppen[121], M.J. Oreglia[33], Y. Oren[155], D. Orestano[136a,136b], N. Orlando[62b], R.S. Orr[161], B. Osculati[53a,53b,*], R. Ospanov[36a], G. Otero y Garzon[29], H. Otono[73], M. Ouchrif[137d], F. Ould-Saada[121], A. Ouraou[138], K.P. Oussoren[109], Q. Ouyang[35a], M. Owen[56], R.E. Owen[19], V.E. Ozcan[20a], N. Ozturk[8], K. Pachal[144], A. Pacheco Pages[13], L. Pacheco Rodriguez[138], C. Padilla Aranda[13], S. Pagan Griso[16], M. Paganini[179], F. Paige[27], G. Palacino[64], S. Palazzo[40a,40b], S. Palestini[32], M. Palka[41b], D. Pallin[37], E.St. Panagiotopoulou[10], I. Panagoulias[10], C.E. Pandini[52], J.G. Panduro Vazquez[80], P. Pani[32], S. Panitkin[27], D. Pantea[28b], L. Paolozzi[52], Th.D. Papadopoulou[10], K. Papageorgiou[9,s], A. Paramonov[6], D. Paredes Hernandez[179], A.J. Parker[75], M.A. Parker[30], K.A. Parker[45], F. Parodi[53a,53b], J.A. Parsons[38], U. Parzefall[51], V.R. Pascuzzi[161], J.M. Pasner[139], E. Pasqualucci[134a], S. Passaggio[53a], Fr. Pastore[80], S. Pataraia[86], J.R. Pater[87], T. Pauly[32], B. Pearson[103], S. Pedraza Lopez[170], R. Pedro[128a,128b], S.V. Peleganchuk[111,c], O. Penc[129], C. Peng[35a,35d], H. Peng[36a], J. Penwell[64], B.S. Peralva[26b], M.M. Perego[138], D.V. Perepelitsa[27], F. Peri[17], L. Perini[94a,94b], H. Pernegger[32], S. Perrella[106a,106b], R. Peschke[45], V.D. Peshekhonov[68,*], K. Peters[45], R.F.Y. Peters[87], B.A. Petersen[32], T.C. Petersen[39], E. Petit[58], A. Petridis[1], C. Petridou[156], P. Petroff[119], E. Petrolo[134a], M. Petrov[122], F. Petrucci[136a,136b], N.E. Pettersson[89], A. Peyaud[138], R. Pezoa[34b], F.H. Phillips[93], P.W. Phillips[133], G. Piacquadio[150], E. Pianori[173], A. Picazio[89], M.A. Pickering[122], R. Piegaia[29], J.E. Pilcher[33], A.D. Pilkington[87], M. Pinamonti[135a,135b], J.L. Pinfold[3], H. Pirumov[45], M. Pitt[175], L. Plazak[146a], M.-A. Pleier[27], V. Pleskot[86], E. Plotnikova[68], D. Pluth[67], P. Podberezko[111], R. Poettgen[84],

R. Poggi[123a,123b], L. Poggioli[119], I. Pogrebnyak[93], D. Pohl[23], I. Pokharel[57], G. Polesello[123a], A. Poley[45], A. Policicchio[40a,40b], R. Polifka[32], A. Polini[22a], C.S. Pollard[56], V. Polychronakos[27], K. Pommès[32], D. Ponomarenko[100], L. Pontecorvo[134a], G.A. Popeneciu[28d], D.M. Portillo Quintero[83], S. Pospisil[130], K. Potamianos[45], I.N. Potrap[68], C.J. Potter[30], H. Potti[11], T. Poulsen[84], J. Poveda[32], M.E. Pozo Astigarraga[32], P. Pralavorio[88], A. Pranko[16], S. Prell[67], D. Price[87], M. Primavera[76a], S. Prince[90], N. Proklova[100], K. Prokofiev[62c], F. Prokoshin[34b], S. Protopopescu[27], J. Proudfoot[6], M. Przybycien[41a], A. Puri[169], P. Puzo[119], J. Qian[92], G. Qin[56], Y. Qin[87], A. Quadt[57], M. Queitsch-Maitland[45], D. Quilty[56], S. Raddum[121], V. Radeka[27], V. Radescu[122], S.K. Radhakrishnan[150], P. Radloff[118], P. Rados[91], F. Ragusa[94a,94b], G. Rahal[181], J.A. Raine[87], S. Rajagopalan[27], C. Rangel-Smith[168], T. Rashid[119], S. Raspopov[5], M.G. Ratti[94a,94b], D.M. Rauch[45], F. Rauscher[102], S. Rave[86], I. Ravinovich[175], J.H. Rawling[87], M. Raymond[32], A.L. Read[121], N.P. Readioff[58], M. Reale[76a,76b], D.M. Rebuzzi[123a,123b], A. Redelbach[177], G. Redlinger[27], R. Reece[139], R.G. Reed[147c], K. Reeves[44], L. Rehnisch[17], J. Reichert[124], A. Reiss[86], C. Rembser[32], H. Ren[35a,35d], M. Rescigno[134a], S. Resconi[94a], E.D. Resseguie[124], S. Rettie[171], E. Reynolds[19], O.L. Rezanova[111,c], P. Reznicek[131], R. Rezvani[97], R. Richter[103], S. Richter[81], E. Richter-Was[41b], O. Ricken[23], M. Ridel[83], P. Rieck[103], C.J. Riegel[178], J. Rieger[57], O. Rifki[115], M. Rijssenbeek[150], A. Rimoldi[123a,123b], M. Rimoldi[18], L. Rinaldi[22a], G. Ripellino[149], B. Ristić[32], E. Ritsch[32], I. Riu[13], F. Rizatdinova[116], E. Rizvi[79], C. Rizzi[13], R.T. Roberts[87], S.H. Robertson[90,o], A. Robichaud-Veronneau[90], D. Robinson[30], J.E.M. Robinson[45], A. Robson[56], E. Rocco[86], C. Roda[126a,126b], Y. Rodina[88,al], S. Rodriguez Bosca[170], A. Rodriguez Perez[13], D. Rodriguez Rodriguez[170], S. Roe[32], C.S. Rogan[59], O. Røhne[121], J. Roloff[59], A. Romaniouk[100], M. Romano[22a,22b], S.M. Romano Saez[37], E. Romero Adam[170], N. Rompotis[77], M. Ronzani[51], L. Roos[83], S. Rosati[134a], K. Rosbach[51], P. Rose[139], N.-A. Rosien[57], E. Rossi[106a,106b], L.P. Rossi[53a], J.H.N. Rosten[30], R. Rosten[140], M. Rotaru[28b], J. Rothberg[140], D. Rousseau[119], A. Rozanov[88], Y. Rozen[154], X. Ruan[147c], F. Rubbo[145], F. Rühr[51], A. Ruiz-Martinez[31], Z. Rurikova[51], N.A. Rusakovich[68], H.L. Russell[90], J.P. Rutherfoord[7], N. Ruthmann[32], E.M. Rüttinger[45], Y.F. Ryabov[125], M. Rybar[169], G. Rybkin[119], S. Ryu[6], A. Ryzhov[132], G.F. Rzehorz[57], A.F. Saavedra[152], G. Sabato[109], S. Sacerdoti[29], H.F-W. Sadrozinski[139], R. Sadykov[68], F. Safai Tehrani[134a], P. Saha[110], M. Sahinsoy[60a], M. Saimpert[45], M. Saito[157], T. Saito[157], H. Sakamoto[157], Y. Sakurai[174], G. Salamanna[136a,136b], J.E. Salazar Loyola[34b], D. Salek[109], P.H. Sales De Bruin[168], D. Salihagic[103], A. Salnikov[145], J. Salt[170], D. Salvatore[40a,40b], F. Salvatore[151], A. Salvucci[62a,62b,62c], A. Salzburger[32], D. Sammel[51], D. Sampsonidis[156], D. Sampsonidou[156], J. Sánchez[170], V. Sanchez Martinez[170], A. Sanchez Pineda[167a,167c], H. Sandaker[121], R.L. Sandbach[79], C.O. Sander[45], M. Sandhoff[178], C. Sandoval[21], D.P.C. Sankey[133], M. Sannino[53a,53b], Y. Sano[105], A. Sansoni[50], C. Santoni[37], H. Santos[128a], I. Santoyo Castillo[151], A. Sapronov[68], J.G. Saraiva[128a,128d], B. Sarrazin[23], O. Sasaki[69], K. Sato[164], E. Sauvan[5], G. Savage[80], P. Savard[161,d], N. Savic[103], C. Sawyer[133], L. Sawyer[82,u], J. Saxon[33], C. Sbarra[22a], A. Sbrizzi[22a,22b], T. Scanlon[81], D.A. Scannicchio[166], J. Schaarschmidt[140], P. Schacht[103], B.M. Schachtner[102], D. Schaefer[33], L. Schaefer[124], R. Schaefer[45], J. Schaeffer[86], S. Schaepe[32], S. Schaetzel[60b], U. Schäfer[86], A.C. Schaffer[119], D. Schaile[102], R.D. Schamberger[150], V.A. Schegelsky[125], D. Scheirich[131], F. Schenck[17], M. Schernau[166], C. Schiavi[53a,53b], S. Schier[139], L.K. Schildgen[23], C. Schillo[51], M. Schioppa[40a,40b], S. Schlenker[32], K.R. Schmidt-Sommerfeld[103], K. Schmieden[32], C. Schmitt[86], S. Schmitt[45], S. Schmitz[86], U. Schnoor[51], L. Schoeffel[138], A. Schoening[60b], B.D. Schoenrock[93], E. Schopf[23], M. Schott[86], J.F.P. Schouwenberg[108], J. Schovancova[32], S. Schramm[52], N. Schuh[86], A. Schulte[86], M.J. Schultens[23], H.-C. Schultz-Coulon[60a], H. Schulz[17], M. Schumacher[51], B.A. Schumm[139], Ph. Schune[138], A. Schwartzman[145], T.A. Schwarz[92], H. Schweiger[87], Ph. Schwemling[138], R. Schwienhorst[93], J. Schwindling[138], A. Sciandra[23], G. Sciolla[25], M. Scornajenghi[40a,40b], F. Scuri[126a,126b], F. Scutti[91], J. Searcy[92], P. Seema[23], S.C. Seidel[107], A. Seiden[139], J.M. Seixas[26a], G. Sekhniaidze[106a], K. Sekhon[92], S.J. Sekula[43], N. Semprini-Cesari[22a,22b],

S. Senkin[37], C. Serfon[121], L. Serin[119], L. Serkin[167a,167b], M. Sessa[136a,136b], R. Seuster[172], H. Severini[115], T. Sfiligoj[78], F. Sforza[165], A. Sfyrla[52], E. Shabalina[57], N.W. Shaikh[148a,148b], L.Y. Shan[35a], R. Shang[169], J.T. Shank[24], M. Shapiro[16], P.B. Shatalov[99], K. Shaw[167a,167b], S.M. Shaw[87], A. Shcherbakova[148a,148b], C.Y. Shehu[151], Y. Shen[115], N. Sherafati[31], A.D. Sherman[24], P. Sherwood[81], L. Shi[153,am], S. Shimizu[70], C.O. Shimmin[179], M. Shimojima[104], I.P.J. Shipsey[122], S. Shirabe[73], M. Shiyakova[68,an], J. Shlomi[175], A. Shmeleva[98], D. Shoaleh Saadi[97], M.J. Shochet[33], S. Shojaii[94a,94b], D.R. Shope[115], S. Shrestha[113], E. Shulga[100], M.A. Shupe[7], P. Sicho[129], A.M. Sickles[169], P.E. Sidebo[149], E. Sideras Haddad[147c], O. Sidiropoulou[177], A. Sidoti[22a,22b], F. Siegert[47], Dj. Sijacki[14], J. Silva[128a,128d], S.B. Silverstein[148a], V. Simak[130], L. Simic[68], S. Simion[119], E. Simioni[86], B. Simmons[81], M. Simon[86], P. Sinervo[161], N.B. Sinev[118], M. Sioli[22a,22b], G. Siragusa[177], I. Siral[92], S.Yu. Sivoklokov[101], J. Sjölin[148a,148b], M.B. Skinner[75], P. Skubic[115], M. Slater[19], T. Slavicek[130], M. Slawinska[42], K. Sliwa[165], R. Slovak[131], V. Smakhtin[175], B.H. Smart[5], J. Smiesko[146a], N. Smirnov[100], S.Yu. Smirnov[100], Y. Smirnov[100], L.N. Smirnova[101,ao], O. Smirnova[84], J.W. Smith[57], M.N.K. Smith[38], R.W. Smith[38], M. Smizanska[75], K. Smolek[130], A.A. Snesarev[98], I.M. Snyder[118], S. Snyder[27], R. Sobie[172,o], F. Socher[47], A. Soffer[155], A. Søgaard[49], D.A. Soh[153], G. Sokhrannyi[78], C.A. Solans Sanchez[32], M. Solar[130], E.Yu. Soldatov[100], U. Soldevila[170], A.A. Solodkov[132], A. Soloshenko[68], O.V. Solovyanov[132], V. Solovyev[125], P. Sommer[141], H. Son[165], A. Sopczak[130], D. Sosa[60b], C.L. Sotiropoulou[126a,126b], S. Sottocornola[123a,123b], R. Soualah[167a,167c], A.M. Soukharev[111,c], D. South[45], B.C. Sowden[80], S. Spagnolo[76a,76b], M. Spalla[126a,126b], M. Spangenberg[173], F. Spanò[80], D. Sperlich[17], F. Spettel[103], T.M. Spieker[60a], R. Spighi[22a], G. Spigo[32], L.A. Spiller[91], M. Spousta[131], R.D. St. Denis[56,*], A. Stabile[94a], R. Stamen[60a], S. Stamm[17], E. Stanecka[42], R.W. Stanek[6], C. Stanescu[136a], M.M. Stanitzki[45], B.S. Stapf[109], S. Stapnes[121], E.A. Starchenko[132], G.H. Stark[33], J. Stark[58], S.H Stark[39], P. Staroba[129], P. Starovoitov[60a], S. Stärz[32], R. Staszewski[42], M. Stegler[45], P. Steinberg[27], B. Stelzer[144], H.J. Stelzer[32], O. Stelzer-Chilton[163a], H. Stenzel[55], T.J. Stevenson[79], G.A. Stewart[56], M.C. Stockton[118], M. Stoebe[90], G. Stoicea[28b], P. Stolte[57], S. Stonjek[103], A.R. Stradling[8], A. Straessner[47], M.E. Stramaglia[18], J. Strandberg[149], S. Strandberg[148a,148b], M. Strauss[115], P. Strizenec[146b], R. Ströhmer[177], D.M. Strom[118], R. Stroynowski[43], A. Strubig[49], S.A. Stucci[27], B. Stugu[15], N.A. Styles[45], D. Su[145], J. Su[127], S. Suchek[60a], Y. Sugaya[120], M. Suk[130], V.V. Sulin[98], DMS Sultan[162a,162b], S. Sultansoy[4c], T. Sumida[71], S. Sun[59], X. Sun[3], K. Suruliz[151], C.J.E. Suster[152], M.R. Sutton[151], S. Suzuki[69], M. Svatos[129], M. Swiatlowski[33], S.P. Swift[2], I. Sykora[146a], T. Sykora[131], D. Ta[51], K. Tackmann[45], J. Taenzer[155], A. Taffard[166], R. Tafirout[163a], E. Tahirovic[79], N. Taiblum[155], H. Takai[27], R. Takashima[72], E.H. Takasugi[103], K. Takeda[70], T. Takeshita[142], Y. Takubo[69], M. Talby[88], A.A. Talyshev[111,c], J. Tanaka[157], M. Tanaka[159], R. Tanaka[119], S. Tanaka[69], R. Tanioka[70], B.B. Tannenwald[113], S. Tapia Araya[34b], S. Tapprogge[86], S. Tarem[154], G.F. Tartarelli[94a], P. Tas[131], M. Tasevsky[129], T. Tashiro[71], E. Tassi[40a,40b], A. Tavares Delgado[128a,128b], Y. Tayalati[137e], A.C. Taylor[107], A.J. Taylor[49], G.N. Taylor[91], P.T.E. Taylor[91], W. Taylor[163b], P. Teixeira-Dias[80], D. Temple[144], H. Ten Kate[32], P.K. Teng[153], J.J. Teoh[120], F. Tepel[178], S. Terada[69], K. Terashi[157], J. Terron[85], S. Terzo[13], M. Testa[50], R.J. Teuscher[161,o], S.J. Thais[179], T. Theveneaux-Pelzer[88], F. Thiele[39], J.P. Thomas[19], J. Thomas-Wilsker[80], P.D. Thompson[19], A.S. Thompson[56], L.A. Thomsen[179], E. Thomson[124], Y. Tian[38], M.J. Tibbetts[16], R.E. Ticse Torres[57], V.O. Tikhomirov[98,ap], Yu.A. Tikhonov[111,c], S. Timoshenko[100], P. Tipton[179], S. Tisserant[88], K. Todome[159], S. Todorova-Nova[5], S. Todt[47], J. Tojo[73], S. Tokár[146a], K. Tokushuku[69], E. Tolley[113], L. Tomlinson[87], M. Tomoto[105], L. Tompkins[145,aq], K. Toms[107], B. Tong[59], P. Tornambe[51], E. Torrence[118], H. Torres[47], E. Torró Pastor[140], J. Toth[88,ar], F. Touchard[88], D.R. Tovey[141], C.J. Treado[112], T. Trefzger[177], F. Tresoldi[151], A. Tricoli[27], I.M. Trigger[163a], S. Trincaz-Duvoid[83], M.F. Tripiana[13], W. Trischuk[161], B. Trocmé[58], A. Trofymov[45], C. Troncon[94a], M. Trottier-McDonald[16], M. Trovatelli[172], L. Truong[147b], M. Trzebinski[42], A. Trzupek[42], K.W. Tsang[62a], J.C-L. Tseng[122], P.V. Tsiareshka[95], G. Tsipolitis[10], N. Tsirintanis[9], S. Tsiskaridze[13], V. Tsiskaridze[51], E.G. Tskhadadze[54a],

I.I. Tsukerman[99], V. Tsulaia[16], S. Tsuno[69], D. Tsybychev[150], Y. Tu[62b], A. Tudorache[28b], V. Tudorache[28b], T.T. Tulbure[28a], A.N. Tuna[59], S. Turchikhin[68], D. Turgeman[175], I. Turk Cakir[4b,as], R. Turra[94a], P.M. Tuts[38], G. Ucchielli[22a,22b], I. Ueda[69], M. Ughetto[148a,148b], F. Ukegawa[164], G. Unal[32], A. Undrus[27], G. Unel[166], F.C. Ungaro[91], Y. Unno[69], K. Uno[157], C. Unverdorben[102], J. Urban[146b], P. Urquijo[91], P. Urrejola[86], G. Usai[8], J. Usui[69], L. Vacavant[88], V. Vacek[130], B. Vachon[90], K.O.H. Vadla[121], A. Vaidya[81], C. Valderanis[102], E. Valdes Santurio[148a,148b], M. Valente[52], S. Valentinetti[22a,22b], A. Valero[170], L. Valéry[13], S. Valkar[131], A. Vallier[5], J.A. Valls Ferrer[170], W. Van Den Wollenberg[109], H. van der Graaf[109], P. van Gemmeren[6], J. Van Nieuwkoop[144], I. van Vulpen[109], M.C. van Woerden[109], M. Vanadia[135a,135b], W. Vandelli[32], A. Vaniachine[160], P. Vankov[109], G. Vardanyan[180], R. Vari[134a], E.W. Varnes[7], C. Varni[53a,53b], T. Varol[43], D. Varouchas[119], A. Vartapetian[8], K.E. Varvell[152], J.G. Vasquez[179], G.A. Vasquez[34b], F. Vazeille[37], D. Vazquez Furelos[13], T. Vazquez Schroeder[90], J. Veatch[57], V. Veeraraghavan[7], L.M. Veloce[161], F. Veloso[128a,128c], S. Veneziano[134a], A. Ventura[76a,76b], M. Venturi[172], N. Venturi[32], A. Venturini[25], V. Vercesi[123a], M. Verducci[136a,136b], W. Verkerke[109], A.T. Vermeulen[109], J.C. Vermeulen[109], M.C. Vetterli[144,d], N. Viaux Maira[34b], O. Viazlo[84], I. Vichou[169,*], T. Vickey[141], O.E. Vickey Boeriu[141], G.H.A. Viehhauser[122], S. Viel[16], L. Vigani[122], M. Villa[22a,22b], M. Villaplana Perez[94a,94b], E. Vilucchi[50], M.G. Vincter[31], V.B. Vinogradov[68], A. Vishwakarma[45], C. Vittori[22a,22b], I. Vivarelli[151], S. Vlachos[10], M. Vogel[178], P. Vokac[130], G. Volpi[13], H. von der Schmitt[103], E. von Toerne[23], V. Vorobel[131], K. Vorobev[100], M. Vos[170], R. Voss[32], J.H. Vossebeld[77], N. Vranjes[14], M. Vranjes Milosavljevic[14], V. Vrba[130], M. Vreeswijk[109], R. Vuillermet[32], I. Vukotic[33], P. Wagner[23], W. Wagner[178], J. Wagner-Kuhr[102], H. Wahlberg[74], S. Wahrmund[47], K. Wakamiya[70], V.M. Walbrecht[103], J. Walder[75], R. Walker[102], W. Walkowiak[143], V. Wallangen[148a,148b], C. Wang[35b], C. Wang[36b,at], F. Wang[176], H. Wang[16], H. Wang[3], J. Wang[45], J. Wang[152], Q. Wang[115], R.-J. Wang[83], R. Wang[6], S.M. Wang[153], T. Wang[38], W. Wang[153,au], W. Wang[36a,av], Z. Wang[36c], C. Wanotayaroj[45], A. Warburton[90], C.P. Ward[30], D.R. Wardrope[81], A. Washbrook[49], P.M. Watkins[19], A.T. Watson[19], M.F. Watson[19], G. Watts[140], S. Watts[87], B.M. Waugh[81], A.F. Webb[11], S. Webb[86], M.S. Weber[18], S.M. Weber[60a], S.W. Weber[177], S.A. Weber[31], J.S. Webster[6], A.R. Weidberg[122], B. Weinert[64], J. Weingarten[57], M. Weirich[86], C. Weiser[51], H. Weits[109], P.S. Wells[32], T. Wenaus[27], T. Wengler[32], S. Wenig[32], N. Wermes[23], M.D. Werner[67], P. Werner[32], M. Wessels[60a], T.D. Weston[18], K. Whalen[118], N.L. Whallon[140], A.M. Wharton[75], A.S. White[92], A. White[8], M.J. White[1], R. White[34b], D. Whiteson[166], B.W. Whitmore[75], F.J. Wickens[133], W. Wiedenmann[176], M. Wielers[133], C. Wiglesworth[39], L.A.M. Wiik-Fuchs[51], A. Wildauer[103], F. Wilk[87], H.G. Wilkens[32], H.H. Williams[124], S. Williams[109], C. Willis[93], S. Willocq[89], J.A. Wilson[19], I. Wingerter-Seez[5], E. Winkels[151], F. Winklmeier[118], O.J. Winston[151], B.T. Winter[23], M. Wittgen[145], M. Wobisch[82,u], A. Wolf[86], T.M.H. Wolf[109], R. Wolff[88], M.W. Wolter[42], H. Wolters[128a,128c], V.W.S. Wong[171], N.L. Woods[139], S.D. Worm[19], B.K. Wosiek[42], J. Wotschack[32], K.W. Wozniak[42], M. Wu[33], S.L. Wu[176], X. Wu[52], Y. Wu[92], T.R. Wyatt[87], B.M. Wynne[49], S. Xella[39], Z. Xi[92], L. Xia[35c], D. Xu[35a], L. Xu[27], T. Xu[138], W. Xu[92], B. Yabsley[152], S. Yacoob[147a], D. Yamaguchi[159], Y. Yamaguchi[159], A. Yamamoto[69], S. Yamamoto[157], T. Yamanaka[157], F. Yamane[70], M. Yamatani[157], T. Yamazaki[157], Y. Yamazaki[70], Z. Yan[24], H. Yang[36c], H. Yang[16], Y. Yang[153], Z. Yang[15], W-M. Yao[16], Y.C. Yap[45], Y. Yasu[69], E. Yatsenko[5], K.H. Yau Wong[23], J. Ye[43], S. Ye[27], I. Yeletskikh[68], E. Yigitbasi[24], E. Yildirim[86], K. Yorita[174], K. Yoshihara[124], C. Young[145], C.J.S. Young[32], J. Yu[8], J. Yu[67], S.P.Y. Yuen[23], I. Yusuff[30,aw], B. Zabinski[42], G. Zacharis[10], R. Zaidan[13], A.M. Zaitsev[132,aj], N. Zakharchuk[45], J. Zalieckas[15], A. Zaman[150], S. Zambito[59], D. Zanzi[91], C. Zeitnitz[178], G. Zemaityte[122], A. Zemla[41a], J.C. Zeng[169], Q. Zeng[145], O. Zenin[132], T. Ženiš[146a], D. Zerwas[119], D. Zhang[36b], D. Zhang[92], F. Zhang[176], G. Zhang[36a,av], H. Zhang[119], J. Zhang[6], L. Zhang[51], L. Zhang[36a], M. Zhang[169], P. Zhang[35b], R. Zhang[23], R. Zhang[36a,at], X. Zhang[36b], Y. Zhang[35a,35d], Z. Zhang[119], X. Zhao[43], Y. Zhao[36b,ax], Z. Zhao[36a], A. Zhemchugov[68], B. Zhou[92], C. Zhou[176], L. Zhou[43], M. Zhou[35a,35d], M. Zhou[150], N. Zhou[36c], Y. Zhou[7],

C.G. Zhu[36b], H. Zhu[35a], J. Zhu[92], Y. Zhu[36a], X. Zhuang[35a], K. Zhukov[98], A. Zibell[177], D. Zieminska[64], N.I. Zimine[68], C. Zimmermann[86], S. Zimmermann[51], Z. Zinonos[103], M. Zinser[86], M. Ziolkowski[143], L. Živković[14], G. Zobernig[176], A. Zoccoli[22a,22b], R. Zou[33], M. zur Nedden[17], L. Zwalinski[32].

[1] Department of Physics, University of Adelaide, Adelaide, Australia
[2] Physics Department, SUNY Albany, Albany NY, United States of America
[3] Department of Physics, University of Alberta, Edmonton AB, Canada
[4] [(a)] Department of Physics, Ankara University, Ankara; [(b)] Istanbul Aydin University, Istanbul; [(c)] Division of Physics, TOBB University of Economics and Technology, Ankara, Turkey
[5] LAPP, CNRS/IN2P3 and Université Savoie Mont Blanc, Annecy-le-Vieux, France
[6] High Energy Physics Division, Argonne National Laboratory, Argonne IL, United States of America
[7] Department of Physics, University of Arizona, Tucson AZ, United States of America
[8] Department of Physics, The University of Texas at Arlington, Arlington TX, United States of America
[9] Physics Department, National and Kapodistrian University of Athens, Athens, Greece
[10] Physics Department, National Technical University of Athens, Zografou, Greece
[11] Department of Physics, The University of Texas at Austin, Austin TX, United States of America
[12] Institute of Physics, Azerbaijan Academy of Sciences, Baku, Azerbaijan
[13] Institut de Física d'Altes Energies (IFAE), The Barcelona Institute of Science and Technology, Barcelona, Spain
[14] Institute of Physics, University of Belgrade, Belgrade, Serbia
[15] Department for Physics and Technology, University of Bergen, Bergen, Norway
[16] Physics Division, Lawrence Berkeley National Laboratory and University of California, Berkeley CA, United States of America
[17] Department of Physics, Humboldt University, Berlin, Germany
[18] Albert Einstein Center for Fundamental Physics and Laboratory for High Energy Physics, University of Bern, Bern, Switzerland
[19] School of Physics and Astronomy, University of Birmingham, Birmingham, United Kingdom
[20] [(a)] Department of Physics, Bogazici University, Istanbul; [(b)] Department of Physics Engineering, Gaziantep University, Gaziantep; [(d)] Istanbul Bilgi University, Faculty of Engineering and Natural Sciences, Istanbul; [(e)] Bahcesehir University, Faculty of Engineering and Natural Sciences, Istanbul, Turkey
[21] Centro de Investigaciones, Universidad Antonio Narino, Bogota, Colombia
[22] [(a)] INFN Sezione di Bologna; [(b)] Dipartimento di Fisica e Astronomia, Università di Bologna, Bologna, Italy
[23] Physikalisches Institut, University of Bonn, Bonn, Germany
[24] Department of Physics, Boston University, Boston MA, United States of America
[25] Department of Physics, Brandeis University, Waltham MA, United States of America
[26] [(a)] Universidade Federal do Rio De Janeiro COPPE/EE/IF, Rio de Janeiro; [(b)] Electrical Circuits Department, Federal University of Juiz de Fora (UFJF), Juiz de Fora; [(c)] Federal University of Sao Joao del Rei (UFSJ), Sao Joao del Rei; [(d)] Instituto de Fisica, Universidade de Sao Paulo, Sao Paulo, Brazil
[27] Physics Department, Brookhaven National Laboratory, Upton NY, United States of America
[28] [(a)] Transilvania University of Brasov, Brasov; [(b)] Horia Hulubei National Institute of Physics and Nuclear Engineering, Bucharest; [(c)] Department of Physics, Alexandru Ioan Cuza University of Iasi, Iasi; [(d)] National Institute for Research and Development of Isotopic and Molecular Technologies, Physics Department, Cluj Napoca; [(e)] University Politehnica Bucharest, Bucharest; [(f)] West University in Timisoara, Timisoara, Romania
[29] Departamento de Física, Universidad de Buenos Aires, Buenos Aires, Argentina

[30] Cavendish Laboratory, University of Cambridge, Cambridge, United Kingdom
[31] Department of Physics, Carleton University, Ottawa ON, Canada
[32] CERN, Geneva, Switzerland
[33] Enrico Fermi Institute, University of Chicago, Chicago IL, United States of America
[34] [(a)] Departamento de Física, Pontificia Universidad Católica de Chile, Santiago; [(b)] Departamento de Física, Universidad Técnica Federico Santa María, Valparaíso, Chile
[35] [(a)] Institute of High Energy Physics, Chinese Academy of Sciences, Beijing; [(b)] Department of Physics, Nanjing University, Jiangsu; [(c)] Physics Department, Tsinghua University, Beijing 100084; [(d)] University of Chinese Academy of Science (UCAS), Beijing, China
[36] [(a)] Department of Modern Physics and State Key Laboratory of Particle Detection and Electronics, University of Science and Technology of China, Anhui; [(b)] School of Physics, Shandong University, Shandong; [(c)] Department of Physics and Astronomy, Key Laboratory for Particle Physics, Astrophysics and Cosmology, Ministry of Education; Shanghai Key Laboratory for Particle Physics and Cosmology, Shanghai Jiao Tong University, Tsung-Dao Lee Institute, China
[37] Université Clermont Auvergne, CNRS/IN2P3, LPC, Clermont-Ferrand, France
[38] Nevis Laboratory, Columbia University, Irvington NY, United States of America
[39] Niels Bohr Institute, University of Copenhagen, Kobenhavn, Denmark
[40] [(a)] INFN Gruppo Collegato di Cosenza, Laboratori Nazionali di Frascati; [(b)] Dipartimento di Fisica, Università della Calabria, Rende, Italy
[41] [(a)] AGH University of Science and Technology, Faculty of Physics and Applied Computer Science, Krakow; [(b)] Marian Smoluchowski Institute of Physics, Jagiellonian University, Krakow, Poland
[42] Institute of Nuclear Physics Polish Academy of Sciences, Krakow, Poland
[43] Physics Department, Southern Methodist University, Dallas TX, United States of America
[44] Physics Department, University of Texas at Dallas, Richardson TX, United States of America
[45] DESY, Hamburg and Zeuthen, Germany
[46] Lehrstuhl für Experimentelle Physik IV, Technische Universität Dortmund, Dortmund, Germany
[47] Institut für Kern- und Teilchenphysik, Technische Universität Dresden, Dresden, Germany
[48] Department of Physics, Duke University, Durham NC, United States of America
[49] SUPA - School of Physics and Astronomy, University of Edinburgh, Edinburgh, United Kingdom
[50] INFN e Laboratori Nazionali di Frascati, Frascati, Italy
[51] Fakultät für Mathematik und Physik, Albert-Ludwigs-Universität, Freiburg, Germany
[52] Departement de Physique Nucleaire et Corpusculaire, Université de Genève, Geneva, Switzerland
[53] [(a)] INFN Sezione di Genova; [(b)] Dipartimento di Fisica, Università di Genova, Genova, Italy
[54] [(a)] E. Andronikashvili Institute of Physics, Iv. Javakhishvili Tbilisi State University, Tbilisi; [(b)] High Energy Physics Institute, Tbilisi State University, Tbilisi, Georgia
[55] II Physikalisches Institut, Justus-Liebig-Universität Giessen, Giessen, Germany
[56] SUPA - School of Physics and Astronomy, University of Glasgow, Glasgow, United Kingdom
[57] II Physikalisches Institut, Georg-August-Universität, Göttingen, Germany
[58] Laboratoire de Physique Subatomique et de Cosmologie, Université Grenoble-Alpes, CNRS/IN2P3, Grenoble, France
[59] Laboratory for Particle Physics and Cosmology, Harvard University, Cambridge MA, United States of America
[60] [(a)] Kirchhoff-Institut für Physik, Ruprecht-Karls-Universität Heidelberg, Heidelberg; [(b)] Physikalisches Institut, Ruprecht-Karls-Universität Heidelberg, Heidelberg, Germany
[61] Faculty of Applied Information Science, Hiroshima Institute of Technology, Hiroshima, Japan
[62] [(a)] Department of Physics, The Chinese University of Hong Kong, Shatin, N.T., Hong Kong; [(b)] Department of Physics, The University of Hong Kong, Hong Kong; [(c)] Department of Physics and

Institute for Advanced Study, The Hong Kong University of Science and Technology, Clear Water Bay, Kowloon, Hong Kong, China
[63] Department of Physics, National Tsing Hua University, Taiwan, Taiwan
[64] Department of Physics, Indiana University, Bloomington IN, United States of America
[65] Institut für Astro- und Teilchenphysik, Leopold-Franzens-Universität, Innsbruck, Austria
[66] University of Iowa, Iowa City IA, United States of America
[67] Department of Physics and Astronomy, Iowa State University, Ames IA, United States of America
[68] Joint Institute for Nuclear Research, JINR Dubna, Dubna, Russia
[69] KEK, High Energy Accelerator Research Organization, Tsukuba, Japan
[70] Graduate School of Science, Kobe University, Kobe, Japan
[71] Faculty of Science, Kyoto University, Kyoto, Japan
[72] Kyoto University of Education, Kyoto, Japan
[73] Research Center for Advanced Particle Physics and Department of Physics, Kyushu University, Fukuoka, Japan
[74] Instituto de Física La Plata, Universidad Nacional de La Plata and CONICET, La Plata, Argentina
[75] Physics Department, Lancaster University, Lancaster, United Kingdom
[76] [(a)] INFN Sezione di Lecce; [(b)] Dipartimento di Matematica e Fisica, Università del Salento, Lecce, Italy
[77] Oliver Lodge Laboratory, University of Liverpool, Liverpool, United Kingdom
[78] Department of Experimental Particle Physics, Jožef Stefan Institute and Department of Physics, University of Ljubljana, Ljubljana, Slovenia
[79] School of Physics and Astronomy, Queen Mary University of London, London, United Kingdom
[80] Department of Physics, Royal Holloway University of London, Surrey, United Kingdom
[81] Department of Physics and Astronomy, University College London, London, United Kingdom
[82] Louisiana Tech University, Ruston LA, United States of America
[83] Laboratoire de Physique Nucléaire et de Hautes Energies, UPMC and Université Paris-Diderot and CNRS/IN2P3, Paris, France
[84] Fysiska institutionen, Lunds universitet, Lund, Sweden
[85] Departamento de Fisica Teorica C-15, Universidad Autonoma de Madrid, Madrid, Spain
[86] Institut für Physik, Universität Mainz, Mainz, Germany
[87] School of Physics and Astronomy, University of Manchester, Manchester, United Kingdom
[88] CPPM, Aix-Marseille Université and CNRS/IN2P3, Marseille, France
[89] Department of Physics, University of Massachusetts, Amherst MA, United States of America
[90] Department of Physics, McGill University, Montreal QC, Canada
[91] School of Physics, University of Melbourne, Victoria, Australia
[92] Department of Physics, The University of Michigan, Ann Arbor MI, United States of America
[93] Department of Physics and Astronomy, Michigan State University, East Lansing MI, United States of America
[94] [(a)] INFN Sezione di Milano; [(b)] Dipartimento di Fisica, Università di Milano, Milano, Italy
[95] B.I. Stepanov Institute of Physics, National Academy of Sciences of Belarus, Minsk, Republic of Belarus
[96] Research Institute for Nuclear Problems of Byelorussian State University, Minsk, Republic of Belarus
[97] Group of Particle Physics, University of Montreal, Montreal QC, Canada
[98] P.N. Lebedev Physical Institute of the Russian Academy of Sciences, Moscow, Russia
[99] Institute for Theoretical and Experimental Physics (ITEP), Moscow, Russia
[100] National Research Nuclear University MEPhI, Moscow, Russia
[101] D.V. Skobeltsyn Institute of Nuclear Physics, M.V. Lomonosov Moscow State University, Moscow,

Russia
[102] Fakultät für Physik, Ludwig-Maximilians-Universität München, München, Germany
[103] Max-Planck-Institut für Physik (Werner-Heisenberg-Institut), München, Germany
[104] Nagasaki Institute of Applied Science, Nagasaki, Japan
[105] Graduate School of Science and Kobayashi-Maskawa Institute, Nagoya University, Nagoya, Japan
[106] [(a)] INFN Sezione di Napoli; [(b)] Dipartimento di Fisica, Università di Napoli, Napoli, Italy
[107] Department of Physics and Astronomy, University of New Mexico, Albuquerque NM, United States of America
[108] Institute for Mathematics, Astrophysics and Particle Physics, Radboud University Nijmegen/Nikhef, Nijmegen, Netherlands
[109] Nikhef National Institute for Subatomic Physics and University of Amsterdam, Amsterdam, Netherlands
[110] Department of Physics, Northern Illinois University, DeKalb IL, United States of America
[111] Budker Institute of Nuclear Physics, SB RAS, Novosibirsk, Russia
[112] Department of Physics, New York University, New York NY, United States of America
[113] Ohio State University, Columbus OH, United States of America
[114] Faculty of Science, Okayama University, Okayama, Japan
[115] Homer L. Dodge Department of Physics and Astronomy, University of Oklahoma, Norman OK, United States of America
[116] Department of Physics, Oklahoma State University, Stillwater OK, United States of America
[117] Palacký University, RCPTM, Olomouc, Czech Republic
[118] Center for High Energy Physics, University of Oregon, Eugene OR, United States of America
[119] LAL, Univ. Paris-Sud, CNRS/IN2P3, Université Paris-Saclay, Orsay, France
[120] Graduate School of Science, Osaka University, Osaka, Japan
[121] Department of Physics, University of Oslo, Oslo, Norway
[122] Department of Physics, Oxford University, Oxford, United Kingdom
[123] [(a)] INFN Sezione di Pavia; [(b)] Dipartimento di Fisica, Università di Pavia, Pavia, Italy
[124] Department of Physics, University of Pennsylvania, Philadelphia PA, United States of America
[125] National Research Centre "Kurchatov Institute" B.P.Konstantinov Petersburg Nuclear Physics Institute, St. Petersburg, Russia
[126] [(a)] INFN Sezione di Pisa; [(b)] Dipartimento di Fisica E. Fermi, Università di Pisa, Pisa, Italy
[127] Department of Physics and Astronomy, University of Pittsburgh, Pittsburgh PA, United States of America
[128] [(a)] Laboratório de Instrumentação e Física Experimental de Partículas - LIP, Lisboa; [(b)] Faculdade de Ciências, Universidade de Lisboa, Lisboa; [(c)] Department of Physics, University of Coimbra, Coimbra; [(d)] Centro de Física Nuclear da Universidade de Lisboa, Lisboa; [(e)] Departamento de Fisica, Universidade do Minho, Braga; [(f)] Departamento de Fisica Teorica y del Cosmos, Universidad de Granada, Granada; [(g)] Dep Fisica and CEFITEC of Faculdade de Ciencias e Tecnologia, Universidade Nova de Lisboa, Caparica, Portugal
[129] Institute of Physics, Academy of Sciences of the Czech Republic, Praha, Czech Republic
[130] Czech Technical University in Prague, Praha, Czech Republic
[131] Charles University, Faculty of Mathematics and Physics, Prague, Czech Republic
[132] State Research Center Institute for High Energy Physics (Protvino), NRC KI, Russia
[133] Particle Physics Department, Rutherford Appleton Laboratory, Didcot, United Kingdom
[134] [(a)] INFN Sezione di Roma; [(b)] Dipartimento di Fisica, Sapienza Università di Roma, Roma, Italy
[135] [(a)] INFN Sezione di Roma Tor Vergata; [(b)] Dipartimento di Fisica, Università di Roma Tor Vergata, Roma, Italy

[136] [(a)] INFN Sezione di Roma Tre; [(b)] Dipartimento di Matematica e Fisica, Università Roma Tre, Roma, Italy
[137] [(a)] Faculté des Sciences Ain Chock, Réseau Universitaire de Physique des Hautes Energies - Université Hassan II, Casablanca; [(b)] Centre National de l'Energie des Sciences Techniques Nucleaires, Rabat; [(c)] Faculté des Sciences Semlalia, Université Cadi Ayyad, LPHEA-Marrakech; [(d)] Faculté des Sciences, Université Mohamed Premier and LPTPM, Oujda; [(e)] Faculté des sciences, Université Mohammed V, Rabat, Morocco
[138] DSM/IRFU (Institut de Recherches sur les Lois Fondamentales de l'Univers), CEA Saclay (Commissariat à l'Energie Atomique et aux Energies Alternatives), Gif-sur-Yvette, France
[139] Santa Cruz Institute for Particle Physics, University of California Santa Cruz, Santa Cruz CA, United States of America
[140] Department of Physics, University of Washington, Seattle WA, United States of America
[141] Department of Physics and Astronomy, University of Sheffield, Sheffield, United Kingdom
[142] Department of Physics, Shinshu University, Nagano, Japan
[143] Department Physik, Universität Siegen, Siegen, Germany
[144] Department of Physics, Simon Fraser University, Burnaby BC, Canada
[145] SLAC National Accelerator Laboratory, Stanford CA, United States of America
[146] [(a)] Faculty of Mathematics, Physics & Informatics, Comenius University, Bratislava; [(b)] Department of Subnuclear Physics, Institute of Experimental Physics of the Slovak Academy of Sciences, Kosice, Slovak Republic
[147] [(a)] Department of Physics, University of Cape Town, Cape Town; [(b)] Department of Physics, University of Johannesburg, Johannesburg; [(c)] School of Physics, University of the Witwatersrand, Johannesburg, South Africa
[148] [(a)] Department of Physics, Stockholm University; [(b)] The Oskar Klein Centre, Stockholm, Sweden
[149] Physics Department, Royal Institute of Technology, Stockholm, Sweden
[150] Departments of Physics & Astronomy and Chemistry, Stony Brook University, Stony Brook NY, United States of America
[151] Department of Physics and Astronomy, University of Sussex, Brighton, United Kingdom
[152] School of Physics, University of Sydney, Sydney, Australia
[153] Institute of Physics, Academia Sinica, Taipei, Taiwan
[154] Department of Physics, Technion: Israel Institute of Technology, Haifa, Israel
[155] Raymond and Beverly Sackler School of Physics and Astronomy, Tel Aviv University, Tel Aviv, Israel
[156] Department of Physics, Aristotle University of Thessaloniki, Thessaloniki, Greece
[157] International Center for Elementary Particle Physics and Department of Physics, The University of Tokyo, Tokyo, Japan
[158] Graduate School of Science and Technology, Tokyo Metropolitan University, Tokyo, Japan
[159] Department of Physics, Tokyo Institute of Technology, Tokyo, Japan
[160] Tomsk State University, Tomsk, Russia
[161] Department of Physics, University of Toronto, Toronto ON, Canada
[162] [(a)] INFN-TIFPA; [(b)] University of Trento, Trento, Italy
[163] [(a)] TRIUMF, Vancouver BC; [(b)] Department of Physics and Astronomy, York University, Toronto ON, Canada
[164] Faculty of Pure and Applied Sciences, and Center for Integrated Research in Fundamental Science and Engineering, University of Tsukuba, Tsukuba, Japan
[165] Department of Physics and Astronomy, Tufts University, Medford MA, United States of America
[166] Department of Physics and Astronomy, University of California Irvine, Irvine CA, United States of America

[167] [(a)] INFN Gruppo Collegato di Udine, Sezione di Trieste, Udine; [(b)] ICTP, Trieste; [(c)] Dipartimento di Chimica, Fisica e Ambiente, Università di Udine, Udine, Italy
[168] Department of Physics and Astronomy, University of Uppsala, Uppsala, Sweden
[169] Department of Physics, University of Illinois, Urbana IL, United States of America
[170] Instituto de Fisica Corpuscular (IFIC), Centro Mixto Universidad de Valencia - CSIC, Spain
[171] Department of Physics, University of British Columbia, Vancouver BC, Canada
[172] Department of Physics and Astronomy, University of Victoria, Victoria BC, Canada
[173] Department of Physics, University of Warwick, Coventry, United Kingdom
[174] Waseda University, Tokyo, Japan
[175] Department of Particle Physics, The Weizmann Institute of Science, Rehovot, Israel
[176] Department of Physics, University of Wisconsin, Madison WI, United States of America
[177] Fakultät für Physik und Astronomie, Julius-Maximilians-Universität, Würzburg, Germany
[178] Fakultät für Mathematik und Naturwissenschaften, Fachgruppe Physik, Bergische Universität Wuppertal, Wuppertal, Germany
[179] Department of Physics, Yale University, New Haven CT, United States of America
[180] Yerevan Physics Institute, Yerevan, Armenia
[181] Centre de Calcul de l'Institut National de Physique Nucléaire et de Physique des Particules (IN2P3), Villeurbanne, France
[182] Academia Sinica Grid Computing, Institute of Physics, Academia Sinica, Taipei, Taiwan
[a] Also at Department of Physics, King's College London, London, United Kingdom
[b] Also at Institute of Physics, Azerbaijan Academy of Sciences, Baku, Azerbaijan
[c] Also at Novosibirsk State University, Novosibirsk, Russia
[d] Also at TRIUMF, Vancouver BC, Canada
[e] Also at Department of Physics & Astronomy, University of Louisville, Louisville, KY, United States of America
[f] Also at Physics Department, An-Najah National University, Nablus, Palestine
[g] Also at Department of Physics, California State University, Fresno CA, United States of America
[h] Also at Department of Physics, University of Fribourg, Fribourg, Switzerland
[i] Also at II Physikalisches Institut, Georg-August-Universität, Göttingen, Germany
[j] Also at Departament de Fisica de la Universitat Autonoma de Barcelona, Barcelona, Spain
[k] Also at Departamento de Fisica e Astronomia, Faculdade de Ciencias, Universidade do Porto, Portugal
[l] Also at Tomsk State University, Tomsk, and Moscow Institute of Physics and Technology State University, Dolgoprudny, Russia
[m] Also at The Collaborative Innovation Center of Quantum Matter (CICQM), Beijing, China
[n] Also at Universita di Napoli Parthenope, Napoli, Italy
[o] Also at Institute of Particle Physics (IPP), Canada
[p] Also at Horia Hulubei National Institute of Physics and Nuclear Engineering, Bucharest, Romania
[q] Also at Department of Physics, St. Petersburg State Polytechnical University, St. Petersburg, Russia
[r] Also at Borough of Manhattan Community College, City University of New York, New York City, United States of America
[s] Also at Department of Financial and Management Engineering, University of the Aegean, Chios, Greece
[t] Also at Centre for High Performance Computing, CSIR Campus, Rosebank, Cape Town, South Africa
[u] Also at Louisiana Tech University, Ruston LA, United States of America
[v] Also at Institucio Catalana de Recerca i Estudis Avancats, ICREA, Barcelona, Spain
[w] Also at Department of Physics, The University of Michigan, Ann Arbor MI, United States of America
[x] Also at Graduate School of Science, Osaka University, Osaka, Japan

[y] Also at Fakultät für Mathematik und Physik, Albert-Ludwigs-Universität, Freiburg, Germany
[z] Also at Institute for Mathematics, Astrophysics and Particle Physics, Radboud University Nijmegen/Nikhef, Nijmegen, Netherlands
[aa] Also at Department of Physics, The University of Texas at Austin, Austin TX, United States of America
[ab] Also at Institute of Theoretical Physics, Ilia State University, Tbilisi, Georgia
[ac] Also at CERN, Geneva, Switzerland
[ad] Also at Georgian Technical University (GTU),Tbilisi, Georgia
[ae] Also at Ochadai Academic Production, Ochanomizu University, Tokyo, Japan
[af] Also at Manhattan College, New York NY, United States of America
[ag] Also at The City College of New York, New York NY, United States of America
[ah] Also at Departamento de Fisica Teorica y del Cosmos, Universidad de Granada, Granada, Portugal
[ai] Also at Department of Physics, California State University, Sacramento CA, United States of America
[aj] Also at Moscow Institute of Physics and Technology State University, Dolgoprudny, Russia
[ak] Also at Departement de Physique Nucleaire et Corpusculaire, Université de Genève, Geneva, Switzerland
[al] Also at Institut de Física d'Altes Energies (IFAE), The Barcelona Institute of Science and Technology, Barcelona, Spain
[am] Also at School of Physics, Sun Yat-sen University, Guangzhou, China
[an] Also at Institute for Nuclear Research and Nuclear Energy (INRNE) of the Bulgarian Academy of Sciences, Sofia, Bulgaria
[ao] Also at Faculty of Physics, M.V.Lomonosov Moscow State University, Moscow, Russia
[ap] Also at National Research Nuclear University MEPhI, Moscow, Russia
[aq] Also at Department of Physics, Stanford University, Stanford CA, United States of America
[ar] Also at Institute for Particle and Nuclear Physics, Wigner Research Centre for Physics, Budapest, Hungary
[as] Also at Giresun University, Faculty of Engineering, Turkey
[at] Also at CPPM, Aix-Marseille Université and CNRS/IN2P3, Marseille, France
[au] Also at Department of Physics, Nanjing University, Jiangsu, China
[av] Also at Institute of Physics, Academia Sinica, Taipei, Taiwan
[aw] Also at University of Malaya, Department of Physics, Kuala Lumpur, Malaysia
[ax] Also at LAL, Univ. Paris-Sud, CNRS/IN2P3, Université Paris-Saclay, Orsay, France
[*] Deceased